

Stellingen

1. Het vloeibare karakter van vloeibaar-kristallijne polymeren is zeer duidelijk waarneembaar in dunne films van dit materiaal, namelijk als de film opbreekt en begint te vloeien bij verwarming in de mesofase.

Dit proefschrift, hoofdstuk 4 en 5.

2. Bij de vorming van een macroscopisch éénkristal in dunne vloeibaar-kristallijne polymeerfilms speelt onderkoeling geen of nauwelijks een rol.

Dit proefschrift, hoofdstuk 3.

3. Een goede polymeerhechting en hoge mate van ordening hoeft niet automatisch te leiden tot stabiele polymeerfilms.

Dit proefschrift, hoofdstuk 2 en 4.

4. De waargenomen bevochtigingsovergang van een dunne homopolymeerfilm (met polymerisatiegraad N_H) op een chemisch identieke 'brush' (met polymerisatiegraad N_{Br}) wordt door Liu et al. gecorreleerd aan de verhouding N_H/N_{Br} . Hierbij wordt voorbij gegaan aan het feit dat de filmdikte en oppervlaktebezetting ook een cruciale rol spelen bij deze overgang.

Liu, Y.; Rafailovich, M.H.; Sokolov, J.; Schwarz, S.A.; Zhong, X.; Eisenberg, A.; Kramer, E.J.; Sauer, B.B.; Satija, S. *Phys. Rev. Lett.*, **1994**, 73, 440.

5. Het nodig zijn van een kritische filmdikte bij polymeerkristallisatie in ultradunne polymeerfilms, sluit niet uit dat polymeerkristallisatie mogelijk is in nog dunnere films.

Frank, C.W.; Rao, V.; Despotopoulou, M.M.; Pease, R.F.W.; Hinsberg, W.D.; Miller, R.D.; Rabolt, J.F. *Science*, **1996**, 273, 912. Reiter, G.; Sommer, J.-U. *Phys. Rev. Lett.*, **1998**, 80, 3771.

6. In de coating-technologie wordt de glasovergangstemperatuur T_g algemeen als grens gezien tussen Fickse en niet-Fickse diffusieverschijnselen. Aangezien de T_g van het systeem kan veranderen door absorptie van laagmoleculaire verbindingen ('penetranten') is deze overgang blijkbaar niet scherp gedefinieerd.

Van der Wel, G.K.; Adan, O.C.G. *Progr. in Org. Coat.*, **1999**, in press.

7. In de wetenschap is de kans groot dat het veel vaker dan eens wordt uitgevonden, aangezien vele grote landen slechts in hun eigen, minder toegankelijke, taal publiceren.

8. Het is op opmerkelijk dat tijdens de fusie tussen de Landbouwniversiteit (LUW) en de Dienst Landbouwkundig Onderzoek (DLO) de gezamenlijke noemer uit de naam verdwenen is.

9. Indien een proefschrift bestaat uit reeds verschenen publicaties, dan is te hopen dat het nawoord, c.q. dankwoord, niet het meest gelezen onderdeel is.

10. Het gezegde: “Ik heb er mijn buik vol van”, kan zeer letterlijk opgevat worden bij hoogzwangere vrouwen.
11. De tijdsaanduiding op een parkeerbewijs vergemakkelijkt de planning van inbraak en diefstal van auto's.
12. De beste stelling is hopelijk die van de schilder.

Stellingen behorende bij het proefschrift

Thin liquid-crystalline polymer films: nucleation, crystallisation, instabilities and growth

Maarten W.J. van der Wielen, Wageningen Universiteit, 30 november 1999.

Thin liquid-crystalline polymer films

nucleation, crystallisation, instabilities and growth

Promotoren: Dr. M.A. Cohen Stuart
hoogleraar in de Fysische Chemie met
bijzondere aandacht voor de Kolloïdchemie

Dr. G.J. FLeer
persoonlijk hoogleraar bij het Laboratorium
voor Fysische Chemie en Kolloïdkunde

1172102501, 2711

Thin liquid-crystalline polymer films

nucleation, crystallisation, instabilities and growth

Maarten Willem Josephus van der Wielen

Proefschrift

ter verkrijging van de graad van doctor

op gezag van de rector magnificus

van Wageningen Universiteit,

dr. C.M. Karssen,

in het openbaar te verdedigen

op dinsdag 30 november 1999

des namiddags te half twee in de Aula.

9970386

Wielen, Maarten W.J. van der

Thin liquid-crystalline polymer films: nucleation, crystallisation, instabilities and growth
[Dunne vloeibaar-kristallijne polymeerfilms: nucleatie, kristallisatie, instabiliteiten en groei]
Thesis Wageningen University

ISBN 90-5808-147-8

Cover design: Patrick van Gerner
Printing: Drukkerij Modern, Bennekom.

Het in dit proefschrift beschreven onderzoek is financieel ondersteund door het Innovatiegericht
Onderzoek Programma verf (IOP-v).

BIBLIOTHEEK
LANDBOUWUNIVERSITEIT
WAGENINGEN

Contents

Chapter 1.	Introduction	1
Chapter 2.	Order in thin films of side-chain liquid-crystalline polymers (Langmuir 1997; 13, 4762-4766)	13
Chapter 3.	Growth of a single-domain smectic phase in a thin liquid -crystalline polymer film (Phys. Rev. E. 1999; in press)	25
Chapter 4.	Autophobicity and layering behaviour of thin liquid-crystalline polymer films (Langmuir 1998; 14, 7065-7071)	37
Chapter 5.	The effect of substrate modification on the ordering and dewetting behaviour of thin liquid-crystalline polymer films (To be submitted)	53
Chapter 6.	Controlled nanometer-scale surface roughening and its effect on the ordering and stability of liquid-crystalline polymers (Advanced Materials 1999; 11, 918-923)	69
Chapter 7.	Side-chain liquid-crystalline polymers in bulk and at surfaces	81
	Summary	93
	Samenvatting	97
	Curriculum Vitae	101
	Dankwoord	103

Chapter 1

Introduction

Abstract

In this thesis thin films of side-chain liquid-crystalline polymers are investigated. In this chapter, first some background on liquid crystallinity (classification and ordering) and thin films in general is given. Then the background and objectives of this project are discussed and, finally, an outline of this thesis is presented.

1.1 General

Polymers with a degree of molecular order which is intermediate between that of a solid crystal and that of an isotropic liquid, are termed *liquid crystalline*, mesomorphic or mesophasic. Such order may be established either in solution (*lyotropic*) or in the melt (*thermotropic*). The term mesomorphic is adopted from the Greek language ($\mu\epsilon\sigma\omicron\sigma$ = intermediate and $\mu\omicron\rho\phi\eta$ = form).

Liquid-crystalline polymers (LCPs) combine liquid-crystalline behaviour (electroactive, magnetoactive, variable optical properties) and typical polymeric properties (mechanical properties such as high melt viscosity and a vitreous state, optical and dielectric properties) in one and the same material¹. The bulk material of such polymers has been the subject of intensive research during the last two decades.

The structural feature which gives liquid crystallinity to a polymer is the presence of rigid or semi-rigid structures within the molecule. This rigid moiety is also called the *mesogenic group*. It usually has a high axial ratio or it is disc-like and is often built up from aromatic rings. The mesogenic groups can be present in the backbone and/or connected to the backbone as side groups. The location of the mesogenic group defines the two major classes of liquid-crystalline polymers, which are correspondingly designated as *main-chain* and *side-chain* types (Figure 1.1a and b). Also other variants exist, for example a combination which is a hybrid between the main-chain and side-chain LCPs (Figure 1.1c).

In this study we focus only on thermotropic side-chain liquid-crystalline polymers, in which the mesogenic groups are linked to the polymer chain as side groups via a flexible spacer. In this way the polymer chains (random coils) and mesogenic groups (LC phases) are partially decoupled. If the mesogenic groups are linked to the polymer chain rigidly, i.e. without a flexible spacer, LC phases are rarely obtained.

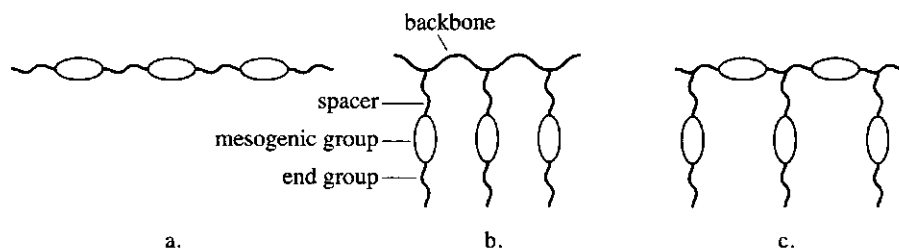


Figure 1.1: Schematic representation of (a) main-chain, (b) side-chain, and (c) combined liquid-crystalline polymers.

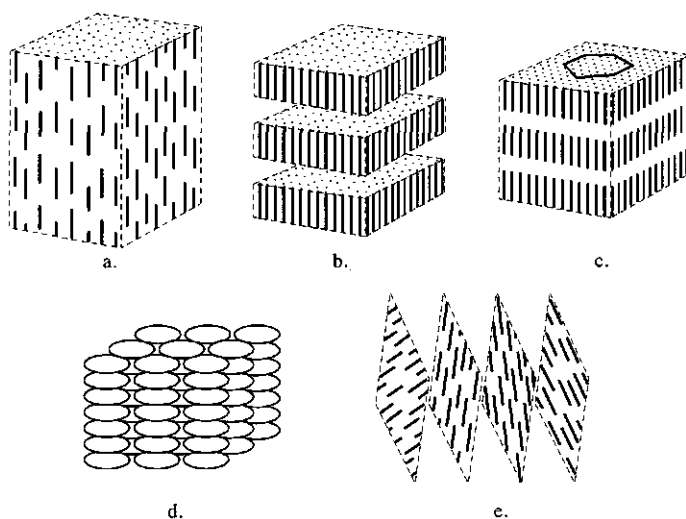


Figure 1.2: Schematic representation of some characteristic liquid-crystalline phases: (a) Nematic, (b) Smectic A, (c) Smectic B, (d) Columnar and (e) Cholesteric.

1.2 Ordering phenomena

Depending on the molecular order and molecular mobility different phases can exist. Types of LC phases which LCPs can exhibit are the so-called nematic, cholesteric, smectic and columnar phases. A schematic representation of these phases is given in Figure 1.2. In the nematic phase the order is present through the alignment of the long axes of neighbouring mesogenic groups (nearly) parallel to each other: the order is in one direction only. The centres of gravity have no long-range order. A special kind of nematic phase is the so-called cholesteric phase. In this phase the preferred direction of the long molecular axis is not constant over the whole sample, as it would be in a 'regular' nematic, but it rather displays a helical distortion (rotating order). Smectics are layered structures with a well-defined interlayer spacing. They have their long axis perpendicular to the layer plane and exhibit order in two directions. In the columnar phase we find piles of rigid building blocks.

With increasing temperature every type of LC phase undergoes a transition towards a liquid (or isotropic) phase at the so-called isotropisation temperature T_i . The temperature below which the LC phase solidifies is called the glass transition temperature T_g and the polymer then is in the glassy LC phase.

In many cases external forces, like that exerted by a substrate, a magnetic field, an electric field or light can play a role in the ordering process of liquid crystals and/or liquid-crystalline polymers. However, the driving force is due to excluded-volume effects.

Onsager and Flory were the first to give an explanation for the isotropic-nematic phase transition in a system of rigid rods. According to their model, the steric interactions between rigid rod-like groups (no overlap) play a major role in selecting the anisotropic state. Rods which are densely packed have more translational freedom (entropy) if they are aligned parallel (nematic) rather than oriented randomly. The average excluded volume is smaller in this ordered phase than in the isotropic phase, which leads to a higher packing entropy in the ordered phase²⁻⁴.

In the liquid-crystalline state of side-chain liquid-crystalline polymers, the backbone must adopt (at least locally) the anisotropic phase structure. Compared with an isotropic melt, this results in a reduction in the chain entropy, because several conformations accessible in the statistical chain conformation are no longer possible. Therefore the chain entropy counteracts the formation of the liquid-crystalline phase structure. Nevertheless, many liquid-crystalline polymer systems exist.

In the Onsager-Flory picture the transition from isotropic to nematic is described in terms of repulsive interactions purely. For smectic ordering it was generally believed in literature that attractive forces are required as well. However, Frenkel et al.⁵ showed that the nematic-smectic phase transition can also occur in the absence of attractive forces, hence, when only repulsive interactions play a role. Therefore, also the nematic-smectic phase transition can be understood on the basis of a competition between two entropic terms. The long range order of smectic layers reduces the ideal entropy but the more efficient packing of the particles leads to a lower excluded volume which, in turn, leads to a gain in packing entropy⁵.

Of course, attractive forces may also play an important role in the ordering process. By changing the chemical structure of the liquid-crystalline polymer these attractive forces are influenced and different LC phases can arise and/or the transition temperatures can change. Small alterations in the mesogenic group, the polymer backbone, the spacer and the degree of polymerisation all affect the phase behaviour⁴ as will be briefly discussed below.

Variation of the mesogenic group: The mesogenic group comprises three components, i.e., the rigid segments, the groups linking different rigid segments together, and substituents of the aromatic rings. Small alterations of each of these components can strongly affect the LC phase behaviour. For example, T_i increases with an increase in polarity of the terminating group. This terminating group determines the strength and direction of the dipole moment. The isotropisation temperature also increases when more benzene rings are present. Also, more ordered phases can then be expected and the thermal stability of the mesophase is enhanced.

Variation of the polymer backbone: The backbone is responsible for the retardation of all relaxation processes. A higher molar mass (due to a longer polymer backbone) results in an increase of the glass transition temperature and of the isotropisation temperature. Increasing the flexibility of the backbone results in wider temperature ranges of the mesophase, and T_i is often increased⁶.

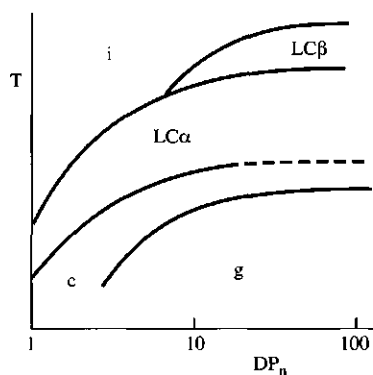


Figure 1.3: Schematic representation of the dependence of the phase behaviour on the degree of polymerisation (DP) (g = glassy, c = crystalline, LC = liquid crystalline, i = isotropic).

Variation of the spacer: With increasing length of the spacer the mobility of the mesogenic groups increases. This results in a decrease of T_i and there is an increasing tendency for the formation of smectic phases. The length and the flexibility of the flexible spacer also determine T_g . Short, flexible spacers strongly elevate T_g , which effect is nearly independent of the chemistry of the main chain, whereas for long flexible spacers the nature of the backbone does become an important feature⁴.

Influence of the degree of polymerisation DP: What kind of mesophases are found often depends on the degree of polymerisation. At high DP more LC phases exist and consequently they can be stabilised differently (Figure 1.3).

In the regime of oligomers ($DP \leq 10$), T_i is strongly affected (increases with DP), while for $10 < DP < 100$ this effect becomes weaker, to approach a constant value of the transition temperature for $DP > 100$. The same holds for LC–LC transitions, e.g., smectic to nematic, and for the glass transition temperature. A schematic example of such behaviour is given in Figure 1.3^{4,7}.

The increase of the LC phase transition temperatures with increasing DP is due to the reduction of the specific volume in going from the monomer to the polymer, which is strong for oligomers. Furthermore, the phase transition temperatures of highly ordered smectic phases are less sensitive to changes in DP than those of the nematic phase.

1.3 Thin films

Thin films (sub-micrometer range) on solid substrates are important in many technological applications and scientific investigations. They can be easily prepared *via* solvent casting procedures (spin-coating and dip-coating), by a Langmuir-Blodgett technique, or by

self-assembly of organic molecules like silanes and thiols. The purpose of these films can be, e.g., to modify the surface behaviour of a material, to form a protective barrier against moisture or solvent penetration, to produce a smooth(er) surface on a rough substrate, or to act as a dielectric insulator. Since thin films offer advantages over thicker films (such as requiring less material), films are made progressively thinner as science and industry strive to exploit these advantages. Upon decreasing the film thickness, though, the films become increasingly susceptible to defects resulting from the coating process⁸, substrate nonuniformities, or conjoining pressure, i.e. negative disjoining pressure which originates from the long-range interactions between molecules of the film and substrate^{9,10}. Upon decreasing the film thickness, the molecular ordering can also change^{11,12}. Therefore, understanding and controlling the processes acting in thin films are of utmost importance. Some important characteristics are surface morphology, film thickness, orientational molecular ordering, chemical composition and surface reactivity, wettability and adhesion, surface topography and roughness, and mechanical properties and stability.

A considerable amount of research has been performed on thin films of isotropic liquids like alkenes, silicon oils and polystyrene^{10,13-16}, but also on more organised films of low-molar-mass liquid crystals (LCs)¹⁷⁻¹⁹, fatty acids and lipids^{20,21}, block-copolymers²²⁻²⁴, and classical self-assembling films formed by chemisorption such as alkylsilanes on silica and alkylthiols on gold²⁵. There is, however, an interesting class of materials exhibiting structured ordered phases in bulk which has hardly been investigated in thin films, namely liquid-crystalline polymers (LCPs).

Since LCPs are hybrid materials (behaving both as liquid crystals and as polymers), they possess a versatility which can make them useful for various applications such as, for instance, optical storage, non-linear optics, gas and liquid chromatography, solid polymer electrolytes, separation membranes and display materials²⁶.

Research on LCPs is not only interesting because of possible applications but also intellectually stimulating from an academic point of view since they provide examples of structurally ordered fluid phases. Although much work has been performed on the synthesis and characterisation of LCPs in bulk^{3,4,27,28}, studies of surface phenomena of LCPs are very scarce. As stated above, the same applies to thin films of LCPs. The work performed so far on side-chain liquid-crystalline polymer films mainly concerns the orientation of the mesogenic group within Langmuir-Blodgett films^{29,30} and within spin-coated films annealed above the glass transition temperature^{12,31,32}. Another feature which has been investigated is the effect of surface roughness on the layer undulations in LB-films³³ and the propagation of the roughness from a boundary in spin-coated films³². The topics described in this thesis contribute to investigations in this unexplored area of surface phenomena of ordered fluids.

1.4 Liquid-crystalline polymers in thin films: background and objectives

As mentioned in section 1.3 there are several applications in which LCPs are used. In this thesis LCPs which could be relevant in the coating technology are studied. An important problem with coatings is the question how old paint layers can be removed. When a paint layer does not meet its requirements (like e.g. protection, decoration) any longer, it has to be removed. It is necessary that this is done in an environmentally friendly way. Techniques used so far are not always adequate in this respect. Therefore there is not only a need to improve existing techniques but also to investigate new paint removal techniques. A novel idea is to make use of a polymer primer layer with a sharp softening temperature. The removal of such a layer is schematically depicted in Figure 1.4. At low T , such a primer layer should adhere well to the substrate and be stable against break-up. Upon heating, e.g., by hot steam under high pressure, the polymer should undergo a phase transition at a certain temperature at which its viscosity suddenly drops so that it becomes possible to remove the coating layer as one intact film, simply by pulling the coating off the primer layer.

There are several reasons why side-chain liquid-crystalline polymers might be suitable for this purpose. First, this kind of polymers can order in parallel layers. By tuning the chemical composition, and thus the polymer-surface interactions, it might even be possible to achieve layering parallel to the substrate surface, i.e., with the mesogenic groups perpendicular to the surface. This will then create more interfaces at which the primer film can split upon heating at suitable temperatures.

Such a suitable temperature probably can be the T_i , since LCPs 'melt' here, and thus undergo an abrupt drop in viscosity. For practical reasons, i.e., in order to remove the coating in an easy way, such an abrupt drop is preferred over the situation occurring for 'classical' polymers where the softening occurs over a long temperature traject and the viscosity remains relatively high even at high temperature³⁴. By varying the chemical constitution of the polymer, the value of T_i can be adjusted.

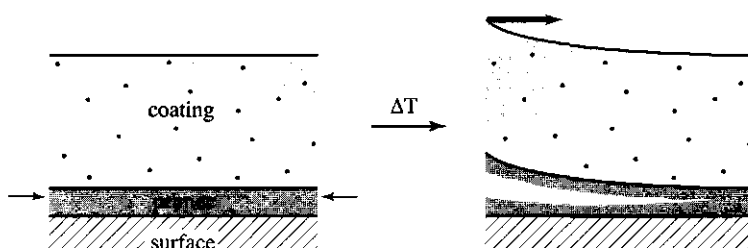


Figure 1.4: Splitting of a liquid-crystalline primer layer.

Another advantage of side-chain LCPs as primers is the fact that ordered layers can prevent and/or slow down the permeation of small molecules (such as water) towards the substrate surface. This has been shown by Gähde et al. in a system where LCPs were used as a primer³⁵. Hence, the interfacial bonds are not weakened as is often the case when water penetrates to the interface; therefore ordered structures can provide protection against corrosion.

All of the properties mentioned above will only constitute real advantages if the primer adheres well to the substrate. Since maleic anhydride moieties, and carboxylic groups in particular, are known to adhere well to metal oxides³⁶⁻³⁹, liquid-crystalline copolymers of *maleic acid anhydride* and *mesogenic alkenes* were synthesised and used in thin films in this project.

The synthesis was performed, in the context of a common project, by R.P. Nieuwhof, at the Laboratory of Organic Chemistry at Wageningen University. The entire project is financially supported by SENTER IOP-verf, which stimulates innovative research programmes in the coating field. Nieuwhof describes the synthesis and characterisation of bulk properties of the polymers in his thesis⁴⁰.

In the present thesis, thin films (in the nanometer range) of these LCPs are investigated. These films are prepared by the spin-coating technique. In this technique substrates covered by a polymer solution are rotated at high velocities (around 3000 rpm) to remove the superfluous material. The remaining solvent evaporates, leaving a thin polymer film behind. By adjusting parameters like the type of solvent, the rotation speed and the polymer concentration, smooth homogeneous films with varying sub-micrometer thicknesses can be prepared. The main techniques used to characterise and study these thin films are

- (i) ellipsometry, to measure the film thickness,
- (ii) atomic force microscopy (AFM) to investigate the surface topography and/or film thickness,
- (iii) optical microscopy (equipped with crossed polarisers and a heating stage) to study the film quality at a macroscopic level, the film stability, the dewetting process, and the appearance of crystalline structures,
- (iv) X-ray reflectivity to study the structures in the film perpendicular to the substrate surface, and
- (v) contact angle measurements to check the quality and hydrophobicity of different substrates.

Several physical properties of the thin liquid-crystalline polymer films are investigated, thereby contributing to the fundamental knowledge in the field of ordered fluid phases and thin films. With the obtained results prudent conclusions might be drawn with respect to the possibilities to use the material as a primer in the proposed novel paint-removal technique.

1.5 Outline of this thesis

This thesis describes different physical properties in thin (nanometer scale) films of side-chain liquid-crystalline polymers. The backbone consists of maleic acid anhydride moieties and the mesogenic side-groups are methoxybiphenyl systems. For the bulk material of LCPs it is known that certain ordered phases appear. However, for thin films little is known about the ordering phenomenon and therefore it is interesting to investigate whether this ordering is also present in thin films.

In Chapter 2 we describe the structures which have been found in the films after annealing the samples above T_g . The combination of AFM and X-ray reflectometry gives a clear picture of the occurrence of ordered structures in thin films, both in parallel as well as in perpendicular directions with respect to the substrate surface.

How this ordering comes about is described in Chapter 3, together with the layering kinetics. We report about the influence of the film thickness and about the effect of the annealing time and temperature. Again the same techniques were used.

Upon prolonged annealing the films do not always remain stable but holes can appear and the film can break up. In Chapter 4 this dewetting behaviour is discussed for the mesophase as well as for the isotropic phase. The film stability is described as a function of the film thickness, the annealing time, and the temperature. The combination of optical microscopy and AFM gives a clear picture of the features on the micrometer to nanometer-scale.

The properties described in Chapters 2,3 and 4 apply to thin films on smooth silicon substrates with a native silica layer. In Chapters 5 and 6 this model substrate was modified chemically and physically, respectively. In Chapter 5 the effect of changes in the polymer-substrate interaction on the film formation, ordering and stability is described. For this purpose, the surface was chemically modified with a variety of chlorosilanes. The results are compared to the behaviour of thin films of a liquid-crystalline polymer with cyanobiphenylic side groups and a methacrylate backbone on unmodified silicon wafers.

In Chapter 6 we describe a new method to roughen the smooth surface, without changing the chemical composition. We make use of colloidal silica particles which are adsorbed onto a pre-adsorbed positively charged polyelectrolyte. By varying the radius of the particles and the particle density the roughness can be controlled. The effect of this nano-roughness on the ordering, stability, and wetting behaviour, has been investigated.

Finally, in Chapter 7, some results in bulk and at surfaces obtained in this IOP-project both from the work of R.P. Nieuwhof as well as from the present work are combined. In the same chapter the perspectives for using this kind of side-chain liquid-crystalline polymers as a primer is discussed.

References

- 1) Nazemi, A.; Williams, G.; Attard, G. S.; Karasz, F. E. *Polymers for Advanced Technologies* **1992**, 3, 157.
- 2) Lekkerkerker, H. N. W. *Physica A* **1991**, 176, 1.
- 3) MacArdle, C. B. *Side Chain Liquid Crystal Polymers*; Blackie & Son: Glasgow and London, 1989.
- 4) Ciferri, A. *Liquid Crystallinity in Polymers*; VCH: New York, 1991.
- 5) Frenkel, D.; Lekkerkerker, H. N. W.; Stroobants, A. *Nature* **1988**, 332, 822.
- 6) Chapoy, L. L. *Recent Advances in Liquid Crystalline Polymers*; Elsevier Appl. Sci.: London, 1985.
- 7) Martellucci, S.; Chester, A. N. *Phase Transitions in Liquid Crystals*; Plenum Press: New York, 1992.
- 8) Stange, T. G.; Mathew, R.; Evans, D. F.; Hendrickson, W. A. *Langmuir* **1992**, 8, 920.
- 9) Kheshgi, H.; Scriven, L. E. *Chemical Engineering Science* **1991**, 46(2), 519.
- 10) Redon, C.; Brzoska, J. B.; Brochard-Wyart, F. *Macromolecules* **1994**, 27, 468.
- 11) Barmantlo, M.; Hoekstra, F. R.; Willard, N. P.; Hollering, R. W. J. *Physical Review A* **1991**, 43(10), 5740.
- 12) Henn, G.; Stamm, M.; Poths, H.; Rücker, M.; Rabe, J. P. *Physica B* **1996**, 221, 174.
- 13) Redon, C.; Brochard-Wyart, F.; Rondelez, F. *Physical Review Letters* **1991**, 66(6), 715.
- 14) Cazabat, A. M.; Heslot, F.; Troian, S. M.; Carles, P. *Nature* **1990**, 346, 824.
- 15) Brochard-Wyart, F.; de Gennes, P.-G.; Hervet, H.; Redon, C. *Langmuir* **1994**, 10, 1566.
- 16) Sharma, A.; Reiter, G. *Journal of Colloid and Interface Science* **1996**, 178, 383.
- 17) Gramsbergen, E. F.; de Jeu, W. H. J. *Phys. France* **1988**, 49, 363.
- 18) Bardon, S.; Valignat, M. P.; Cazabat, A. M.; Stocker, W.; Rabe, J. P. *Langmuir* **1998**, 14(10), 2916.
- 19) Mullin, C. S.; Guyot-Sionnest, P. G.; Shen, Y. R. *Physical Review A* **1989**, 39(7), 3745.
- 20) Roberts, G. *Langmuir-Blodgett Films*; Plenum Press: New York, 1990.
- 21) Ulman, A. *An Introduction to Ultrathin Organic Films from Langmuir-Blodgett to Self-Assembly*; Academic Press: Boston, 1991.
- 22) Ausserré, D.; Chatenay, D.; Coulon, G.; Collin, B. *J. Phys. France* **1990**, 51, 2571.
- 23) Mayes, A. M.; Russell, T. P.; Bassereau, P.; Baker, S. M.; Smith, G. S. *Macromolecules* **1994**, 27, 749.
- 24) Russell, T. P.; Coulon, G.; Miller, D. C. *Macromolecules* **1989**, 22(12), 4600.
- 25) Dubois, L. H.; Nuzzo, R. G. *Annu. Rev. Phys. Chem.* **1992**, 43, 437.
- 26) Hsu, C.-S. *Prog. Polym. Sci.* **1997**, 22, 829.
- 27) Gray, G. W. *Thermotropic Liquid Crystals*; John Wiley & Sons: New York, 1987.
- 28) Collyer, A. A. *Liquid Crystal Polymers*; Elsevier Appl. Sci.: London, 1992.
- 29) Jegou, C.; Leroux, N.; Agricole, B.; Mingotaud, C. *Liquid Crystals* **1996**, 20(6), 691.
- 30) Geer, R.; Qadri, S.; Shashidhar, R.; Thibodeaux, A. F.; Duran, R. S. *Liquid Crystals* **1994**, 16(5), 869.

- 31) Elben, H.; Strobl, G. *Macromolecules* **1993**, *26*, 1013.
- 32) Mensinger, H.; Stamm, M.; Boeffel, C. *J. Chem. Phys.* **1992**, *96*(4), 3183.
- 33) Geer, R. E.; Qadri, S. B.; Shashidhar, R.; Thibodeaux, A. F.; Duran, R. S. *Physical Review E* **1995**, *52*(1), 671.
- 34) van Krevelen, D. W. *Properties of polymers*; Elsevier: Amsterdam, 1990.
- 35) Gähde, J.; Mix, R.; Goering, H.; Schulz, G.; Funke, W.; Hermann, U. *J. Adhesion Sci. Technol.* **1997**, *11*(6), 861.
- 36) Gähde, J.; Mix, R.; Krüger, R.-P.; Goering, H. *J. Adhesion* **1996**, *58*, 243.
- 37) Kurbanova, R. A.; Mirzaoglu, R.; Kurbanov, S.; Karatas, I.; Pamuk, V.; Ozcan, E.; Okudan, A.; Güler, E. *J. Adhesion Sci. Technol.* **1997**, *11*(1), 105.
- 38) Frost, A. M.; Kolosentseva, I. A.; Razumovskii, V. V. *Zh. Prikl. Khim.* **1974**, *47*(4), 731.
- 39) Thery, S.; Jacquet, D.; Mantel, M. *J. Adhesion* **1996**, *56*, 15.
- 40) Nieuwhof, R. P. Dissertation Wageningen University, 1999.

Chapter 2

Order in thin films of side-chain liquid-crystalline polymers[‡]

Abstract

Spin-coated side-chain liquid-crystalline polymer films, based on alternating copolymers of maleic acid anhydride and α -olefins carrying terminal mesogenic methoxybiphenyloxy groups, on silicon wafers show lamellar ordering upon annealing above the glass transition temperature. In the surface topography (atomic force microscopy measurements) structures are visible with a height corresponding to a bilayer. Also within the film, the side chains are ordered perpendicularly to the surface as measured by X-ray reflectometry. There are indications that directly at the substrate surface the side chains are aligned parallel to the surface. By the two complementary techniques, a rather complete picture is obtained. Even though the films are very thin (nanometer-scale thickness), the structure has a high degree of perfection and the bilayer spacing is the same as measured for bulk polymer.

[‡] Based on: M.W.J. van der Wielen, M.A. Cohen Stuart, G.J. Fleer, D.K.G. de Boer, A.J.G. Leenaers, R.P. Nieuwhof, A.T.M. Marcelis, E.J.R. Sudhölter, *Langmuir*, **1997**, 13(17), p. 4762-4766.

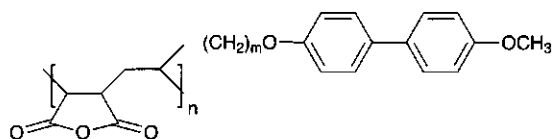
2.1 Introduction

There has been increasing interest in the properties of thermotropic liquid-crystalline polymers (LCP) during the past several years¹⁻⁴. Most of these studies were concerned with bulk material; much less work was done on the thin films of such polymers. The use of X-ray reflectometry (XRR) or atomic force microscopy (AFM) to study thin films of liquid-crystalline polymers is even more scarce⁵⁻⁸. It is important to investigate the behaviour of these polymers in thin films because such films can be used in several applications, e.g., in optical and electrical devices. For these and other applications, it is crucial that the adhesion of the thin films on the substrate is good and that the phase behaviour is known. Because the molecular ordering may be affected by both the substrate-polymer interface and the polymer-air interface, the behaviour could well be different from that of bulk material.

In this study thin films of side-chain thermotropic liquid-crystalline polymers are investigated. The polymer backbone is modified with anhydride groups, and the side chains contain mesogenic groups, in this case methoxybiphenyloxy groups, separated from the backbone with an alkyl spacer. The anhydride groups are expected to improve the adhesion⁹, and the mesogenic groups are responsible for an ordered structure. Atomic force microscopy is used in combination with X-ray reflectometry to study the behaviour of films of these side-chain liquid-crystalline polymers and to extract information on the ordering. A similar approach was used in a recent study by Henn et al.⁶. With AFM, it is possible to investigate lateral structures in the topography on the nanometer length scale. If thin films would not adhere sufficiently, dewetting is expected to take place upon annealing, which should be detectable with AFM. Vertical structures inside the film can be detected with XRR, with a depth resolution better than 1 nm¹⁰. With XRR, one obtains information on the layer thickness, the order within the film, the electron density profile, and the interfacial roughness.

2.2 Experimental

The liquid-crystalline side-chain polymers under study were synthesised by Nieuwhof et al.¹¹. The synthesis of these polymers is based on an alternating copolymerisation of maleic acid anhydride and α -olefins carrying terminal mesogenic methoxybiphenyloxy groups. The radical polymerisation was performed in tetrahydrofuran under an argon atmosphere. The molecular structure of the repeating unit is depicted in Figure 2.1. Also shown in this figure are some aspects of the phase behaviour of the polymers in the bulk as determined by differential scanning calorimetry (DSC), X-ray diffraction, and polarisation microscopy. Full details of the synthesis and bulk properties will be published elsewhere¹¹. The numbers used in the abbreviations for the liquid-crystalline polymers LCP-C4 and LCP-C9 refer to the number of carbon atoms (*m*) in the alkyl spacer of the side-chain, 4 and 9, respectively. The symbols *g*, *S_B*, *S_{Ad}* and *I* correspond to the glass, smectic B, smectic A_d, and isotropic phase as described



LCP-C4 ($m=4$): $T_g=130^{\circ}\text{C}$, $T_{SAd \rightarrow I}=136^{\circ}\text{C}$

LCP-C9 ($m=9$): $T_g=99^{\circ}\text{C}$, $T_{SB \rightarrow SAd}=112^{\circ}\text{C}$, $T_{SAd \rightarrow I}=164^{\circ}\text{C}$

Figure 2.1: Molecular structure of the repeating unit of the side-chain liquid-crystalline polymers LCP-C4 and LCP-C9. Also indicated is the phase behaviour of these polymers. The explanation of the symbols is given in the text.

by Collyer¹². These smectic phases are interdigitated bilayers; they are distinguished by differences in the short-range positional order. The polymers have a degree of polymerisation (DP) of about 9 and a polydispersity of 1.4.

Films were prepared by spin-coating, with a homebuilt spin-coater, on smooth silicon substrates ($1 \times 1 \text{ cm}^2$ for AFM measurements and $2 \times 2 \text{ cm}^2$ for XRR measurements) with a 3-nm-thick native oxide layer. The cleaning procedure of the substrates is successive: (i) ultrasonic cleaning for 5 min in demineralised water, (ii) ultrasonic cleaning for 5 min in 1 M KOH, (iii) UV-ozone treatment for 20 min, and (iv) ultrasonic cleaning for 5 min in isopropyl alcohol. Before spin-coating, the wafers were dried in a nitrogen flow. The polymers were deposited on the wafer from 1,2-dichloroethane by spinning at 4500 rpm during 1 min. Film thicknesses are a function of the polymer concentration in the solution and were found to be in the range 3 – 40 nm as determined by ellipsometry (Gaertner ellipsometer Model L116C, with a rotating analyser) at an angle of incidence of 70° , and/or by XRR and/or by AFM.

The surface topography of the films was investigated by AFM at room temperature directly after spin-coating and after annealing at several temperatures for different time intervals. The images were measured with a Nanoscope III (Digital Instruments, Santa Barbara, CA) operating in the tapping mode (TM-AFM) at a resonance frequency of about 370 kHz. This mode enables one to minimise the lateral forces. Silicon cantilevers with a spring constant between 25 and 110 N/m and resonance frequency in the range of 305 – 493 kHz were used. Some measurements were performed in the contact mode (CM-AFM) with silicon nitride cantilevers with a spring constant of about 0.58 N/m. In this mode, high forces can be applied to the surface to remove the material from the substrate and to determine the thickness of the film afterwards.

An optical microscope (Olympus BX60) was used to study the films on larger length scales to see whether dewetting took place or whether ordering could be made visible by use of crossed polarisers. Some of the films were also characterised by X-ray reflectometry. Again, the films, untreated or annealed, were investigated at room temperature.

The XRR measurements were performed using a Philips reflectometer with a copper-anode tube. The incidence angle with respect to the sample surface is typically below 4° . An asymmetric germanium monochromator with a divergence of 0.02° is used for the incident beam, and the reflected beam is measured using a conventional gas-filled detector with a $50\text{ }\mu\text{m}$ slit. The wavelength of the CuK_α beam is 0.154 nm . Layer densities, thicknesses, and interface roughnesses are extracted from the reflectivity measurement via model-fit calculations¹³. It should be noted that in specular XRR, the roughness profile is laterally averaged over the projected X-ray coherence length ($10 - 100\text{ }\mu\text{m}$). If the roughness is assumed to be distributed normally, an error-function-shaped density profile results, which cannot be distinguished from a similar profile at the atomic scale. We use the Nèvot-Croce method¹⁴ to account for error-function-shaped profiles. In a model fit, the reflectivity is calculated (I_c) and compared with the experimental data (I_m) by iteratively minimising $\sum (\log I_m - \log I_c)^2$ ¹⁵.

2.3 Results and discussion

2.3.1 Atomic force microscopy

The procedure of spin-coating described above always resulted in homogeneous films, as determined by AFM: the roughness was below 1 nm . An example is shown in Figure 2.2a, in which the topography of an 16.9-nm -thick film of LCP-C9 is imaged over an area of $3 \times 3\text{ }\mu\text{m}^2$. Upon annealing, the topography changes. Films of this polymer which were annealed in the mesophase (at $110\text{ }^\circ\text{C}$, in between the glass transition temperature (T_g) and the isotropisation temperature (T_i)) showed terrace-like structures with a characteristic height of roughly $3.4 (\pm 0.2)\text{ nm}$, as can be seen from Figure 2.2b. The holes in this figure cover $25 - 30\%$ of the film area. The minimum annealing time to obtain such terraces is not precisely known, but 30 min appeared to be enough to get this terrace-like image. The formation of such structures is independent of the film thickness, as was checked for the range of $8.7 - 40\text{ nm}$. Films of LCP-C9 which were annealed above T_i , at $168\text{ }^\circ\text{C}$, and subsequently imaged at room temperature, already showed a change in topography after annealing for just 0.5 min , as shown in Figure 2.2c for a 17.8-nm -thick film. Holes of different diameters, all with about the same characteristic depth, are visible over the whole sample surface.

The same kind of topography is found for thin films of LCP-C4 (not shown). Again, a homogeneous topography is obtained immediately after spin-coating, and holes or terrace-like structures appear after annealing (several minutes above T_i at $140\text{ }^\circ\text{C}$). For this polymer, the height of the structures is typically about 2.5 nm .

Similar structures were recently found by Sheiko et al.¹⁶ for films of polymethacrylates with fluorocarbon side chains which were annealed in the mesophase. These structures were

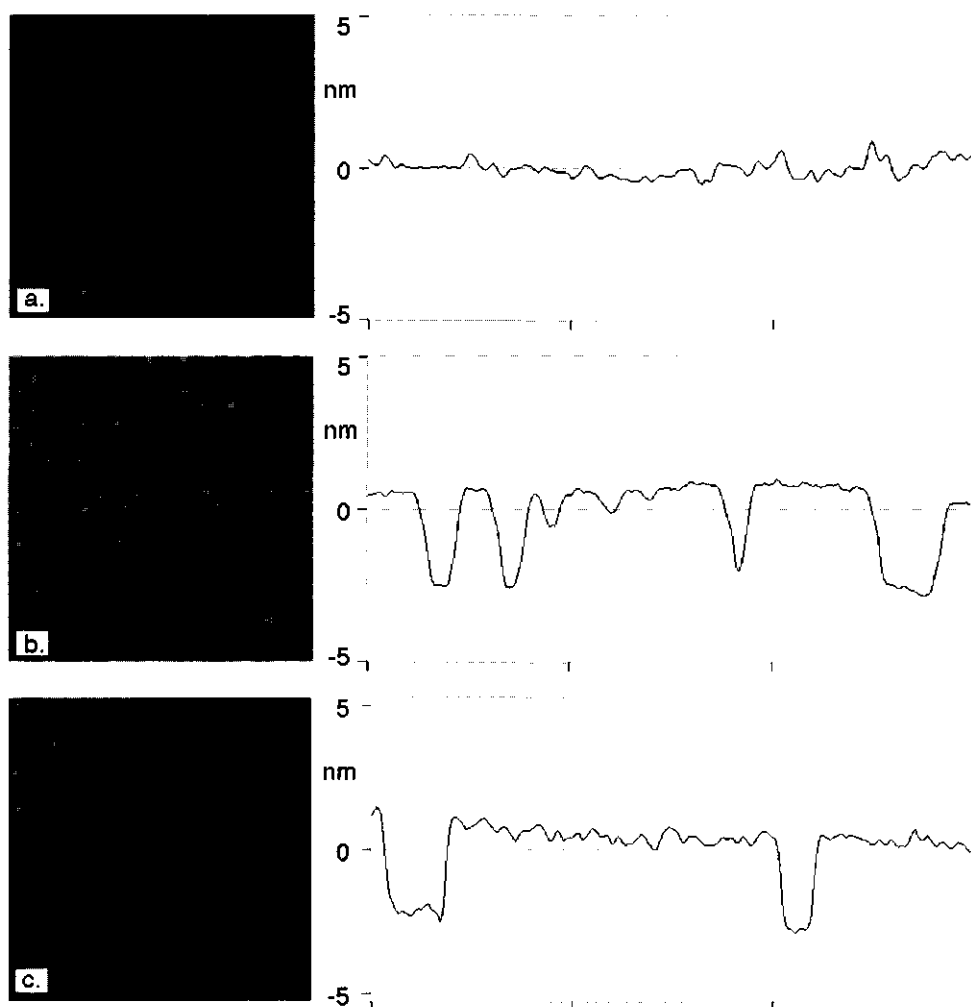


Figure 2.2: AFM image ($3 \times 3 \mu\text{m}^2$) of an about 17 nm thick film of LCP-C9 on a silicon substrate: a) as prepared by spin-coating, b) annealed at $T = 110^\circ\text{C}$ for 30 minutes, c) annealed at $T = 168^\circ\text{C}$ for 0.5 minute (black-white contrast in all images: 10 nm). The cross-sectional profiles along the lines in the images (left) are depicted on the right.

ascribed to bilayer formation in which the side chains were in a rather extended conformation and oriented perpendicularly to the surface, facing the side chains of the next macromolecule.

Also in our case, the characteristic heights are approximately equal to the calculated bilayer spacings for the two polymers, 3.3 and 2.6 nm, respectively, for LCP-C9 and LCP-C4. This calculation was done by summation over the atom-atom distances in the side chain and assuming total overlap of the mesogenic groups oriented perpendicularly with respect to the

substrate. The X-ray diffraction pattern of the bulk material of LCP-C9, measured by Nieuwhof et al.^[1], gave a comparable spacing of about 3.17 nm for the mesophase ordering. These findings seem to indicate that, indeed, bilayer formation takes place in the thin films of these polymers at the polymer–air interface, after annealing above T_g .

The holes most probably arise because there is not enough material to complete a full top bilayer. This assumption is confirmed by experiments in which the surface was covered with insufficient material to obtain a complete bilayer (e.g., 25 % coverage). The fact that the height of the structures corresponds with a bilayer spacing might be an indication that the side chains are alternatively directed up and down; otherwise, one would expect to measure the height of half a bilayer for incomplete bilayers.

Further annealing above T_i for thin films of both polymers (containing several bilayers) resulted in less ordered structures, although also here (even more) terrace-like structures are present (not shown). The size of these structures increases upon longer annealing times. Later, holes of several hundred of nanometers in diameter appear. Dewetting of the surface occurs in some cases. This was also visible with optical microscopy. These dewetting phenomena are under further study and will not be treated in detail in this paper.

Also, even thinner films of LCP-C4 and LCP-C9 (thickness 3 – 4 nm) were prepared by spin-coating, annealed for 30 min in the mesophase and imaged at room temperature. To study the configuration of the first layer in the thin films, the polymer was removed from a small area of the surface by applying a high force on the tip in the contact mode. A schematic representation is given in Figure 2.3. The numbers 1 and 2 indicate the “underlayer” and the outer layer structure, respectively. The height of both layers for the two polymers is given in Table 2.1. These results should be treated rather qualitatively because it is not very accurate to determine the height of structures in the contact mode. In this mode the surface is very sensitive to damage induced by the tip, especially after the ‘scratching’ procedure. In spite of this, it is clear from Table 2.1 that there is still a thin layer under the bilayer structures. Most probably this is a layer of side chains which are aligned parallel to the substrate surface.

2.3.2 X-ray reflectometry

In the reflectograms of as-prepared films of LCP-C9, Kiessig fringes are visible with XRR, which indicates the presence of smooth surfaces, just as found with AFM. The Kiessig fringes originate from interferences of beams reflected at the air–polymer and polymer–substrate interface, respectively. The fringes can be fitted very nicely, assuming no order in the film. An example is given in Figure 2.4 (lower curve) for a film which in the model fit has a thickness of 16.85 nm, an electron density of 334 e/nm³, and a surface roughness of 0.65 nm.

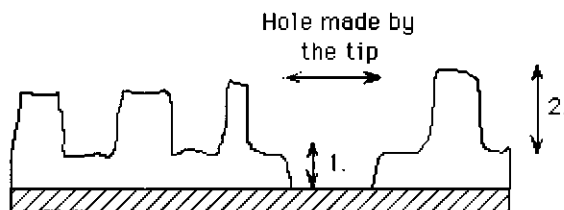


Figure 2.3: Schematic representation of the profile of an CM-AFM image of an annealed thin layer of LCP. The explanation of the numbers is given in the text.

Table 2.1: The height of the ‘underlayer’ (1) and outer layer (2) of an annealed thin (about 4 nm) layer of LCP-C4 and LCP-C9.

LCP	‘underlayer’ (nm)	outer layer (nm)
C4	0.7 ± 0.2	2.5 ± 0.2
C9	0.4 ± 0.2	3.6 ± 0.2

Annealing for 30 min in the mesophase at 110 °C of a 17.8-nm-thick LCP-C9 film and measuring at room temperature resulted in a spectrum where Bragg reflections became visible (upper curve in Figure 2.4). From these Bragg reflections, arising from the periodicity of layers in the film, together with Kiessig fringes, from which the total film thickness can be derived, it was concluded that the film consists of 5.5 (bi)layers. This number of layers, together with the thickness and the composition of the film, was used in model calculations to fit the reflectivity spectrum. The fit is also given in Figure 2.4. Some of the data used for the fitting, or extracted from it, are listed in Table 2.2. The accuracy of the fit results is 5 – 10 % for the electron density and 0.02 – 0.05 nm for the thickness and roughness. In Figure 2.5, these data are represented graphically, by plotting the fluctuations in the electron density as a function of the distance perpendicular to the substrate. The wavy character of this figure is due to the roughness of the layers, modelled by an error-function-shaped profile as explained in section 2.2. Due to this wavy character, the values for the electron densities are lower as compared to the values given in Table 2.2. Small changes in the fit parameters do not change the density profile. At the left side in Figure 2.5, the silicon surface is located, with an electron density of about $712 \text{ e}/\text{nm}^3$, which corresponds to the bulk density typical for this material¹⁰. The density of the LCP film is of the same order of magnitude as has been found by Mensinger et al.⁵ and Henn et al.⁶ for different ordered LCP films. In our case, we relate the different electron densities to backbone regions, spacer regions and mesogen regions, respectively. Although we

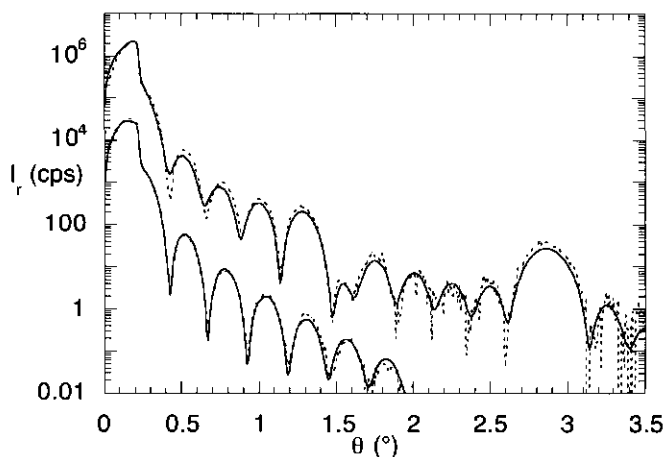


Figure 2.4: Reflected X-ray intensity I_r as a function of the angle of incidence θ , for a 16.9 nm thick film of LCP-C9 on a silicon substrate as prepared by spin-coating (lower curve) and of a 17.8 nm thick film annealed at $T = 110^\circ\text{C}$ for 30 minutes (upper curve). The reflection curve for the film as prepared is shifted down over two decades. The solid curves are the model fits.

do not have hard evidence which electron density we have to assign to which region, we think we have reasonable indications to the assignment as described below. We plan to do some more X-ray and AFM measurements and some modeling to further verify this model.

The region close to the substrate surface is difficult to interpret with XRR. We expect that the backbone will be at the silicon substrate due to its good adhesion properties. Furthermore, when we assume that the configuration of the molecules at the substrate is the same as in an about 4-nm-thick film, the layer at the substrate surface consists of side chains lying parallel to the surface and a backbone region (see section 2.3.1). Probably, regions with backbones on the substrate exist next to regions with side chains on the substrate. This structure gives rise to the shoulder near the silicon surface (at the left side in Figure 2.5). Layer 1 in Table 2.2 corresponds to this region. One must keep in mind that the picture of the first layer in the schematic representation is somewhat speculative.

The peaks in Figure 2.5 with a high electron density of about $410\text{ e}^-/\text{nm}^3$ (corresponding to the value $428\text{ e}^-/\text{nm}^3$ in Table 2.2, layers 4, 8, 12, and 16) we assign to the backbone region because we expect that this layer will have the highest density due to its oxygen atoms in the anhydride group. Compared with the mesogen region, the volume of the backbone region is much smaller and the mesogen region will be more diffuse. This conclusion is also supported by making estimates of the number of electrons per unit volume in the different regions. The density of $340\text{ e}^-/\text{nm}^3$ (the top of the smaller peaks in Figure 2.5) is assigned to the mesogenic groups. The reason that the density of the mesogenic groups does not reach the value of

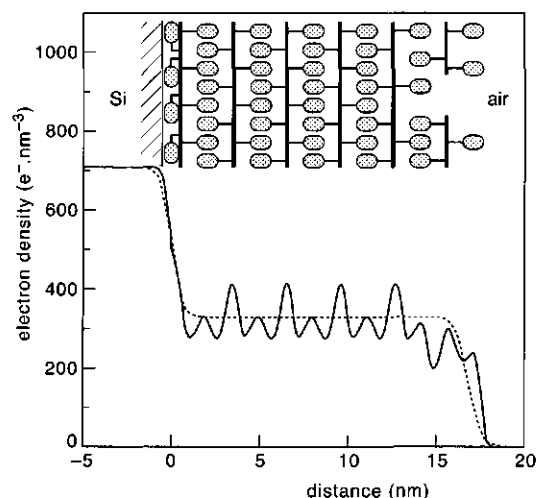


Figure 2.5: Electron density profile of the LCP-C9 film as given in Figure 2.4 as a function of the depth (bottom). The dashed curve is the electron density profile for the as prepared film. The solid curve is for the annealed film. An illustration of the corresponding layer ordering (5.5 bilayers) is given in the top diagram. The symbols refer to backbone (fat lines), alkyl spacers (stripes) and mesogenic groups (circles), respectively.

Table 2.2: Results of the model fit (shown in Figure 2.4 as a solid line) for a 17.8 nm thick annealed (30 min. at $T = 110\text{ }^{\circ}\text{C}$) LCP-C9 film.

Layer	Thickness (nm)	Roughness (nm)	Density (e^-/nm^3)	
Si	∞	0.45	712	
SiO ₂	3.0	0.45	712	
1	1.40	0.30	260	
2	0.49	0.33	411	4 x
3	0.93	0.25	261	
4	0.74	0.21	428	
5	0.93	0.25	261	
18	0.49	0.20	360	
19	0.93	0.20	196	
20	0.74	0.60	321	
21	0.93	0.20	196	
22	0.45	0.40	357	

411 e⁻/nm³ (Table 2.2: layer 2, 6, 10, and 14) is due to the large roughness as compared to the layer thickness, 0.33 and 0.49 nm, respectively, which results in the wavy character as described before. Finally, the lowest density of about 260 e⁻/nm³, in Figure 2.5 and in the odd layers of Table 2.2 (except for layer 1), we assign to the region of the spacers. The electron density here is low compared to the backbone and mesogenic groups, because the spacers contain no atoms with a high electron density. Figure 2.5 (top) gives a schematic representation of the corresponding layer ordering in the 5.5 bilayers.

An alternative model, in which the electron density maxima would be assigned to the mesogen groups, results in a worse fit. In that case also, the structure of the top layer cannot be explained.

The top layer shows a density which is about three-fourths of the density found in the four periodic layers (e.g., for the spacers, these are 196 and 261 e⁻/nm³, respectively). This can be explained with the AFM results in which holes were detected in the surface topography (25 – 30 %, see section 2.3.1) which will give rise to a lower mean value for the electron density.

One periodic bilayer has a thickness of 3.1 nm (summation over the thicknesses of layers 3 – 6, Table 2.2), which is quite close to the layer-spacing as found for the bulk material (3.17 nm)¹¹. For the top bilayer (layers 19 – 22 of Table 2.2), we find 3.1 (± 0.2) nm (with the uncertainty determined by the surface roughness), in good agreement with the AFM terrace height of 3.4 (± 0.2) nm.

An LCP-C9 film of about 9 nm has also been investigated by XRR, both untreated (film thickness of 9.24 nm, an electron density of 400 e⁻/nm³ and a surface roughness of 0.45 nm) and after annealing in the mesophase (at 110 °C for 30 min). The reflection curve for the as-prepared film shows Kiessig fringes. For the annealed film, again, these fringes change, indicating a change in the ordering (Figure 2.6). A comparable model as found for the 18-nm-thick film, now assuming 2.5 interdigitated bilayers, reasonably describes the reflection curve of the film (Figure 2.6), but not as well as in the case of the 18-nm film. Apparently the ordering is less perfect in a thin film.

2.4 Conclusions

The combination of atomic force microscopy and X-ray reflectometry is very useful in describing the morphology of and the structures in thin films of side-chain liquid-crystalline polymers. Although the two techniques measure different properties of the films, there is good agreement between the results from both techniques as to surface roughness, density and top-layer thickness. We can conclude that directly after spin-coating, the LCP-C9 films are not oriented and rather smooth. Annealing above the T_g results in ordered layers parallel to the substrate surface and holes and/or islands with a depth of one bilayer appear in the toplayer. This is also the case for thin films of LCP-C4.

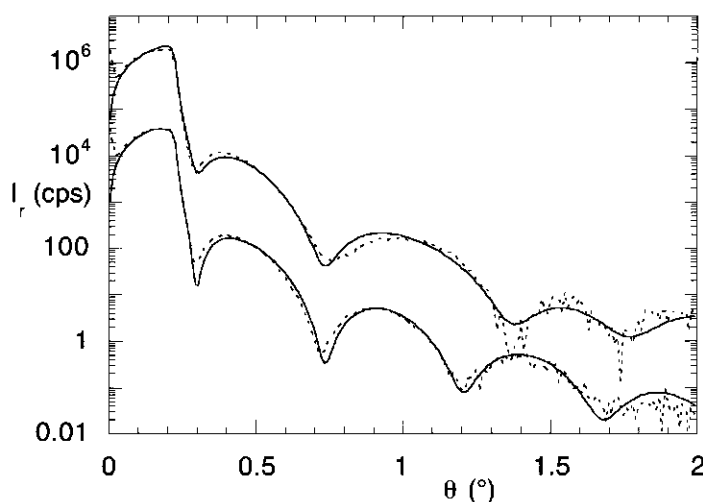


Figure 2.6: Reflected X-ray intensity I_r as a function of the angle of incidence θ , for a 9.24 nm thick film of LCP-C9 on a silicon substrate as prepared by spin-coating (lower curve) and of a 9 nm thick film after annealing at $T = 110^\circ\text{C}$ for 30 minutes (upper curve). The reflection curve for the film as prepared is shifted down over two decades. The solid curves are the model fits.

From AFM measurements it becomes clear that when annealing takes place above T_i the ordering is achieved much faster than in the case of lower annealing temperatures, probably because the molecules are less mobile in the latter case. Furthermore, the ordering seems to be independent of the film thickness, as checked for the range of 8.7 – 40 nm with AFM.

The inner layer spacings, measured by XRR, in an annealed thin film (17.8 nm) of LCP-C9 are the same as measured by Nieuwhof et al.¹¹ for the same material in bulk. Also, for a 9-nm thin film of LCP-C9 ordering of (2.5) interdigitated bilayers is observed after annealing in the mesophase. However, this ordering is not as perfect as in case of the thicker films. This leads to the conclusion that the molecular ordering in these thin films is not, or only slightly, influenced by the substrate-polymer and polymer-air interface for this polymer.

Only at the substrate surface the configuration of the LCP molecules is different. Directly at the substrate, the side chains are most probably ordered parallel to the substrate surface instead of the perpendicular configuration they have within the bilayers.

As discussed above, specular XRR cannot distinguish smearing of the electron density at an atomic scale from that due to interface roughness at larger lateral scales. This distinction can be made by nonspecular reflection. Preliminary nonspecular measurements show that diffuse scattering is present, indicating that roughness at larger scales certainly plays a role.

Acknowledgement

We acknowledge the Dutch Department of Economy Affairs for financial support of 'IOP-verf'-project IVE94.802 and J.W.Th. Lichtenbelt (AKZO-Nobel, Arnhem, The Netherlands) for making available his ellipsometer.

References

- 1) Ciferri, A. *Liquid Crystallinity in Polymers*; VCH: New York, 1991.
- 2) Chapoy, L. L. *Recent Advances in Liquid Crystalline Polymers*; Elsevier Applied Science: London, 1985.
- 3) Gray, G. W. *Thermotropic Liquid Crystals*; John Wiley & Sons: New York, 1987.
- 4) MacArdle, C. B. *Side Chain Liquid Crystal Polymers*; Blackie & Son: Glasgow and London, 1989.
- 5) Mensinger, H.; Stamm, M.; Boeffel, C. *J. Chem. Phys.* **1992**, 96(4), 3183.
- 6) Henn, G.; Stamm, M.; Poths, H.; Rücker, M.; Rabe, J. P. *Phys. B* **1996**, 221, 174.
- 7) Elben, H.; Strobl, G. *Macromolecules* **1993**, 26, 1013.
- 8) Wong, G. C. L.; Commandeur, J.; Fischer, H.; de Jeu, W. H. *Phys. Rev. Lett.* **1996**, 77 (26), 5221.
- 9) Frost, A. M.; Kolosentseva, I. A.; Razumovskii, V. V. *Zh. Prikl. Khim.* **1974**, 47(4), 731.
- 10) Russell, T. P. *Mater. Sci. Rep.* **1990**, 5, 171.
- 11) Nieuwhof, R. P.; Marcelis, A. T. M.; Sudhölter, E. J. R.; Picken, S. J.; de Jeu, W. H. *Macromolecules* **1999**, 32, 1398.
- 12) Collyer, A. A. *Liquid Crystal Polymers: From structures to applications*; Elsevier Applied Science: London, 1992.
- 13) de Boer, D. K. G.; Leenaers, A. J. G.; van den Hoogenhof, W. W. *X-ray Spectrom.* **1995**, 24, 91.
- 14) Nèvot, L.; Croce, P. *Rev. Phys. Appl.* **1980**, 15, 761.
- 15) Leenaers, A. J. G.; de Boer, D. K. G. *X-ray Spectrom.* **1997**, 26, 115.
- 16) Sheiko, S.; Lermann, E.; Möller, M. *Langmuir* **1996**, 12(16), 4015.

Chapter 3

Growth of a single-domain smectic phase in a thin liquid-crystalline polymer film[‡]

Abstract

The ordering process and kinetics in thin films (200 – 800 nm thick) of a thermotropic side-chain liquid-crystalline polymer have been investigated vertically and laterally, respectively, by X-ray reflectivity and atomic force microscopy. The original smooth and amorphous spin-coated films initially become corrugated upon annealing in the smectic mesophase. The roughening of the surface results from the formation of randomly oriented micro-crystalline domains in the film. At the same time, however, a laterally macroscopic crystal starts to grow from the substrate surface in the direction of the polymer–air interface at the expense of these domain structures. Finally, a nicely ordered single crystal with parallel ordered bilayers is formed in the film as well as at the polymer–air interface. This one-dimensional crystallisation, actually recrystallisation, depends strongly on the temperature due to viscosity effects. At low temperatures, just above the glass transition temperature, the ordering is very slow, but with increasing temperature the crystal growth is faster. An Arrhenius-type plot gives an activation energy of 122 kJ/mol, which we ascribe to the expected reorientations of the mesogenic groups during the recrystallisation process.

[‡] Based on: M.W.J. van der Wielen, M.A. Cohen Stuart, G.J. Fleer, A.R. Schlatmann, D.K.G. de Boer, *Physical Review E*, 1999, in press.

3.1 Introduction

Liquid-crystalline materials represent an important field of study with many practical applications. Part of this field concerns liquid-crystalline polymers (LCPs). The study of thin films of such materials started about 5 years ago with the discovery that in thin films of thermotropic liquid-crystalline polymers (on a smooth substrate) perfect ordering can be achieved by a thermal treatment¹⁻⁴. This kind of epitaxy results in a perfectly ordered one-dimensional single crystal. As a result of the ordering process, nanoscale surface structures appear. So far, the layering process (a kind of one-dimensional crystallisation) and its kinetics have not been studied systematically.

In the case of classical polymers, crystallisation can take place when their melts or solutions are cooled. Crystallisation has also been investigated for thin films and close to interfaces^{5,6}. One finding is that in thin films the crystal growth is definitely slower as compared to that in bulk due to the slowing down of the diffusion of molecules. Between the melting temperature and the glass transition temperature the crystallisation rate of polymers has a maximum. Starting from the melting point the rate of secondary nucleation increases as undercooling increases. However, at lower temperatures transport processes are slower due to the increasing viscosity which will reduce the growth rate^{7,8}.

As for crystallisation of classical polymers, the annealing temperature, the annealing time, and the film thickness of thin LCP films will play a crucial role in the ordering (crystallisation) process. By changing these parameters it should be possible to influence the dynamics of ordering in and the final surface topography of thin liquid-crystalline polymer films and hence, to control the formation of (nanoscale) surface structures. Therefore, it is important to know how the crystallisation process in thin LCP films takes place and on what time scale the ordering is completed.

The combination of X-ray reflectometry (XRR) and atomic force microscopy (AFM) gives a good view on the morphology of and structures in the film and their changes in time. This motivates the present study.

3.2 Experimental section

Films were prepared by spin-coating from a 1,2-dichloroethane solution of the liquid-crystalline polymer LCP-C9 (depicted in Figure 3.1) on silicon wafers (Wacker Chemitronics). Film thicknesses of about 200 and 800 nm were prepared. For the synthesis of the polymer, the cleaning of the substrates and the spin-coating conditions we refer to previous work⁹⁻¹¹. The main step in the cleaning procedure is a plasma treatment.

The polymer used has a degree of polymerisation of around 10 and has a glass transition temperature, T_g , of 99 °C. Above this temperature two interdigitated smectic phases appear: a smectic B phase above 99 °C and a smectic Ad phase above 112 °C. The isotropisation

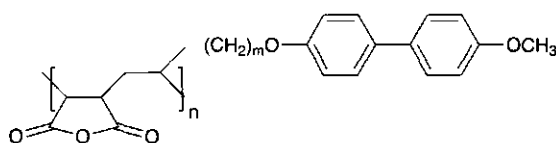


Figure 3.1: Molecular structure of the repeating unit of the side-chain liquid-crystalline polymer LCP-C9. The polymer studied has $m=9$, $n=10$, $T_g=99$ °C, $T_{SB \rightarrow S_{Ad}}=112$ °C and $T_{S_{Ad} \rightarrow I}=164$ °C.

(melting) temperature (T_i) is at 165 °C. Full details about the synthesis and bulk characterisation can be found elsewhere^{10,11}.

The samples were annealed on a hot stage at different temperatures for varying time intervals. Because of the finite time needed to heat up the sample (a few seconds) an uncertainty is present in the annealing time and temperature. To minimise the relative uncertainty as much as possible all samples were annealed for at least 20 s, after which they were immediately cooled down on a cold red copper plate (stored in a refrigerator at -6 °C). In this way the temperature of the film is dropped rapidly to below T_g and the structure within the film is quenched.

In between the heating steps the films were analysed at room temperature using a X-ray reflectometer (X'pert MRD, Philips) with a copper-anode tube. Symmetrical θ -2 θ scans were performed with an incidence angle below 1.75° and the specular reflection was measured. A germanium 4-crystal monochromator (Ge220AS) with a divergence of 0.0042° was used for the incident beam, and the reflected beam is measured using a gas-filled detector with a 0.1 mm slit. The wavelength of the Cu K_α beam is 0.154 nm. Analysis of the reflectivity data, resulting in electron density profiles, thicknesses, and interfacial roughnesses, requires model assumptions. In model-fit calculations (programme Philips WinGixa V1.1) the reflectivity is calculated and compared with the experimental data. Details about this programme and the underlying method have been described by De Boer et al.^{12,13}.

The surface topography was investigated by AFM (Nanoscope III, Digital Instruments, Santa Barbara, CA) at room temperature, both for the as-prepared films and after annealing, in both contact mode (silicon nitride cantilevers, spring constant about 0.58 N/m) as well as tapping mode (silicon cantilevers, spring constant between 25 and 110 N/m, and drive frequency about 370 kHz).

3.3 Results and discussion

3.3.1 Crystallisation processes

The investigated films (thickness 200 and 800 nm) are initially amorphous after spin-coating (at room temperature) and have a smooth surface (roughness less than 1 nm), as determined by XRR and AFM. Upon annealing the films for several seconds in the mesophase

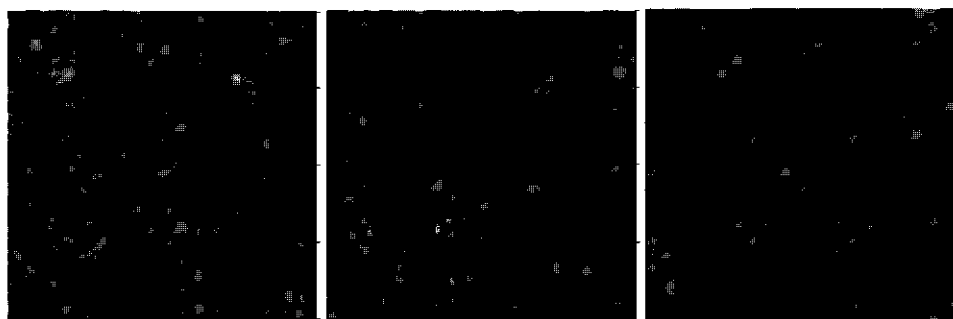


Figure 3.2: AFM images ($10 \times 10 \mu\text{m}^2$) of a 210 nm thick film, annealed at 140 °C for 30 s (a), 1.5 min (b), and for 20 min (c) (black-white contrast in all images 40 nm).

temperature range the polymer surface begins to roughen. Irregular structures are formed, the size of which increases with the film thickness. As an example we show in Figure 3.2a the surface topography (AFM-image) of a film of 210 nm thickness annealed at 140 °C for 30 s. In Figure 3.2a the width and height of the corrugations are typically about 500 nm and 25 nm, respectively. Under an optical microscope with crossed polarisers one also sees these small structures in the film.

After prolonged annealing (a few minutes) the domains which were initially visible under crossed polarisers disappear. However, the film does *not* become smooth. Under the AFM, a complicated structure with multiple terraces is found. This is shown in Figure 3.2b, which has been taken after a total annealing time at 140 °C of 1.5 min. It can be seen that the terraces are bounded by a smooth circumference. The typical lateral size of the ‘hills’ is now about 1 μm . Further annealing (total annealing time 20 min) results in the growth of the terraces together with a reduction in their number, as shown in Figure 3.2c. For this growth to occur molecules have to be transported within the bilayers, as well as cross over from one bilayer into a neighbouring one. Ausserré et al.¹⁴ have modelled this process of permeation and interlayer transport of molecules.

A very striking ‘landscape’ is given in Figure 3.3 for a film of about 800 nm thickness which was annealed at 145 °C for 10 min. Up to 20 terrace levels can be seen. The step height between terraces (3.2 nm) corresponds precisely to the spacing of one interdigitated bilayer⁴. The lateral size of the terraces is of the order of microns. When we compare Figure 3.2b and c with Figure 3.3, it seems that the thickness of the original film has an influence on the final size of the terraced ‘hills’. It is striking that the terraces are all perfectly parallel to the substrate. We note that the terraces have sharp edges but very smooth perimeters (Figure 3.2b and c and Figure 3.3) which is indicative of a tendency to minimise the length of circumference, i.e., a line tension operates. The time scale in which this layering process takes place is another striking point, it all happens (for these temperatures) within a few minutes.

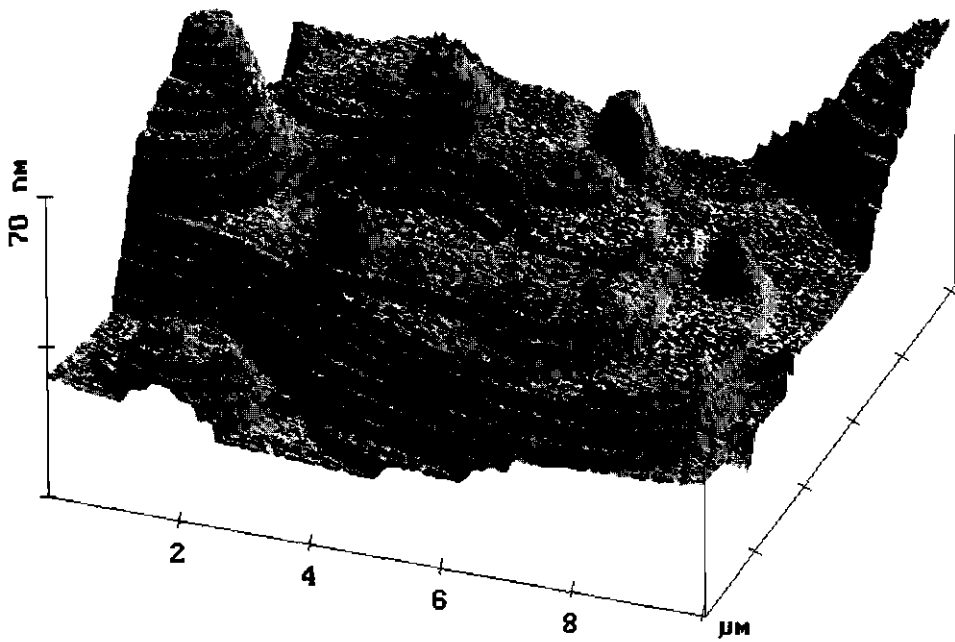


Figure 3.3: AFM image ($10 \times 10 \mu\text{m}^2$) of a 800 nm thick film, annealed at 145 °C for 10 min.

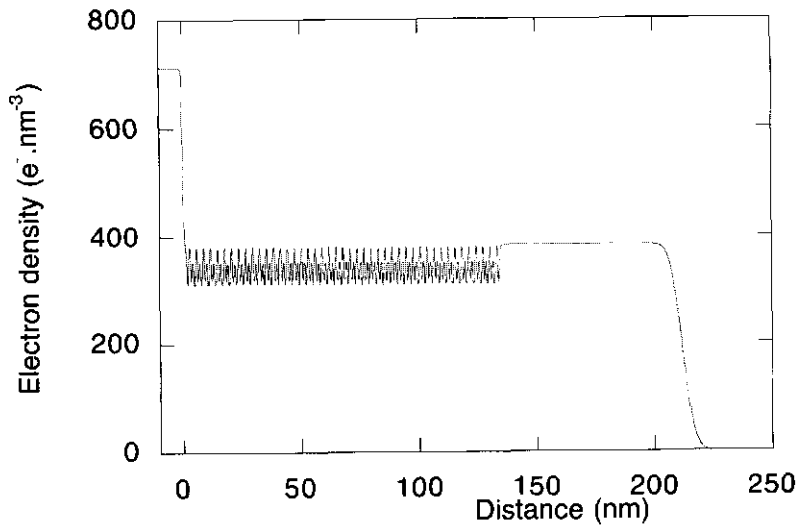


Figure 3.4: Electron density profile (from X-ray reflectivity) for a 210 nm thick film, annealed at 140 °C for 20 s. At the left side the silicon substrate is located with a density of approximately 700 $\text{e}^- \cdot \text{nm}^{-3}$.

In the following, we try to interpret these results. Clearly, a description in terms of equilibrium does not make sense, since this would always require the total free energy and, hence, the total surface area to be minimal. Hence, we have to consider the sample history. This brings us to the following scenario.

Below the isotropisation temperature (T_i) the amorphous phase is metastable. As soon as the initially vitreous polymer is heated to a temperature above T_g in the smectic range, LC domains may nucleate anywhere in the film. These nuclei are oriented randomly. As they grow, they will eventually reach the surface of the film, but this does not stop their growth. Should the crystallisation go on, this would eventually lead to a polycrystalline material with a concomitant rough surface. However, this is not the only process. Simultaneously with the crystallisation in the bulk of the film, a macroscopic crystal begins to grow from the surface of the substrate upward. The presence of such a crystal could be demonstrated with X-ray reflectivity. An extensive description of the X-ray data is given in section 3.2. However, in Figure 3.4 we already present an electron density profile (as extracted from a model fit of the X-ray reflection spectrum⁴) for a film of 210 nm thickness which was annealed during 20 s at 140 °C. After such a short time the topography of the free surface of this polymer film (as monitored by AFM) does not show any terraces yet (surface topography comparable with the one given in Figure 3.2a). Still, we find that about 45 ordered layers are present at the substrate surface, whereas the top layer is not yet stratified in this way. This proves that a large crystal is growing from the wafer in the direction of the polymer–air interface. It seems that the substrate acts as an external field in imposing the orientation. This is not very surprising, because we expect attractions between the maleic acid anhydride groups in the polymer backbone and the silicon surface¹⁵⁻¹⁸ which will help to impose the ordering. Some ordering is even present above the isotropisation temperature in the form of a single stable bilayer as shown in previous work⁹. Obviously, the *free* surface does not act like an external field (in contrast to the case of lamellar ordering in thin copolymer films^{19,20}) and this surface then becomes rough. Somewhat later, the terraces appear. Apparently, the large stable crystal grows at the expense of the smaller domains that were responsible for the roughness. It is this Ostwald ripening process, or recrystallisation, which produces the layering, while preserving the corrugations formed in the first few seconds, with terraces as a result. Apparently, molecules are not transported over large distances, so that macroscopic smoothing cannot occur, or occurs very slowly.

Somewhat similar ‘landscapes’ have been observed during deposition of thin silver films²¹. However, the mechanism of formation is different: the Ag terraces are a consequence of layer-by-layer growth of an Ag(111) crystal from the vapour phase, induced by the presence of surface active additives like Sb. Hence, new material is *added* in the course of time, in contrast to what occurs in our system where there is *no* transport from a dilute phase.

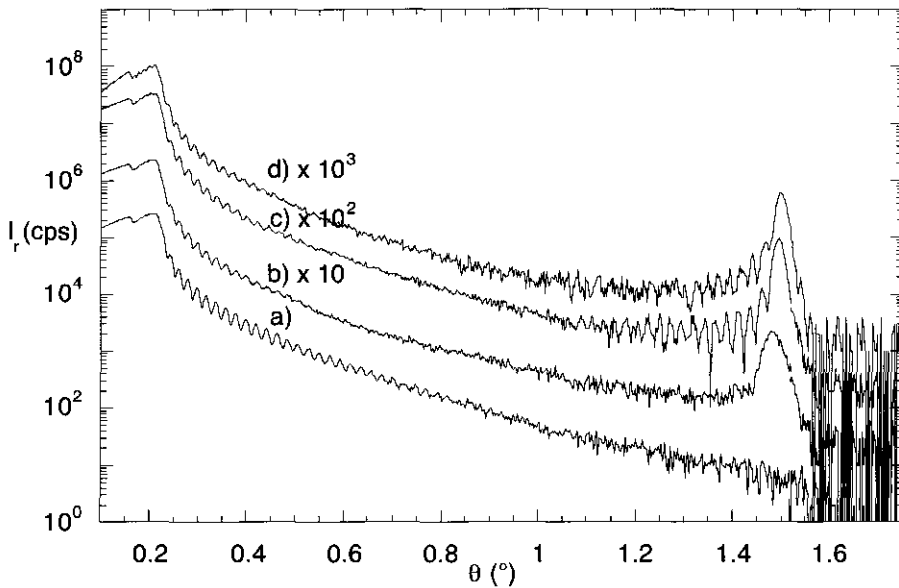


Figure 3.5: XRR-spectra of a 210 nm thick film annealed at 140 °C for 0 (a), 20 (b) and 120 s (c), and of a film annealed at 160 °C for 20 s (d). The data have been offset for clarity.

3.3.2 Kinetics of one-dimensional (re)crystallisation

The growth of the layered structures in time in films of about 200 nm thickness was examined more closely by XRR. With this technique it is possible to follow the layering process in the direction perpendicular to the substrate surface. The samples were annealed at different temperatures in the mesophase at 105, 115, 140, 147, 155, 160 and 164 °C, respectively. The as-prepared films show Kiessig fringes in the reflectograms (an example is given in Figure 3.5, trace a), which indicates that the surfaces are smooth.

Upon annealing these fringes remain, but also a Bragg peak appears at a certain moment in the reflectivity curves at all temperatures mentioned above. In Figure 3.5 examples are given for films annealed at 140 °C and 160 °C, respectively.

The Bragg reflectivity arises from the periodicity of the layers. Its intensity increases with annealing time, which reflects the increase in the number of ordered layers in time. The Bragg peak occurs around $\theta = 1.5^\circ$. From Figure 3.5 it is clear that in the course of time the position of the peak shifts to higher angles, from about 1.45 to 1.5°. This corresponds to a (small) decrease in layer spacing from 3.0 to 2.9 nm. Furthermore, upon reaching the final stage of layering the Bragg peak becomes narrower and additional Kiessig fringes appear around the Bragg peak. The observations mentioned above (intensity increase, sharpening and

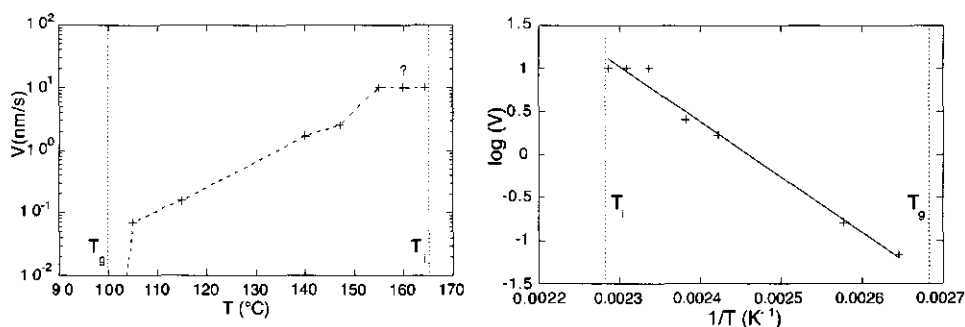


Figure 3.6: a) 1-Dimensional crystal growth rate at different temperatures; b) $^{10}\log$ Arrhenius plot of a).

structuring of the peak) indicate that the system becomes more and more ordered. Finally, a perfect one-dimensional crystal appears.

The time after which the Bragg reflections appear depends on the annealing temperature. At 105 °C, just above the T_g , the Bragg peak is hardly visible even after annealing for 7 min (not shown). At higher annealing temperatures the Bragg peak appears sooner and its intensity increases faster. When annealed just below T_i , the Bragg peak has already reached its maximum intensity and established its detailed surrounding fringe structure within the first annealing treatment of 20 s (Figure 3.5). A further annealing step has hardly any further effect on the reflectivity curves. This was even the case at temperatures very close to T_i , i.e. nearly 164 °C!

From the reflectivity spectra it is possible to extract the number of ordered layers by using model-fit calculations. In the model we make use of the fact that we have a stack of interdigitated bilayers each of which can be separated into four regions. As reported in another paper⁴ the different regions within one bilayer are successively a backbone region, a spacer region, a mesogenic region and another spacer region. Important parameters in the model are film thickness, interfacial roughness, electron density per region, number of bilayers, and (sometimes) fluctuations or a gradient in the bilayer spacing.

The number of bilayers was determined after successive annealing steps. Because of the fluctuations in the ordering it was sometimes not possible to do this with high precision. The overall accuracy is about 5 – 10%. From the number of layers found at different annealing times and temperatures the rate of monocrystal growth (nm/s) can be determined. This rate is plotted in Figure 3.6a as a function of temperature. As was stated above, the crystal layer growth depends strongly on the temperature. In the case of annealing above 155 °C layering was already complete in less than 20 s of annealing, corresponding to a growth rate of at least 10 nm/s. Since our sample preparation (annealing) procedure does not allow us to determine the actual rate in this case, a question mark is shown in Figure 3.6a.

As mentioned in the introduction, the viscosity and the undercooling together determine the rate of crystal growth of common (polymer) crystals. However, in our case we are dealing with a kind of recrystallisation. The driving force is then not the free energy difference at the phase boundary (which is proportional to the undercooling for common crystal growth) but it is the reduction of the domain surface energy²². Indeed, in our case it seems that undercooling plays no (or only a very minor) role, since even at less than 1 degree below the isotropisation temperature, i.e. hardly any undercooling, the layering occurs very fast.

An important aspect of the recrystallisation process is the difference in orientation between the large crystal which starts from the substrate surface and the polycrystalline domains. Since this difference determines domain boundaries, reorientation of only the mesogenic groups at the grain boundary is enough to produce growth of the large single crystal; transport over large distances is not necessary. The viscosity plays the major part in these reorientations, hence also in our ordering process.

When the material is less viscous it is easier for the mesogenic groups to rotate around the backbone. In terms of dielectric spectroscopy this rotational motion gives rise to the so-called δ -relaxation, which has been studied for different side-chain liquid-crystalline polymers (spacer length about 5 – 8 carbon atoms)²³⁻²⁶. In those studies this reorientation process was investigated as a function of the temperature, showing an Arrhenius-like temperature dependence from which the activation energy E_{act} can be derived. Typical values found are around 150 – 180 kJ/mol. In the case of small nematogens, i.e. low molecular weight liquid-crystals, activation energies in the range of 60 – 90 kJ/mol have been reported²⁷. In the former case, the rotation is evidently more co-operative and micro-Brownian motions of the polymer are a necessary prerequisite.

When we make an Arrhenius-plot of our data (Figure 3.6b), we also obtain a straight line. The activation energy, derived from the slope according to the Arrhenius equation

$$\ln V = \frac{-E_{act}}{RT} + const., \quad 3.1$$

gives $E_{act} = 122$ kJ/mol. This value is in between the values obtained from dielectric measurements for other LCP and LC-systems, as discussed above. Since our polymers are very short ($n = 10$) and are actually oligomers, it is plausible that the motion of the mesogenic groups is less restricted by the motion of the backbone than for polymers of high molar mass ($n \approx 50$). Compared to small nematogens, of course, the motion will be more restricted. Hence, one may anticipate an intermediate activation energy, in between that for LCPs and for LCs, as indeed found for our system.

3.4 Conclusions

Initially rough films of an isotropic polymer normally tend to become smooth upon heating in order to lower the surface free energy. However, films of a thermotropic side-chain liquid-crystalline polymer can be highly anisotropic and behave quite differently. Initially, the crystallisation process in the film occurs in randomly oriented domains. However, at the substrate surface a large crystal of parallel ordered (bi)layers starts to grow from the surface. This laterally macroscopic crystal grows at the expense of the randomly oriented domain structures until the whole film is layered parallel to the substrate surface. The crystal growth rate depends strongly on the temperature and increases by more than two orders of magnitude over the whole mesophasic temperature range. In this crystallisation process the effect of polymer viscosity dominates; the effect of undercooling is very small since our films undergo a recrystallisation process. Rotation of the mesogenic groups around the polymer backbone is enough to promote layer growth in the film. The activation energy for this process is 122 kJ/mol, as derived from an Arrhenius-plot. This value is in the expected range, taking data for other systems (LCP and LC) obtained by dielectric spectroscopy into account.

At the end of the recrystallisation process a super crystal remains with very striking nanosized surface patterns. This 'molecular landscaping' process may have interesting applications if it can be externally controlled. It is clear from our result that the growth of the macroscopic crystal retains to some extent the initial surface topography. We therefore could speculate that it would be possible to mechanically impose a certain surface topography, which subsequently could be annealed towards a perfectly terraced surface structure.

Acknowledgements.

We thank A.J.G. Leenaers (Philips Research Laboratories, Eindhoven) for participating in the X-ray reflectivity measurements and R.P. Nieuwhof (Wageningen University) for providing the liquid-crystalline polymer. This work is supported by the Dutch Ministry of Economic Affairs through the SENTER 'IOP-verf' programme.

References

- 1)Mensinger, H.; Stamm, M.; Boeffel, C. *J. Chem. Phys.* **1992**, 96(4), 3183.
- 2)Elben, H.; Strobl, G. *Macromolecules* **1993**, 26, 1013.
- 3)Henn, G.; Stamm, M.; Poths, H.; Rücker, M.; Rabe, J. P. *Physica B* **1996**, 221, 174.
- 4)van der Wielen, M. W. J.; Cohen Stuart, M. A.; Fleer, G. J.; de Boer, D. K. G.; Leenaers, A. J. G.; Nieuwhof, R. P.; Marcelis, A. T. M.; Sudhölter, E. J. R. *Langmuir* **1997**, 13, 4762.
- 5)Reiter, G.; Sommer, J.-U. *Physical Review Letters* **1998**, 80(17), 3771.
- 6)Izumi, K.; Ping, G.; Hashimoto, M.; Toda, A.; Miyaji, H.; Miyamoto, Y.; Nakagawa, Y. *Advances in the understanding of crystal growth mechanisms*; Elsevier Science B.V., 1997.

- 7) Bovey, F. A.; Winslow, F. H. *Macromolecules*; Academic Press: New York, 1979.
- 8) Elias, H.-G. *Macromolecules I*; Plenum Press: New York, 1983.
- 9) van der Wielen, M. W. J.; Cohen Stuart, M. A.; Fleer, G. J. *Langmuir* **1998**, *14*(24), 7065.
- 10) Nieuwhof, R. P.; Marcelis, A. T. M.; Sudhölter, E. J. R.; van der Wielen, M. W. J.; Cohen Stuart, M. A.; Fleer, G. J. *Macromolecular Symposia* **1998**, *127*, 115.
- 11) Nieuwhof, R. P.; Marcelis, A. T. M.; Sudhölter, E. J. R.; Picken, S. J.; de Jeu, W. H. *Macromolecules* **1999**, *32*, 91.
- 12) de Boer, D. K. G.; Leenaers, A. J. G.; van den Hoogenhof, W. W. *X-ray Spectrometry* **1995**, *24*, 91.
- 13) Leenaers, A. J. G.; de Boer, D. K. G. *X-Ray Spectrom.* **1997**, *26*, 115.
- 14) Ausserré, D.; Brochard-Wyart, F.; de Gennes, P.-G. *C.R. Acad. Sci. Paris II* **1995**, *320*, 131.
- 15) Funke, W. *Progress in Organic Coatings* **1996**, *28*, 3.
- 16) Gähde, J.; Mix, R.; Krüger, R.-P.; Goering, H. *J. Adhesion* **1996**, *58*, 243.
- 17) Gähde, J.; Mix, R.; Goering, H.; Schulz, G.; Funke, W.; Hermann, U. *J. Adhesion Sci. Technol.* **1997**, *11*(6), 861.
- 18) Kurbanova, R. A.; Mirzaoglu, R.; S., K.; Karatas, I.; Pamuk, V.; Ozcan, E.; Okudan, A.; Güler, E. *J. Adhesion Sci. Technol.* **1997**, *11*(1), 105.
- 19) Russell, T. P.; Coulon, G.; Miller, D. C. *Macromolecules* **1989**, *22*(12), 4600.
- 20) Mayes, A. M.; Russell, T. P.; Bassereau, P.; Baker, S. M.; Smith, G. S. *Macromolecules* **1994**, *27*, 749.
- 21) Vrijmoeth, J.; van der Vegt, H. A.; Meyer, J. A.; Vlieg, E.; Behm, R. J. *Physical Review Letters* **1994**, *72*(24), 3843.
- 22) Doremus, R. H. *Rates of Phase Transformations*; Academic Press: New York, 1985.
- 23) Wendorff, J. H.; Fuhrmann, T. *Dielectrics Newsletter*; Novocontrol GmbH: Hundsangen, 1994.
- 24) Attard, G. S.; Williams, G.; Gray, G. W.; Lacey, D.; Gemmel, P. A. *Polymer* **1986**, *27*, 185.
- 25) Heinrich, W.; Stoll, B. *Colloid & Polymer Science* **1985**, *263*, 895.
- 26) Zentel, R.; Strobl, G. R.; Ringsdorf, H. *Macromolecules* **1985**, *18*, 960.
- 27) Davies, M.; Moutran, R.; Price, A. H.; Beevers, M.; Williams, G. *J. Chem. Soc., Farad. Trans. II* **1976**, *72*, 1447.

Chapter 4

Autophobicity and layering behaviour of thin liquid-crystalline polymer films[‡]

Abstract

The stability against breaking-up of thin spin-coated films of liquid-crystalline polymers depends on the film thickness and annealing temperature. This study concerns side-chain liquid-crystalline polymers, based on alternating copolymers of maleic acid anhydride and mesogenic alkenes. The mesogenic group is a methoxybiphenyl. The as-prepared films are homogeneous and remain stable below the glass transition temperature. Upon annealing above this temperature the films start to dewet. At the final stage of dewetting only droplets remain on top of a rather stable bilayer, which itself does not participate in the dewetting. This indicates an autophobic behaviour. The bilayer is even present above the isotropisation temperature. In the mesophase we have a layered film and dewetting may occur over several ordered layers. In all cases the dewetting is not linear in time and polymer slippage seems to take place on top of the stable bilayer. In case of polymer slippage, a $t^{2/3}$ dependence is expected for the growth rate. That is indeed found above the isotropisation temperature. In the mesophase the dewetting differs from the 'normal' slippage behaviour and a weaker time-dependence is observed. Around the isotropisation temperature there is a strong increase in the (initial) dewetting velocity of over more than two orders of magnitude, due to the sudden drop in viscosity.

[‡] Based on: M.W.J. van der Wielen, M.A. Cohen Stuart, G.J. Fleer, *Langmuir*, **1998**, 14, p. 7065-7071.

4.1 Introduction

The adhesion between a polymer and a solid substrate is of great importance in many practical applications, such as coatings and optical and electrical devices. In these applications the polymer film should be stable with respect to morphology and thickness. When the polymer film is thicker than a few micrometers, gravity affects the film stability. Thinner polymer films (< 100 nm) are often unstable because intermolecular forces, such as van der Waals forces, become dominant so that the films can break up and spontaneously dewet the substrate¹. The final topology of the film is determined by the balance between the interface (surface tension) and long range (van der Waals) energy contributions².

For polymer films, the dewetting process starts only after first heating the film above the glass transition temperature³. With increasing temperature, the dewetting rate increases, mainly due to the decrease in viscosity of the polymer.

Methods used to prevent dewetting rely upon the modification of the interfacial tension between the liquid and the substrate. This can be done by chemical surface modification, or by grafting a polymer brush on the substrate.

In the present study thin films of thermotropic side-chain liquid-crystalline polymers (LCP) were investigated. In materials of this kind the properties of low-molecular-mass liquid crystals are combined with polymeric properties. The ordering of such material in thin films has been studied for different side-chain LCPs⁴⁻⁷. In our case, the polymer backbone of the LCP is modified with anhydride groups and the side-chains contain mesogenic groups, in this case methoxybiphenyl groups, separated from the backbone with an alkyl spacer. The anhydride groups are expected to improve adhesion^{8,9} (a chemical reaction is possible with the silanol groups at the surface) and the mesogenic groups are responsible for a certain ordering. We recently reported about the order obtained in thin films of this polymer upon annealing above the glass transition temperature (T_g)⁷. The combination of the anhydride groups and the ordering properties might contribute to the stability of the LCP-films. However, it has also been noticed that after annealing for longer times these films start to dewet. This dewetting process is described in more detail in this paper.

So far, not much work was done on the stability of thin LCP films. Sheiko et al.¹⁰ found ordering in and dewetting of thin films of poly(perfluoralkyl methacrylate). They proposed a qualitative model for the observed (self-)dewetting.

A more quantitative mechanism for dewetting of spin-coated films was given by Redon et al.^{11,12} and Brochard-Wyart et al.¹³. However, the films studied by these authors (poly(dimethylsiloxane) on silanized (n-hexa-decyl-trichlorosilane) silicon wafers), were not liquid crystalline. After nucleation of a hole in a thick film (μm -scale), the rate of growth $V = dR/dt$ of the dry patch radius R was found to be constant in time t . The dewetting velocity V was predicted to be inversely proportional to the viscosity η :

$$V = \eta^{-1} \cdot \gamma (12 \cdot L \cdot \sqrt{2})^{-1} \cdot \theta^3 \quad 4.1$$

where γ is the surface tension, θ the static contact angle, and L a dimensionless parameter describing the divergence of the viscous dissipation near the contact line. For films of simple liquids $L = \ln(x_{\max}/x_{\min})$, where x_{\max} is the rim size and x_{\min} a molecular cut-off. The same authors found that in microscopic films (thickness $< 1 \mu\text{m}$) the velocity decreases in time, which was ascribed to strong polymer slippage at the surface of the substrate. The melt slips at the surface and the bulk of the film moves like a solid in that case. The growth of the hole radius is given by¹²

$$R \approx \left(\frac{\gamma}{\eta}\right)^{2/3} \cdot \theta_e^{5/3} \cdot \left(\frac{b^{2/3}}{e^{1/3}}\right) \cdot t^{2/3} \quad 4.2$$

where b is the distance from the wall at which the velocity extrapolates to zero (the so-called extrapolation length) and e the film thickness. The thin poly(dimethylsiloxane) films were unstable and the holes opened spontaneously^{11,12}.

A similar slippage effect was also found by Henn et al.¹⁴ for films of sulfonated polystyrene on an adsorbed brushy monolayer on which dewetting takes place. The films were annealed above the T_g . In the case of thin unmodified polystyrene films, however, the growth velocity is constant as found by Reiter³.

In this paper we describe the dewetting behaviour of LCP-films as a function of temperature. In this way information can be obtained about the change in viscosity of the polymer around the isotropisation temperature¹¹. Because often the film stability depends on the film thickness (the thicker the films the more stable they can be), we have also investigated this dependency.

4.2 Experimental

The molecular structure of the repeating unit of the liquid-crystalline polymer, denoted as LCP-C9, is shown in Figure 4.1. The polymer was synthesised by Nieuwhof et al. and the synthesis and characterisation have been reported elsewhere^{15,16}. The symbols g, S_B, S_{Ad} and I in the legend of Figure 4.1 correspond to the glass, smectic B, smectic A_d, and isotropic phases as described by Collyer¹⁷. The smectic phases are interdigitated bilayers; they are distinguished by differences in the short-range positional order. Concerning its chemical structure the polymer is stable at least up to 190 °C, as measured by infrared spectroscopy and differential scanning calorimetry DSC. The polymer has a degree of polymerisation DP of about 9 and a polydispersity index of 1.4.

Films were prepared on smooth crystalline (100) silicon substrates (Wacker Chemitronics) with a native oxide layer of about 2 nm. The cleaning procedure of the substrates consisted of successively: (i) ultrasonic cleaning for 5 min. in demineralised water, (ii) drying

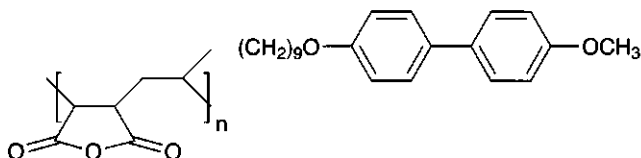


Figure 4.1: Molecular structure of the repeating unit of the side-chain liquid-crystalline polymer LCP-C9. Also indicated are the transition temperatures of the polymer. The polymer studied has $m=9$, $n=10$, $T_g=99$ °C, $T_{SB \rightarrow SAd}=112$ °C and $T_{SAd \rightarrow I}=164$ °C. The explanation of the symbols is given in the text.

in a nitrogen flow, and (iii) plasma treatment (Harrick Plasmacleaner/sterilizer PDC-32G) for 2 minutes. This treatment results in hydrophilic surfaces with a zero contact angle for water. The polymers were deposited on the wafer by spin-coating from 1,2-dichloroethane at the spinning rate 4500 rpm during 1 minute. Film thicknesses are a function of the polymer concentration in the solution and were found to be in the range 30 – 800 nm as determined by ellipsometry (Sentech ellipsometer model SE400, with a rotating analyser) at different angles of incidence.

The dewetting dynamics were observed using an optical microscope in reflection mode (Olympus BX60) fitted with a colour video camera (Sony model DXC 151AP) and a heating stage. Annealing times and temperatures were varied.

The surface topography of the films was investigated by atomic force microscopy (AFM) at room temperature directly after spin-coating, and after annealing at several temperatures for different time intervals. The images were taken with a Nanoscope III (Digital Instruments, Santa Barbara, CA) operating in the contact mode (CM-AFM) with silicon nitride cantilevers with a spring constant of about 0.58 N/m. In this mode it is also possible to apply high forces to the surface in order to remove the material from the substrate and to determine the residual thickness of the film in dewetted areas.

4.3 Results and discussions

Most of the as-prepared films were homogeneous on a small scale (micrometers) as determined by AFM. However, in 800 nm thick films regions with differences in colour were visible with optical microscopy as a result of differences in height. These structures are aligned radially around the centre of the substrate and result from the spin-coating procedure.

Below the glass transition temperature the films are stable for long times, irrespective of the film thickness (in the range 30 – 800 nm). However, the films become unstable above T_g . Both above the isotropisation temperature as well as in the mesophase break up and dewetting occur. These processes were followed in time. The material from the patch accumulates into a rim and this rim of liquid material recedes under capillary forces. When two rims come into

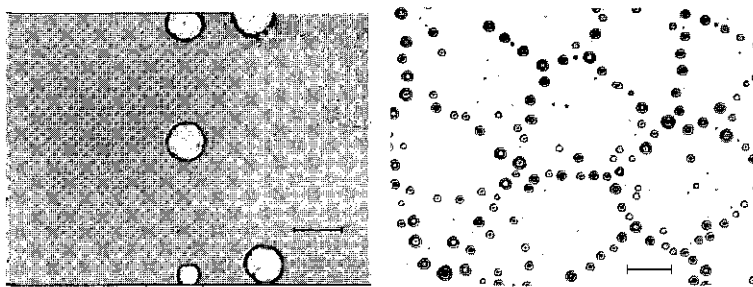


Figure 4.2: Optical micrograph of a 30 nm film at an early stage (40 s) (left) and at the final stage of dewetting (right), after annealing at 180 °C. The bar in both figures represents 100 μm .

contact they form a ribbon which decays into droplets due to Rayleigh instabilities. By way of illustration we show in Figure 4.2 a polymer film (thickness about 30 nm) in the early stages (left), and near the end of the dewetting process (right). These films were annealed at 180 °C, for 40 s and 790 s, respectively. In the final stages the film breaks up completely, leading to a polygon pattern of droplets.

By measuring and analysing the growth rate of the dry patch for different temperatures, information is inferred about the temperature dependence of the viscosity, which determines the growth rate (see equation 4.1 and 4.2). The film stability was examined for three different thickness regimes: thin films (about 32 nm), medium-thickness films (about 180 nm) and thick films (about 800 nm).

For these three regimes, the growth of the hole radius R as a function of time is given in Figure 4.3 for different annealing temperatures. In all cases the rim velocity goes down in time, and it increases with increasing temperature. In sections 4.3.1 and 4.3.2 the dependence of the dewetting process on the film thickness as well as on the temperature will be discussed.

4.3.1 Dependence of dewetting on the film thickness

In Table 4.1 the number of initial holes per unit area as well as the average size and number of droplets per unit area at the final stage of dewetting are given for films (thickness 32 and 180 nm) annealed at 180 °C. With increasing film thickness the number of nuclei decreases. Thermal fluctuations will cause a modulation of the surface, with a wavelength proportional to the square of the film thickness. When these modulations become sufficiently large, holes will appear in the film. Hence, the average distance between the holes depends on the film thickness: the thicker the film, the larger this separation, and the lower the density of nuclei. This is also the reason why the number of remaining droplets at the final stage becomes less with increasing film thickness. Due to mass conservation these droplets will have a larger size³.

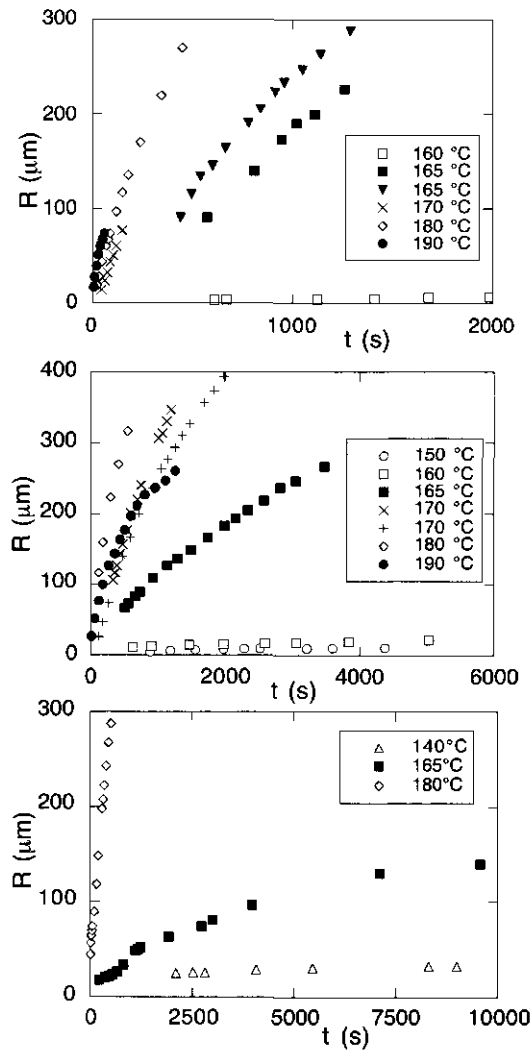


Figure 4.3: Growth in time of the hole radius in LCP-C9 films of thickness 30 nm (top), 180 nm (middle) and 800 nm (bottom), during annealing at different temperatures. For the thin and medium-thickness films, only half of the total annealing time in the mesophase is shown.

Table 4.1: The number of initial holes, N_h , the average size of the remaining droplets, D_d , and their number, N_d , for films of two thicknesses, e , annealed at 180 °C.

e (nm)	N_h (per μm^2)	D_d (μm)	N_d (per μm^2)
32	$1 \cdot 10^{-3}$	18	$3 \cdot 10^{-2}$
180	$2 \cdot 10^{-4}$	100	$2 \cdot 10^{-3}$

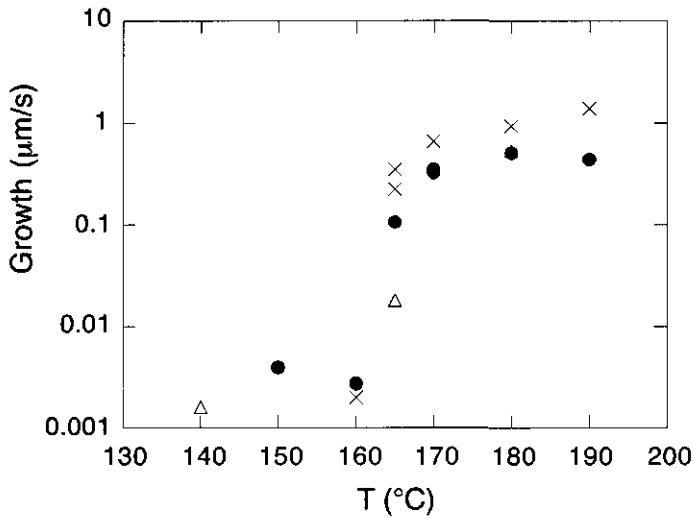


Figure 4.4: Initial dewetting velocity as a function of the temperature for three different film thicknesses: 32 nm (x), 180 nm (•) and 800 nm (Δ).

In Figure 4.4 the initial growth rate is plotted as a function of temperature for the different film thicknesses. This is the velocity as determined in the steep first part in Figure 4.3. The formation of the nuclei as well as their growth are slower for medium-thickness films, as compared to the thin films (Figure 4.3 top and middle, and Figure 4.4).

The theories as given in the introduction describe two limiting cases of dewetting: no-slip conditions (only viscous dissipation) or full slippage (no viscous dissipation). Whether or not slippage occurs for our LCP films will be discussed below.

When slippage occurs the shape of the rim should be asymmetric¹³. This is what we indeed found by AFM: the rim is steeper on the side towards the dry patch than on the side facing the unperturbed film.

In the case of polymer slippage one would also expect a decrease in dewetting velocity according to $R \approx e^{-1/3} \cdot t^{2/3}$ (equation 4.2), where e is the film thickness. In the absence of slippage no dependency on the film thickness is expected (equation 4.1). This slowing down of the growth rate with increasing film thickness is clearly observed for the medium-thickness films as compared to the thin films. However, in thick films the growth of the holes is not much slower than that for medium-thickness films. This is most probably because in the thick films the dewetting often occurs over a rather thick remaining polymer film, as visible by optical microscopy (see section 4.3.2 and Figure 4.8). Hence, the dewetting in that case does not occur over the full 800 nm thickness, and is therefore comparable to that in films of medium thickness.

Both observations mentioned above (i.e., the rim asymmetry and the thickness-dependence of the growth rate) suggest that in our liquid-crystalline polymer films slippage is

present in the dewetting process. Other indications for polymer slippage are given in section 4.3.2.

4.3.2 Dependence of dewetting on the temperature

As discussed in the previous section, we expect polymer slippage at the substrate. Then the hole radius $R(t)$ should grow as $t^{2/3}$ (equation 4.2). In all cases (whatever the film thickness or temperature) we indeed observe a decrease in growth rate with time (Figure 4.3). We therefore tried to fit the $R(t)$ curves in Figure 4.3 by a power law of the form

$$R(t) = a(t - t_0)^x \quad 4.3$$

where R is the radius of the dry patch and t_0 a lag time. Hence, a , t_0 and x are the fit parameters. One example of such a curve fit is given in Figure 4.5. The values of the exponent x at different temperatures are given in Table 4.2. The value of x depends on whether the film is annealed in the mesophase or in the isotropic phase, as will be discussed below.

4.3.2.1. Isotropic phase. Dynamics. When the films are annealed in the isotropic phase ($T \geq 165^\circ\text{C}$), the exponent x in equation 4.3 is in most cases close to the theoretical value $x = 0.67$. This indicates that there is slippage at the surface, with the bulk of the film moving like a solid. For ordinary polymers, entanglements are held responsible for such behaviour¹⁸. In our LCP case we do not expect many entanglements (the molecular mass of our compound is rather low), but we expect that there are still small domains of oriented mesogens in the melt which might act as weak reversible crosslinks, thus creating slippage behaviour.

From Figure 4.3 it becomes clear that the holes do not appear instantaneously but after a few seconds or, in some cases, after a few minutes. The t_0 values obtained from fitting the curves by equation 4.3 are almost always smaller than 1 minute. This is sufficient to create a hole, as it also takes some time to heat up the sample.

At 165°C , which is at the isotropisation temperature, small fluctuations in temperature will result in switching between the two different phases (meso- and isotropic phase). Because the dewetting process in the mesophase is different from that in the isotropic phase (see the second part of this section), the value of x at the coexistence temperature is subject to a large error. This could explain why the two exponent values in Table 4.2 for the 32 nm-thick-film at 165°C are different.

At 190°C the exponent is smaller (0.48 for thin and medium-thickness films) than the theoretical value. This might be an experimental error due to the fact that at that temperature the dewetting process is very fast and more difficult to follow precisely.

In the case of the thick films, the rims are quite large in comparison with the diameter of the holes. Therefore, the conditions assumed by Brochard-Wyart et al.¹³ underlying the derivation of equation 4.2 are not fulfilled. Hence, these dewetting curves cannot be fitted by equation 4.3.

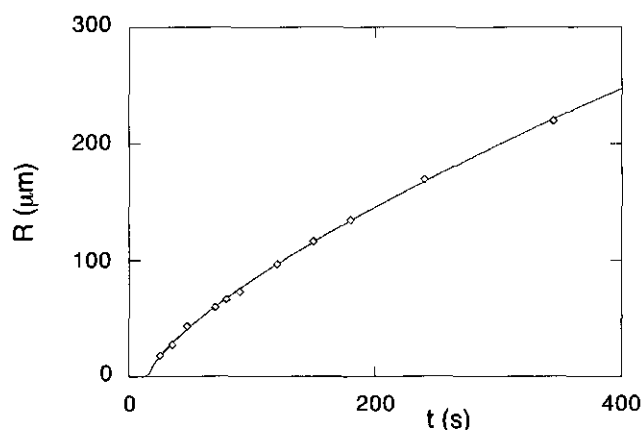


Figure 4.5: Power law curve fit according to eq. 4.3 for a thin film annealed at 180 °C. In this example $x = 0.72 \pm 0.01$.

Table 4.2: Exponent values, x , and their errors, σ , for the fitting of the curves in Figure 4.3 with eq. 4.3.

d=32nm			d=180nm		
T	x	σ	T	x	σ
160	0.48	0.06	150	0.26	0.02
165	0.68	0.12	160	0.40	0.03
165	0.54	0.02	165	0.67	0.02
170	0.90	0.06	170	0.68	0.03
180	0.72	0.01	170	0.64	0.02
190	0.48	0.04	180	0.58	0.06
			190	0.48	0.02

Morphology. In the final stage of dewetting, the dewetted areas were examined more closely by AFM, for all thicknesses. In between the droplets the surface topography appears to be homogeneous. When a high force is applied on a small area of this surface a scratch is observed, which indicates that a residual polymer layer ('underlayer') is still present after dewetting. The thickness of this residual layer after annealing in the temperature range of 165 – 190 °C is typically 3.1 ± 0.4 nm, and is independent of the initial film thickness. Such a thickness of about 3 nm corresponds with a bilayer spacing, as follows from X-ray measurements for ordered thin films of the same material when annealed above T_g ⁷. From the X-ray data we concluded that the mesogenic groups are interdigitated, forming bilayers

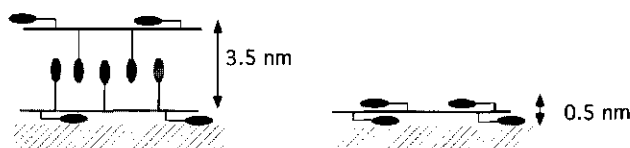


Figure 4.6: Schematic representation of two possible LCP-structures in the remaining thin polymer film at the final stage of dewetting after annealing at 180 °C.

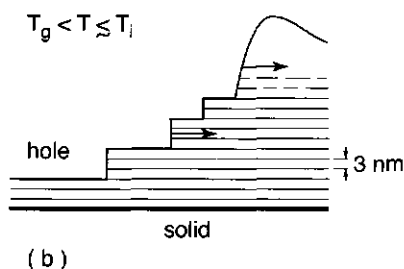
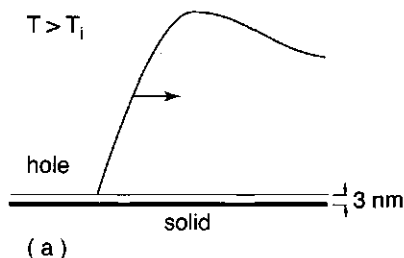


Figure 4.7: Schematic representation of a dewetting film in the isotropic phase (a) and in the mesophase (b). One layer represents a bilayer as illustrated in Figure 4.6 (left).

throughout the film, also directly at the substrate. Although the remaining layer, after dewetting, has not yet been investigated by X-ray measurements in this study, we are rather confident that it is a bilayer, for two reasons. First, with the same material we corroborated in the previous study⁷ the existence of bilayers. Second, in another ordered situation, e.g. a homeotropic alignment, a larger spacing than 3 nm would be expected. We thus conclude that the dewetting occurs from a remaining stable bilayer. A schematic picture of such a bilayer is shown in Figure 4.6 (left). This bilayer is stabilised by the substrate even above the isotropisation temperature.

In Figure 4.7a a schematic representation is given of a dewetting film in the isotropic phase. The ‘underlayer’ represents the stable interdigitated bilayer as given in Figure 4.6 (left), and the bulk material of this film recedes over this remaining bilayer.

To see whether this thin underlayer can still further dewet, some films were annealed for 25 hours at 170 – 180 °C. Afterwards, again a high force was applied by AFM to determine the

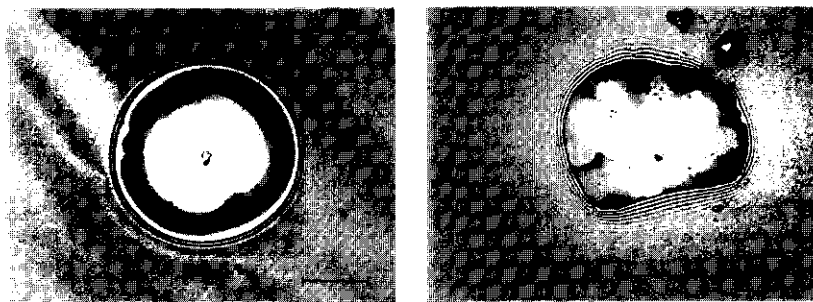


Figure 4.8: Optical micrographs of nucleations in LCP-C9 films of 800-nm-thickness after annealing at 140 °C (left) and 165 °C (right) for 25 and 193 min, respectively. The bar in these figures represents 25 (left) and 50 μm (right).

thickness of the remaining film, if any. In most cases the thin film of about 3 nm was still present. Thus, it seems that this bilayer is very stable. Only in a few cases we found an even thinner layer of 0.7 ± 0.2 nm. In such an ultrathin film both the backbone and the mesogen groups are most probably aligned parallel to and flat on the substrate surface, as schematically depicted in Figure 4.6 (right).

When we examined different ‘dry’ patches in a 180 nm thick film, annealed at 165 °C, before the final stage was reached we found an underlayer that was thicker than 3 nm. Two layer thicknesses were observed for different ‘dry’ patches: 6.7 ± 0.2 nm and 9.7 ± 0.3 nm respectively. This suggests that at some places two bilayers remain and at others three. The underlayers are even visible by optical microscopy in the case of the thick films (Figure 4.8, right). As stated above, at 165 °C we are at (or very close to) the isotropisation temperature which makes it possible that the film switches from the isotropic phase into the smectic A_d phase due to small fluctuations in temperature. This is probably the reason why we see a remnant of the mesophase (i.e., the presence of some layered structures), even though the growth of the holes is still quite fast. A schematic illustration of the dewetting film around T_i (or in the mesophase) is given in Figure 4.7b. Dewetting can occur over several ordered bilayers.

4.3.2.2. Mesophase. Dynamics. In the mesophase the measurements were never extended up to the final stage of dewetting, because the dewetting was very slow. Yet the dynamics could be investigated. As in the isotropic phase, the growth of the holes slows down in time. However, it is clear from Table 4.2 that the exponents for the dewetting process, found in the mesophase, are lower than the theoretical value 0.67. This can be explained by the fact that in the mesophase the side chains are interdigitated⁷ and the mesogen groups (biphenyls) overlap, which results in a layered structure. During the dewetting the mesogen–mesogen interactions have to be disrupted at the dewetting interface, which can cause a retardation in the dewetting. This might explain that we did not find the theoretical value $x = 0.67$ but a lower

one. Furthermore, it is also possible that there is simultaneous slip at *several levels* in the film, due to a layered structure in the film (see also mesophase morphology and the illustration in Figure 4.7b), which can also influence the dewetting velocity in time. This complicates the analysis considerably.

When we take another look at Figure 4.4, we see a large increase in growth rate, of more than 2 orders of magnitude, around T_i (164 °C). This is probably mostly a viscosity effect related to the breaking up of the mesogen–mesogen interactions. Because $V \approx \eta^{-1}$ according to Redon et al.¹¹ we might speculate that there is also a jump in the viscosity of more than 2 orders of magnitude around the isotropisation temperature of this LCP in the thin film. However, because equation 4.1 and 4.2 are not unambiguously valid, we cannot be more precise as to the viscosity.

Morphology. The topography of the films which were annealed in the mesophase was completely different from that of the films annealed above the isotropisation temperature. Dewetting is still in its initial stage and layered structures are visible (Figure 4.9) in between the nuclei. In the case of the medium-thickness films, some small holes (diameter 300 nm – 1 μ m) were also found. The depth of these holes was in the range of 33 – 120 nm. These holes can be the nuclei which will further grow and dewet the (substrate or polymer) surface.

The multiple terrace structures as found in Figure 4.9, have also been followed in time¹⁹ by AFM. The terraces grow in size but there is also a reduction in their number. From these measurements we can conclude that molecules have to be transported within the bilayers, as well as permeate from one bilayer into a neighbouring one. Such a process of permeation and interlayer transport of molecules has been modelled by Ausserré et al.²⁰ in a description of a dewetting process where “holes” (bare regions) and “towers” (two-layer regions) nucleate and grow. According to this model the radius of the depressions (or towers) increases as $R^2(t) \propto t$. Although this may also be the case in our system, we emphasise once more that the AFM-images (terrace-like structures) are *in between* the nuclei which were followed by optical microscopy. To what extent such a process of permeation and interlayer transport contributes to the dewetting process is difficult to say. It seems likely that there must be some effect on the dewetting dynamics.

In places where the film was broken up the substrate was still covered with a rather thick polymer film (as compared to the initial film thickness). This is also sketched in Figure 4.7b. Some examples of the thickness of the remaining film within the dewetted areas will be given below.

In thin films a remaining polymer film of about 10 nm in thickness was measured. This might correspond to three bilayers. For medium-thickness films layered structures were present in the dewetted areas. The thickness of the remaining film was 10 – 15 nm. The thickness of the residual layer for initially thick films was even 25 and 54 nm, respectively, as measured in two cases of annealing at 140 °C.

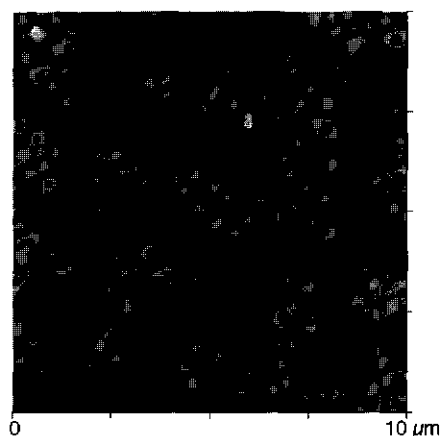


Figure 4.9: AFM image ($10 \times 10 \mu\text{m}^2$) of an film of 32 nm, annealed at 105 °C for 75 min (black-white contrast: 30 nm).

For the thick films terrace-like structures are even visible by optical microscopy (Figure 4.8, left). The different layers suggest that dewetting is possible between any pair of ordered bilayers, e.g. self-dewetting takes place. This supports the view that there can be slip at several arbitrary levels in the film, which in turn would influence the time dependence of the dewetting velocity.

4.4 Conclusions

We studied films of various thicknesses (30, 180 and 800 nm) of a side-chain liquid-crystalline polymer on silicon wafers. The polymer is an alternating copolymer of maleic acid anhydride and mesogenic (methoxybiphenyl) alkenes. The films were obtained by spin-coating and annealed above the glass transition temperature.

Thin films (8 – 40 nm) show lamellar ordering upon annealing for short periods above the glass transition temperature, as has been reported previously⁷. After prolonged heating, the films break up and start to dewet. These processes were followed in time for the different film thicknesses and for different annealing temperatures. In all cases the growth of the holes slows down in time.

Thickness dependence: This dewetting is dependent on the film thickness. With increasing film thickness the number of holes decreases and the rates of breaking up and dewetting slow down. This last observation suggests that polymer slippage occurs in the dewetting process.

Temperature dependence: In the *isotropic phase* a $t^{2/3}$ dependence is found for the growth of the holes in time. This also supports the view that there is polymer slippage at the surface.

In the final stage of dewetting polygon patterns (Voronoi tessellations)²¹ are formed by the remaining droplets. These droplets sit on top of a rather stable bilayer (3.1 ± 0.4 nm) which does not participate in the dewetting. This typical autophobic behaviour indicates that the adhesive forces of this polymer to the (oxidised) silicon substrate are stronger than the cohesive forces between the mesogenic groups.

The autophobic behaviour is even more pronounced in the *mesophase* ($T_g < T < T_i$), where the annealing was stopped before the final stage of dewetting had been reached. In this range, AFM measurements show different bilayer structures. The layering seems to modify the 'normal' slippage behaviour in the mesophase, so that the predicted $t^{2/3}$ dependence is not found. During the dewetting the mesogen-mesogen interactions have to be disrupted at the dewetting interface, which will retard the dewetting process.

Around the isotropisation temperature there is a strong increase (two orders of magnitude) in the dewetting velocity. This is most probably due to the strongly decreasing viscosity because of the breaking up of the mesogen-mesogen interactions.

Side-chain liquid-crystalline polymers with maleic acid anhydride groups in the backbone adhere well to a silicon surface. Thin films of this material are metastable on a large timescale when kept below the isotropisation temperature. This thermal stability against break-up might be improved by increasing the film thickness and/or increasing the molecular weight.

Acknowledgement

We acknowledge SENTER IOP-verf for financial support of this project and R.P. Nieuwhof (Laboratory of Organic Chemistry, Wageningen Agricultural University) for providing us with the polymer.

References

- 1) Brochard, F.; Redon, C.; Rondelez, F. *C.R. Acad. Sci. Paris II* **1988**, 306, 1143.
- 2) Brochard Wyart, F.; Daillant, J. *Can. J. Phys.* **1990**, 68, 1084.
- 3) Reiter, G. *Langmuir* **1993**, 9, 1344.
- 4) Elben, H.; Strobl, G. *Macromolecules* **1993**, 26, 1013.
- 5) Mensinger, H.; Stamm, M.; Boeffel, C. *J. Chem. Phys.* **1992**, 96(4), 3183.
- 6) Henn, G.; Stamm, M.; Poths, H.; Rücker, M.; Rabe, J. P. *Physica B* **1996**, 221, 174.
- 7) van der Wielen, M. W. J.; Cohen Stuart, M. A.; Fleer, G. J.; de Boer, D. K. G.; Leenaers, A. J. G.; Nieuwhof, R. P.; Marcelis, A. T. M.; Sudhölter, E. J. R. *Langmuir* **1997**, 13, 4762.
- 8) Frost, A. M.; Kolosentseva, I. A.; Razumovskii, V. V. *Zh. Prikl. Khim.* **1974**, 47(4), 731.
- 9) Kurbanova, R. A.; Mirzaoglu, R.; S., K.; Karatas, I.; Pamuk, V.; Ozcan, E.; Okudan, A.; Güler, E. *J. Adhesion Sci. Technol.* **1997**, 11(1), 105.
- 10) Sheiko, S.; Lermann, E.; Möller, M. *Langmuir* **1996**, 12(16), 4015.

- 11) Redon, C.; Brochard-Wyart, F.; Rondelez, F. *Physical Review Letters* **1991**, 66(6), 715.
- 12) Redon, C.; Brzoska, J. B.; Brochard-Wyart, F. *Macromolecules* **1994**, 27, 468.
- 13) Brochard-Wyart, F.; de Gennes, P.-G.; Hervet, H.; Redon, C. *Langmuir* **1994**, 10, 1566.
- 14) Henn, G.; Bucknall, D. G.; Stamm, M.; Vanhoorne, P.; Jérôme, R. *Macromolecules* **1996**, 29, 4305.
- 15) Nieuwhof, R. P.; Marcelis, A. T. M.; Sudhölter, E. J. R.; Picken, S. J.; de Jeu, W. H. *Macromolecules* **1999**, 32, 1398.
- 16) Nieuwhof, R. P.; Marcelis, A. T. M.; Sudhölter, E. J. R.; van der Wielen, M. W. J.; Cohen Stuart, M. A.; Fleer, G. J. *Macromolecular Symposia* **1998**, 127, 115.
- 17) Collyer, A. A. *Liquid Crystal Polymers: From structures to applications*; Elsevier Appl. Sci.: London, 1992.
- 18) de Gennes, P. G. *Reviews of Modern Physics* **1985**, 57(3), 827.
- 19) van der Wielen, M. W. J.; Cohen Stuart, M. A.; Fleer, G. J.; Schlatmann, A. R.; de Boer, D. K. G. *to be published*.
- 20) Ausserré, D.; Brochard-Wyart, F.; de Gennes, P.-G. *C.R. Acad. Sci. Paris II* **1995**, 320, 131.
- 21) Stange, T. G.; Mathew, R.; Evans, D. F.; Hendrickson, W. A. *Langmuir* **1992**, 8, 920.

Chapter 5

The effect of substrate modification on the ordering and dewetting behaviour of thin liquid-crystalline polymer films[‡]

Abstract

Liquid-crystalline polymers with maleic acid anhydride moieties in the backbone and methoxybiphenyl groups in the side-chain have been investigated with respect to the ordering in and stability of thin films on chemically modified silicon substrates. For unmodified silicon wafers, it is known that the polymer-substrate interaction induces parallel layering in the film, resulting in rather stable films. By changing the surface groups, i.e. by silylation, the interaction between the polymer and the surface can be tuned. This results in unstable films with a dewetting behaviour which is strongly temperature and substrate dependent. At low temperatures in the mesophase holes nucleate which are encircled by unstable rims. Upon annealing at higher temperature the rim instability decreases and the dewetting velocity increases. This feature also occurs for another completely different side-chain liquid-crystalline polymer with a methacrylate backbone and cyanobiphenyl groups in the side chains. We ascribe the peculiar dewetting behaviour to the presence of polycrystalline domains in the thin films. Especially their size and orientation and their ability to deform under shear are held responsible for the rim instabilities and, consequently, for the droplets remaining behind in the dry patches.

[‡] Based on: M.W.J. van der Wielen, E.P.I. Baars, M. Giesbers, M.A. Cohen Stuart, G.J. Fleer, *To be published.*

5.1 Introduction

The properties of thin films of organic materials are of great importance in many fields like, e.g., coatings, corrosion protection, membranes, wetting/dewetting, microelectronics, biological interfaces and adhesion, but these films are also relevant for the general understanding of the physics and chemistry of surfaces and interfaces. In the present study we report about thin liquid-crystalline polymer (LCP) films (30 nm).

Recently, we have shown that thin films of LCPs, with maleic acid anhydride moieties in the backbone and methoxybiphenyl as the mesogenic group in the side chains, become ordered in layers parallel to a smooth silicon substrate upon annealing in the mesophase¹. In the ordered state, the mesogenic groups are oriented perpendicularly with respect to the substrate plane. We proposed that this ordering is induced by the substrate surface due to the strong backbone–substrate attraction. According to the literature a strong bond of the carboxylate type can be formed between the maleic anhydride and a metal oxide surface^{2,3}. Upon further annealing, these films become unstable and show autophobic behaviour, which finally results in droplets sitting on top of a remaining stable polymer (bi)layer⁴. Especially in the isotropic phase the films dewet rapidly.

Because of the interactions between the anhydride and metal oxide, we expect that the ordering behaviour in, and the stability of thin LCP films can be influenced by modifications in the molecular structure or by modifications of the substrate top-layer. In this study we will consider the effect of surface modifications on ordering and dewetting on a thin organic coating (silane monolayer) on the silica substrate.

It is known that subtle changes in the interactions at the interfaces by, e.g., surface treatment, may have dramatic effects on the wetting properties. For liquid crystals it has been demonstrated that the molecular orientation in the first LC layer at the substrate can be affected by the presence of silane layers^{5,6}. Such surface modifications can also influence the film stability against break-up (dewetting); an example was reported by Reiter et al. for polystyrene films^{7,8}.

Since in our system polymeric properties are combined with liquid-crystalline behaviour, both the ordering and the film stability can be affected by substrate modifications, and both these aspects will be investigated.

5.2 Experimental

Silicon wafers with a thin native oxide layer were modified by various chlorosilane compounds with different end-groups (–X). The silane group forms a chemical bond with the silicon surface, and the end-groups are exposed at the coating–air interface. In this way, several chemically different surfaces were created. Before exposing the wafers to the silanes, the following thorough cleaning procedure was used: (i) ultrasonic treatment in demineralised water

for 5 min, (ii) ultrasonic treatment in chloroform for 5 min, (iii) drying in a nitrogen flow, (iv) UV-Ozone treatment for 20 min, and, finally (v) plasma treatment for 2 min.

The silane reagents are *n*-decyldimethylchlorosilane [$\text{C}_{10}\text{H}_{21}\text{Si}(\text{CH}_3)_2\text{Cl}$], allyldimethylchlorosilane [$\text{C}_2\text{H}_5\text{-CH}_2\text{Si}(\text{CH}_3)_2\text{Cl}$], phenethyldimethylchlorosilane [$\text{C}_6\text{H}_5(\text{CH}_2)_2\text{Si}(\text{CH}_3)_2\text{Cl}$], 4-chlorobutyldimethylchlorosilane [$\text{ClC}_4\text{H}_8\text{Si}(\text{CH}_3)_2\text{Cl}$], 10-carbomethoxydecyldimethylchlorosilane [$\text{CH}_3\text{CO}_2\text{C}_9\text{H}_{18}\text{Si}(\text{CH}_3)_2\text{Cl}$], and 3-cyanopropyldimethylchlorosilane [$\text{CNC}_3\text{H}_6\text{Si}(\text{CH}_3)_2\text{Cl}$], all purchased from United Chemical Technologies, Inc. For convenience, we will refer to a specific coating by means of its terminal functional groups. A 4-chlorobutyldimethylchlorosilane will thus be called a chloride surface ($-\text{X} = -\text{Cl}$).

The modification reactions were performed in 2 % (v/v) solutions of the chlorosilanes in (dried) toluene, in a reflux set-up (80 °C) for at least 12 hours. After this procedure the wafers were kept in the silane solution and stored at room temperature.

Since water/air contact angles are very sensitive to the molecular structure of the topmost few angstroms of the underlying substrate, measurements of these contact angles gives a good idea of the modification quality. One should keep in mind that a contact angle is a macroscopic property of the system. We employed the sessile drop method using a Krüss goniometer, and the values were comparable with values given in literature for thiol self-assembling monolayers on gold with the same end-groups (Table 5.1)^{9,10}. Hence, we conclude that for our purpose we succeeded quite well in preparing dense and homogeneous monolayers.

Since polymer films spin-coated on these wafers undergo a thermal treatment, the effect of the annealing procedure on the coating stability was investigated. In order to do this, the water contact angle on the wafers was also measured after heating the modified wafers (without LCP film) at 190 °C for several minutes (Table 5.1). The contact angle did not change, hence we conclude that all surfaces remain stable upon annealing.

Liquid-crystalline polymer films were prepared by spin-coating from 1,2-dichloroethane. Smooth homogeneous films of about 30 nm in thickness could be prepared by spin-coating from a 0.5 wt% LCP-solution at 3000 rpm.

The structure of the repeating units, as well as the phase transition temperatures for the polymers used are given in Figure 5.1. LCP94 was purchased from Merck and LCP-C9 was synthesised by Nieuwhof et al.¹¹. Both polymers are side-chain liquid-crystalline polymers with smectic order in the mesophase.

The thicknesses of the coating and of the LCP layer were measured by ellipsometry (Sentech ellipsometer model SE400, with a rotating analyser). The thickness of the coatings was always less than 2 nm, and is around 25 – 30 nm for the LCP films.

The surface topography of these layers was imaged using a Nanoscope III atomic force microscope (AFM Digital Instruments, Santa Barbara, CA). The contact mode (CM-AFM) with silicon nitride cantilevers with a spring constant of about 0.58 N/m as well as the tapping mode (TM-AFM) with silicon cantilevers (resonance frequency about 370 kHz) were used. In a few

Table 5.1: Water contact angles for different chemically modified substrates ($-X$) for different situations: as-prepared, literature values for monolayers on gold (lit.), after annealing at 190 °C (Ann.), and after removing a dewetted (Dew.) LCP-film.

$-X$	$\theta(H_2O)$	$\theta(H_2O)$ lit.	$\theta(H_2O)$ Ann.	$\theta(H_2O)$ Dew.
$-\text{CH}_3$	112	112 ⁹ , 110 ¹⁰		
$-\text{CH}=\text{CH}_2$	100	107 ⁹		
$-\text{C}_6\text{H}_5$	78 (82 [*])	95	78	78 (83 [*])
$-\text{Cl}$	83	83 ⁹	80	80
$-\text{CO}_2\text{CH}_3$	68 (74 [*])	67 ⁹ , 95 ¹⁰	68	68 (76 [*])
$-\text{CN}$	64	64 ⁹	64	76

Values measured for a second batch of modified wafers.

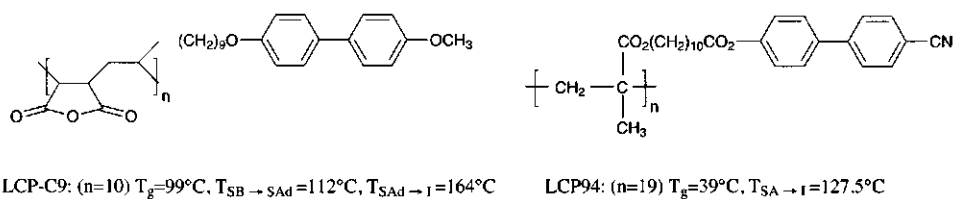


Figure 5.1: Schematic representation of the liquid-crystalline polymers.

cases, which will be specifically mentioned in the text, also oxide-sharpened silicon nitride tips were used to reveal tip-convolution effects.

An optical microscope (Olympus BX60), equipped with a hot-stage and crossed polarisers, was used to investigate the film stability against break-up and the formation of macroscopic polycrystalline domains.

5.3 Results and discussions

5.3.1 Wetting by LCPs

It appeared to be impossible to prepare uniform thin LCP-C9 films on all modified substrates. Whether or not film formation was successful is indicated in Table 5.2. It is clear that film formation is impossible on very hydrophobic coatings ($\theta_{\text{H}_2\text{O}} > 100^\circ$) due to a bad solvent wettability. The wettability of the polymer itself is determined by melting a small amount of the polymer powder and by measuring its (advancing) contact angle at different temperatures. These values can also be found in Table 5.2. The contact angle hardly depends on the temperature and is highest (about 54°) on the wafers onto which no film could be prepared and lowest on the bare silicon wafer (about 32°). For the other wafers there is hardly any difference between the measured contact angles (on average 43°). LCP94 on silicon has a contact angle of about 35° . The contact angle depends on the size of the droplet, i.e., it decreases with decreasing droplet size.

Upon annealing the films above the glass transition temperature all films start to break-up at a certain moment and finally only droplets remain. This process of break-up is described in more detail in section 5.3.2 for the different substrates at different temperatures. The contact angle of the remaining tiny polymer droplets is measured by determining a cross-sectional height profile of the droplet by AFM. This gives the receding contact angle of the polymer on the different substrates. Also here, within the error of the measurement and for all substrates, no dependency of the contact angle on the temperature could be found. Therefore, only the average values are given in Table 5.2 for LCP-C9. After dewetting the LCP94 contact angle on silicon is $12 \pm 3^\circ$.

The contact angle hysteresis of about $10 - 20^\circ$ is not unusual and, probably results from surface heterogeneities and/or differences in droplet size. As found for the advancing contact angle, the angle decreases with decreasing droplet size. The size of the droplets in the receding case is even smaller (nanometer scale) than in the advancing case (micrometer scale), which can contribute to the difference in measured contact angles.

5.3.2 Ordering and dewetting behaviour

The films were investigated by optical microscopy and AFM. From the AFM images it becomes clear that the initially smooth and amorphous films become corrugated upon annealing in the mesophase (not shown). These corrugations result from the formation of randomly oriented polycrystalline domains. For film thicknesses as used here (around 30 nm) the

Table 5.2: Several characteristics of LCP-C9 on different chemically modified silicon wafers ($-X$): possibility of film formation (ff), its advancing (θ_a) and receding (θ_r) contact angle for wetting of the polymer melt at different temperatures, and, the time t needed to complete film break-up at different temperatures.

$-X$	ff	θ_a (LCP-C9)			θ_r (LCP-C9)		t (s) for complete dewetting		
		T (°C)			T (°C)		T (°C)		
		140	150	170	140-170	140	150	170	
$-\text{CH}_3$	-	53	52	56					
$-\text{CH}=\text{CH}_2$	-								
$-\text{C}_6\text{H}_5$	+	41	42	42	$23 \pm 4^{**}$	>1350	~ 50	~ 15	
				55^*	$32 \pm 4^*$	~ 560	~ 15	~ 3.5	
$-\text{Cl}$	+	43	44	46	$23 \pm 5^{**}$	$\sim >800$	~ 30	~ 12	
$-\text{CO}_2\text{CH}_3$	+	41	40	41	$29 \pm 1^{**}$	~ 340	~ 12	~ 8	
				51^*	$40 \pm 3^*$	~ 180	~ 10	~ 4	
$-\text{CN}$	+				8 ± 3	∞	~ 0	~ 0	
$-\text{OH}$	+	31	32	33	10 ± 2				

* Values measured for a second batch of modified wafers (see Table 5.1).

** Oxide-sharpened tips used.

corrugations are too small to be visible by optical microscopy. However, for thicker films it is known that the corrugations are also visible under crossed polarisers, indicating the polycrystalline character. This formation of corrugations and their dependence on the initial film thickness, were studied for LCP-films on unmodified silicon wafers¹². On these wafers the corrugations disappear in time and nicely ordered parallel layers appear^{1,12}.

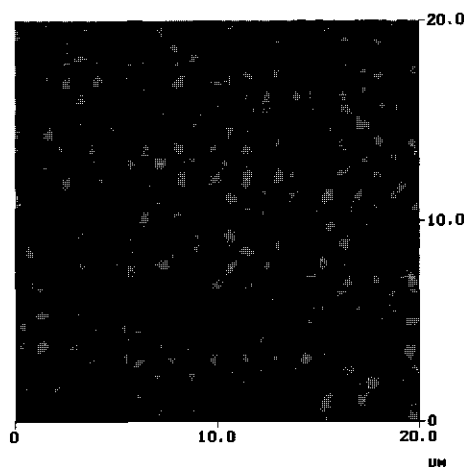


Figure 5.2: Topography of an about 30 nm thick LCP-C9 film on a cyano substrate, annealed at 150 °C for a few seconds. (Area 20 × 20 µm², b/w-contrast 100 nm).

In the experiments reported presently, the same material does not form layered structures parallel to the substrate whenever the $-\text{Cl}$, $-\text{C}_6\text{H}_5$, $-\text{CO}_2\text{CH}_3$, and $-\text{CN}$ substrates were used. Instead, upon increasing the temperature the films become unstable at about 140 °C and start to break up rapidly, while still in the mesophase. This is clearly visible by optical microscopy on $-\text{Cl}$, $-\text{C}_6\text{H}_5$ and $-\text{CO}_2\text{CH}_3$ substrates. In the case of $-\text{CN}$ substrates no dewetting is visible by optical microscopy. However, by AFM it becomes clear that the film breaks up immediately into very small droplets when annealed above about 150 °C (Figure 5.2).

From the data we infer that the time t needed for complete film break-up depends on the nature of the substrate and on the temperature. The t -values for the various situations are given in Table 5.2. The break-up is faster at higher temperatures. This is not surprising because with increasing temperature the viscosity decreases, which will enable the rim accumulating around the dry patch to recede faster.

In the case of phenyl and carbomethoxy surfaces a second batch of modified wafers was obtained with higher contact angles (Table 5.2). It is clear that for surfaces with the same functionalities but higher contact angle the dewetting is also faster. This is the expected behaviour, since the dewetting velocity is known to be proportional to $\theta^{3/3}$.

For the carbomethoxy surface, the dewetting pattern is independent of the modification quality. However, on the phenyl wafers it varies with θ . We tend to ascribe this to the quality of the polymer film, since it was clear by optical microscopy that the film quality on the first phenyl batch was worse than that on all other modified wafers.

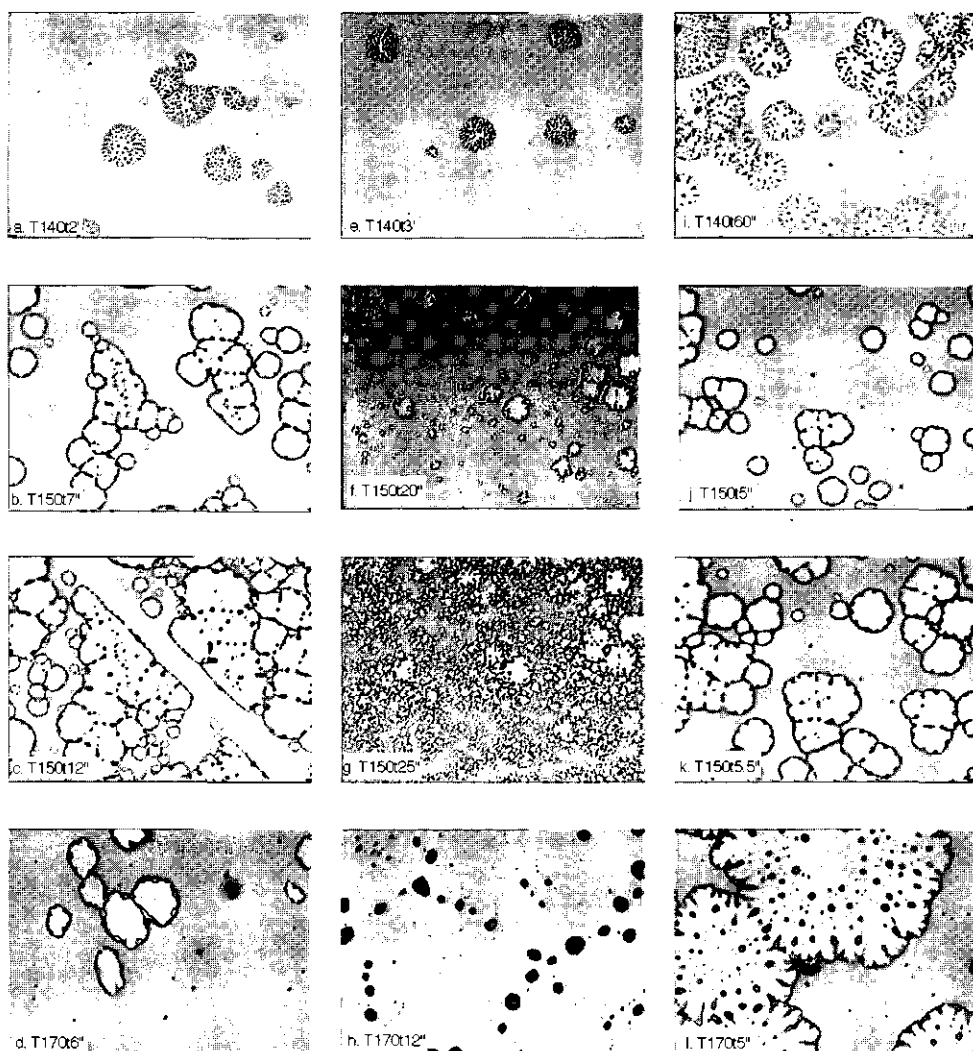


Figure 5.3: Optical micrographs ($162 \times 125 \mu\text{m}^2$) at different stages of dewetting of about 30 nm thick LCP-C9 films on phenyl (a–d), chloride (e–h) and carbomethoxy (i–l) substrates, annealed at different temperatures. The annealing temperature (T) and time (t) are indicated. For example, T140t3' means that the film is annealed at 140 °C for 3 min.

The different stages of hole formation and growth at different temperatures on the cyano, phenyl, chloride and carbomethoxy surfaces are depicted in Figure 5.2 and Figure 5.3. These situations will be discussed separately below.

Cyano surface: The dewetting pattern on -CN-modified surfaces is completely different from that of the other investigated substrates. For the latter (Figure 5.3) we found nucleation and growth of holes, but for cyano surfaces the film instantaneously breaks up into tiny droplets (Figure 5.2). Also, the break-up appears at higher temperature, namely at 150 °C instead of 130 °C. Perhaps the silane coating is modified in one way or another during the annealing of the polymer film, even though the water contact angles do not show any evidence of this (see Table 5.1). Another possibility is the occurrence of silane-LCP interactions when annealing the sample, which can cause or modify the dewetting pattern. In order to check the properties of the substrate after annealing, the remaining small droplets of LCP-C9 at the final stage of dewetting were rinsed off by 1,2-dichloroethane, and the water contact angle of the surface was measured again. In the case of the -CN-surface the water contact angle had changed from 64 to 76°, indicating that a modification had indeed taken place during the annealing. For the other wafers (-C₆H₅, -Cl and -CO₂CH₃) there was no such change in the water contact angle (Table 5.1). Hence, we conclude that the latter three coatings remain stable and unchanged and, hence, we will now further report results for these three coatings only.

Phenyl surface: Thin LCP films on this surface start to become unstable at about 130 °C. Holes appear, which grow in time. The rim around these holes is very unstable and many tiny droplets are left behind. This situation is given in Figure 5.3a for a film annealed at 140 °C for 120 s. For the first batch (Table 5.2), the dewetting pattern was different. Holes appeared which hardly grew. However, since the quality of the polymer film was bad, we do not discuss that result any further.

With increasing temperature, the holes appear faster and grow faster. Also, less droplets are left behind (Figure 5.3b vs. Figure 5.3a). The number of holes increases and at 150 °C the dewetting is completed within 1 min. The situation after 12 s at 150 °C is given in Figure 5.3c.

At 170 °C, in the isotropic phase, we see again nucleation and growth, but even faster. The snapshot (Figure 5.3d) is for the first batch of samples, but the image looks the same for the second batch; the dewetting on the wafer from the second batch being somewhat faster (Table 5.2). At the final stages of dewetting, in both cases a polygonal droplet pattern is left on the surface. A similar pattern was also found for the same material on unmodified silicon wafers at this temperature⁴. In contrast to the dewetting on unmodified silicon, dewetting does not leave a polymer monolayer behind: dewetting is not driven by autophobicity. The absence of such a monolayer could be demonstrated by applying a high force by AFM in between the droplets: there was no remaining polymer material in these areas.

Chloride surface: Several holes become visible at 140 °C after annealing for about 1 min. The rim around the patches is very unstable and, as a result, many small droplets are left behind. Figure 5.3e illustrates the situation after 3 min at 140 °C. At 150 °C these rim instabilities are less pronounced (Figure 5.3f,g). At this temperature the growth of the holes is slower and many more new holes appear. Due to the high density of these new holes, the initial

holes can hardly grow in the period needed to complete film break-up. The numerous new holes occupy almost the complete surface within 25 s (Figure 5.3g).

At 170 °C holes nucleate virtually instantaneously and grow very fast. The situation after 4 s of annealing is comparable with the situation depicted in Figure 5.3d, for a phenyl surface ($\theta_i \sim 23^\circ$). At the final stages of dewetting a polygonal structure is visible (Figure 5.3h). As with the phenyl surface no polymer monolayer is left.

Carbomethoxy surface: As in the case of the phenyl and chloride substrates, the film breaks up and the rim is very unstable at 140 °C, decaying into small droplets. These remaining droplets are somewhat larger in size than for the phenyl and chloride substrates (Figure 5.3i vs a and e). At 150 °C the rate of nucleation is more or less balanced by the hole grow rate (Figure 5.3j,k). At 170 °C the dewetting seems 'normal' and the situation after 3 s of annealing is comparable with the situation in Figure 5.3d for the phenyl surface. However, in a few cases (Figure 5.3l where $\theta_i \sim 29^\circ$) the rims become more unstable and consequently form fingers which decay into droplets. These fingers are larger in size than the instabilities at 140 °C. For the second batch such instabilities are less frequent and the situation looks more like that in Figure 5.3d,h.

Although the chemical structure of LCP94 is rather different from that of LCP-C9, its dewetting patterns are very similar. We discuss only unmodified substrates.

LCP94 on bare silicon: Thin films (10 – 500 nm) of this material on silicon substrates get corrugated above T_g and no layering parallel to the substrate surface could be detected in the mesophase. This is comparable with the LCP-C9 films on the chemically modified wafers.

In time, holes nucleate and grow. Depending on the temperature, either small droplets are left behind due to rim instabilities (below 120 °C), or numerous new holes are formed (above 120 °C). Both cases are depicted in Figure 5.4 (a and b). These dewetting patterns were found consistently, appearing both when the samples were annealed on a hot stage and in the oven. In the dry patches an ultrathin remaining polymer layer of about 2 – 4 nm in thickness could be detected by scratching with the AFM tip and analysing this scratched area afterwards. This result indicates autophobic behaviour and explains the rather low polymer contact angle as measured from the dewetted films (section 5.3.1).

Above T_i , the LCP94 dewetting behaviour is a 'normal' nucleation-and-growth-of-circular-holes (Figure 5.4c), comparable to the situation of traditional polymers like polystyrene. The rims are rather stable at this temperature.

When the holes, which were initially formed in the isotropic phase, were imaged during an additional annealing in the mesophase, no further growth was observed. New holes (of the same type as depicted in Figure 5.4a and b) could be observed, however.

When we compare the LCP94 dewetting behaviour on silicon with the dewetting behaviour of LCP-C9 on the chemically modified wafers, we see clear similarities. With increasing temperature, we seem to encounter three different regimes:

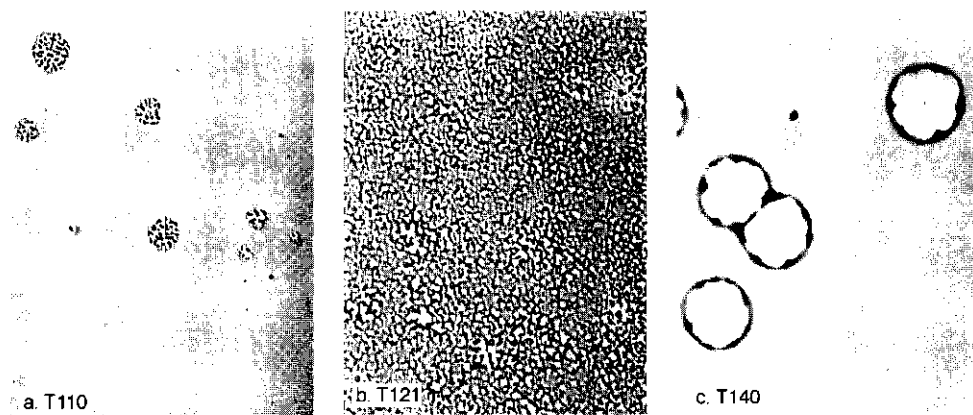


Figure 5.4: Optical micrographs ($125 \times 162 \mu\text{m}^2$) at different stages of dewetting of about 30 nm thick LCP94 films on silicon. (Indications as in Figure 5.3).

(a) the rims around the dry patches are very unstable and decay into very tiny droplets (at 'low' temperatures in the mesophase), (b) (numerous) new holes appear in the film which rapidly disintegrate the entire film without a significant growth of the holes (at higher temperatures in the mesophase), and (c) 'normal' nucleation and growth with rather stable rims (in the isotropic phase). This is a peculiar temperature dependence.

With respect to the instabilities, several explanations may be suggested:

- (i) the presence of gradients in the surface tension, induced by a temperature gradient and resulting in a Marangoni effect¹⁴,
- (ii) order–disorder transitions and/or heterogeneities of the coating¹⁵,
- (iii) surface ordering phenomena due to the polymer–substrate interactions, and
- (iv) hydrodynamic instabilities originating from the rheological properties of the polymers.

We have some indications that we can exclude (i) and (ii). Since the dewetting behaviour is independent of the kind of heating set-up, i.e. on a hot stage or in an oven, we can exclude a spreading process which is driven by a gradient in temperature. A temperature gradient will induce a gradient in surface tension, which is different for both heating devices and consequently will result in a different dewetting pattern. Since this is not the case we exclude explanation (i). Moreover, the films are extremely thin, which indeed makes it unlikely that significant temperature gradients will develop.

We also exclude order–disorder transitions (ii) in the coating layer as a reason for the instabilities, since the special characteristics upon increasing temperature (rim instabilities followed by the formation of numerous new holes) are present in systems on modified as well as on unmodified wafers. This is an indication that the modification is not the cause of this process. Furthermore, upon changing the temperature the polymer contact angle on the different wafers does not change significantly, again indicating a stable coating surface.

As there are clear similarities between the different LCPs it is most likely that the patterns have something to do with the properties of LCP-materials, so that explanation (iii) or (iv) are more likely.

In the literature information about dewetting of liquid-crystalline material is scarce. We reported autophobic behaviour in LCP films on silicon⁴, and Vix et al.¹⁶ found similar behaviour in thin films of main-chain liquid-crystalline polyesters. Herminghaus et al.¹⁷ investigated the dewetting morphology of thin films of a (low-molar-mass) liquid crystal (tris-trimethylsiloxy-silane-ethoxy-cyanobiphenyl) on silicon and these authors claim that both nucleation and spinodal dewetting occur in these films.

More is known about dewetting in systems without LC properties^{7,13,18-24}. Rim instabilities are found, but not frequently⁷. The instabilities as described by Reiter⁷ are for polystyrene films on octadecyltrichlorosilane (OTS) layers. The films break up and holes appear which grow upon heating the sample above its glass transition temperature. The rims around the holes are unstable and fingering instabilities are present. At higher molar mass of the polystyrene, i.e. higher viscosity and more entanglements of the polymer molecules, the fingers are more stable, which finally results in the formation of larger droplets.

In our laboratory, Maas²⁵ also found fingers for high-molar-mass polystyrene ($M_n = 3 \cdot 10^6$ g/mol) films on silica. These fingers remained present with increasing temperature, even though the dewetting velocity increased.

Our polymers have relatively low molar masses; LCP94 has a higher M_w than LCP-C9. Extrapolating from the findings of Reiter⁷ we would expect the length of the fingers to be different, which is, however, not what we observe. Furthermore, we observe the fingering to become less with increasing temperature, which is different from the findings of Maas described above.

Although the dewetting patterns are comparable for both side-chain liquid-crystalline polymers on the different substrates, they differ from the mesophase dewetting behaviour of LCP-C9 on silicon, as reported recently⁴. In the latter case a single crystal is present which consists of smectic layers parallel to the substrate. This layering makes the film more stable and leads to autophobic behaviour. In the present experiments, polycrystalline domains are present in the mesophase.

When, during dewetting, a hole is formed and a rim recedes, these polycrystalline LC-domains have to flow. Such flow cannot occur without deformation of LC domains, and probably leads to their break-up and rearrangement. The ease with which this occurs must depend on the effective local viscosity in the film, which is determined by the size and the orientation of the domains with respect to the direction of the flow of the rim. For example, for mesogens oriented in the flow direction, i.e. flow perpendicularly to the ordered layers, one can imagine that the flow is more difficult than for an mesogen alignment perpendicularly to the flow direction. Shear may align the mesogens, however, and therefore LCPs are likely to be

shear-thinning. Small differences in velocity along the receding rim are then amplified, leading to fingerings just like we find both for LCP-C9 and LCP94.

With increasing temperature the viscosity becomes less dependent on orientation and shear, and, as a result, there is less fingering. This is indeed what we observe. Also, at higher T the overall viscosity decreases, so that the growth rate increases. This explanation is also consistent with the findings of Maas described above²⁵, since in our case the fingering becomes less pronounced upon increasing the temperature, whereas in his case of isotropic viscosity the fingering remained.

Further evidence for the scenario proposed above is that the holes which were initially formed in the isotropic phase (in the LCP94 films), did not grow any further in the mesophase. We expect that due to the big size of the rims formed in the isotropic phase, large LC-domains will appear in these rims at temperatures in the mesophase, since locally the film thickness is larger. Such large domains are less easily deformed under a shear stress, and may even behave elastically at low stress.

Between the different substrates we find not only differences in dewetting velocity, as described above, but also in droplet formation. Because the (macroscopic) contact angles for LCP-C9 on the different substrates are so similar, one wonders whether microscopic polymer-surface interactions play a role in this droplet formation. For the various substrates the interaction at the polymer-substrate surface may perhaps cause differences in domain formation, leading to differences in size and orientation of domains. Again, this will influence the dynamics of the dewetting.

Above the isotropisation temperature the LCPs are in an isotropic liquid state with a low viscosity. No LC domains are then present and the rims, with liquid material from the dry patches, recede very fast. Yet, even though there are no domains in the rims, they are not always perfectly circular and sometimes fingering is seen (LCP-C9). This fingering above T_i is most clearly visible for the carbomethoxy surface with $\theta_i \sim 29^\circ$ (Figure 5.31). This system has a high rim velocity, a condition which is also expected to be responsible for instabilities of a moving rim⁷. Although the contact angles only slightly differ in the other cases, the rims show less instabilities. Apparently, the contact angle is very critical in causing unstable rims.

5.4 Conclusions

By tuning the interactions between a thin liquid-crystalline polymer film and a solid substrate the stability of such a film against break-up changes, as well as the ordering behaviour. In the case of LCP-C9, uniform films cannot be prepared on very hydrophobic wafers ($-methyl$ and $-allyl$ terminated). Films on the modified phenyl, chloride and carbomethoxy wafers are less stable than those on unmodified silicon wafers, which is ascribed

to the absence of smectic layers in the LCP-film parallel to the substrate. Therefore, the dewetting pattern was also different.

A similar dewetting behaviour as found for LCP-C9 on modified wafers was also found for the other side-chain liquid-crystalline polymer LCP94 on unmodified silicon wafers upon annealing. At low temperatures in the mesophase, holes are surrounded by unstable rims and consequently many tiny droplets are left behind in the dry patch as the rim recedes. Upon increasing the temperature, the number of nucleations increases, and the rim instabilities decrease.

These findings are ascribed to hydrodynamic instabilities which arise from the fact that the ease of deformation of domains in polycrystalline LC material under shear depends on domain size and orientation. Hence, in the mesophase the local effective viscosity depends strongly on shear and history, and is lowered under shear. This effect tends to amplify the velocity differences and leads to fingering. We conjecture that this is a general trend for side-chain LCPs.

Acknowledgements

We acknowledge R.P. Nieuwhof for providing us with LCP-C9, A. Elyousfi and W.H. de Jeu for useful discussions and SENTER IOP-verf for financial support.

References

- 1) van der Wielen, M. W. J.; Cohen Stuart, M. A.; Fleer, G. J.; de Boer, D. K. G.; Leenaers, A. J. G.; Nieuwhof, R. P.; Marcelis, A. T. M.; Sudhölter, E. J. R. *Langmuir* **1997**, *13*, 4762.
- 2) Gähde, J.; Mix, R.; Goering, H.; Schulz, G.; Funke, W.; Hermann, U. *J. Adhesion Sci. Technol.* **1997**, *11*(6), 861.
- 3) Thery, S.; Jacquet, D.; Mantel, M. *J. Adhesion* **1996**, *56*, 15.
- 4) van der Wielen, M. W. J.; Cohen Stuart, M. A.; Fleer, G. J. *Langmuir* **1998**, *14*(24), 7065.
- 5) Abbott, N. L. *Current Opinion in Colloid & Interface Science* **1997**, *2*, 76.
- 6) Barmentlo, M.; Hoekstra, F. R.; Willard, N. P.; Hollering, R. W. J. *Physical Review A* **1991**, *43*(10), 5740.
- 7) Reiter, G. *Langmuir* **1993**, *9*, 1344.
- 8) Sharma, A.; Reiter, G. *Journal of Colloid and Interface Science* **1996**, *178*, 383.
- 9) Bain, C. D.; Troughton, E. B.; Tao, Y.-T.; Evall, J.; Whitesides, G. M.; Nuzzo, R. G. *J. Am. Chem. Soc.* **1989**, *111*, 321.
- 10) Dubois, L.; Zegarski, B. R.; Nuzzo, R. G. *J. Am. Chem. Soc.* **1990**, *112*, 570.
- 11) Nieuwhof, R. P.; Marcelis, A. T. M.; Sudhölter, E. J. R.; Picken, S. J.; de Jeu, W. H. *Macromolecules* **1999**, *32*, 1398.

- 12)van der Wielen, M. W. J.; Cohen Stuart, M. A.; Fleer, G. J.; Schlattmann, A. R.; de Boer, D. K. *G. Phys. Rev. E* **1999**, in press.
- 13)Redon, C.; Brochard-Wyart, F.; Rondelez, F. *Physical Review Letters* **1991**, 66(6), 715.
- 14)Cazabat, A. M.; Heslot, F.; Troian, S. M.; Carles, P. *Nature* **1990**, 346, 824.
- 15)Ulman, A. *Thin films: Self-assembled monolayers of thiols*; Academic Press, Boston, 1998, p.149.
- 16)Vix, A.; Stocker, W.; Rabe, J. P.; Müller-Buschbaum; Stamm, M. *Conference Proceedings: Workshop on Wetting and Self-Organization in Thin Liquid Films* Munich, 1998.
- 17)Herminghaus, S., Jacobs, K., Mecke, K., Bischof, J., Fery, A., Ibn-Elhaj, M., Schlagowski, S. *Science* **1998**, 282, 916.
- 18)Brochard, F.; Redon, C.; Rondelez, F. *C.R. Acad. Sci. Paris II* **1988**, 306, 1143.
- 19)Henn, G.; Bucknall, D. G.; Stamm, M.; Vanhoorne, P.; Jérôme, R. *Macromolecules* **1996**, 29, 4305.
- 20)Jacobs, K.; Herminghaus, S.; Mecke, K. R. *Langmuir* **1998**, 14, 965.
- 21)Khanna, R.; Sharma, A. *Journal of Colloid and Interface Science* **1997**, 195, 42.
- 22)Redon, C.; Brzoska, J. B.; Brochard-Wyart, F. *Macromolecules* **1994**, 27, 468.
- 23)Reiter, G.; Auroy, P.; Auvray, L. *Macromolecules* **1996**, 29, 2150.
- 24)Stange, T. G.; Evans, D. F.; Hendrickson, W. A. *Langmuir* **1997**, 13, 4459.
- 25)Maas, J. H. *Unpublished results*.

Chapter 6

Controlled nanometer-scale surface roughening and its effect on the ordering and stability of liquid-crystalline polymer films[†]

Abstract

A silicon surface was roughened by adsorbing colloidal silica particles onto a preadsorbed positively charged polyelectrolyte. By changing the radius of particles and the particle density the degree of roughness can be tuned. The effect of this nanometer-scale roughness on the stability and ordering of thin films of side-chain liquid-crystalline polymers has been investigated. On smooth silicon substrates the films show layering behaviour and autophobicity above T_g . On roughened substrates this does no longer occur. The initially smooth films get rough above T_g by the formation of random polycrystalline domains which, in time, grow in size and decrease in number (Ostwald ripening). Above T_i the domains coalesce as an effect of the surface tension and the liquid film remains then stable. Decreasing the density of silica particles at the surface results not only in the formation of crystal domains in the film, but also in layered structures, which however, disappear in time and eventually only big crystals remain. Hence, just a few rough silica patches (5 % coverage) are enough to suppress the layering behaviour.

[†] Based on: M.W.J. van der Wielen, M.A. Cohen Stuart, G.J. Fleer, *Advanced Materials*, **1999**, 11, p. 918-923.

6.1 Introduction

Thin polymer films are of great importance in many fields like polymer electronics, data storage, display devices, adhesives and non-linear optical devices. An important aspect in these technologies is the surface roughness. Sometimes, surface roughness is necessary or preferred, like in liquid-crystal display devices, where the surface patterning can induce a certain liquid-crystalline alignment^{1,2}. However, in other applications, like coatings on optical surfaces, supermirrors, and waveguides, the purpose is to prepare uniform high quality films. When the substrate is rough its roughness can propagate to the rest of the film. For simple liquid films the roughness, induced by the substrate, is strongly damped. However, for thin polymer films the decay length of the surface modulation is much longer^{3,4}. Clearly, surface roughness is a very important parameter in surface science. Especially a controllable roughening on the molecular level is of great interest in, e.g., nanotechnology, surface ordering, LC displays, and wetting processes^{1,2,5,6}.

Rough substrates can be produced by rubbing, polishing, oblique evaporation, ion-beam etching, or by the formation of surface gratings. An attractive alternative is to make use of colloids since the size and deposition density of colloidal particles can be well controlled. In this paper we describe a new method whereby silica particles are first adsorbed onto a smooth surface and sintered afterwards, leaving behind a roughened surface. This procedure is described in the Experimental section.

We will also focus on the effect of nanoscale surface roughness on the ordering and film stability of liquid-crystalline polymers films. In bulk, LCPs show ordering upon annealing above the glass transition temperature. By spin-coating polymer films from solution on substrates one can obtain thin uniform films of liquid-crystalline polymers in which ordering can also be induced⁷⁻¹⁰. For LCPs with methoxy biphenyl as the mesogenic group in the side chains and maleic acid anhydride moieties in the backbone (Figure 6.1), the ordering as well as the (de)wetting behaviour have already been studied in thin films on smooth silicon substrates^{10,11}. Upon annealing the mesogenic groups become oriented perpendicularly to the surface. The mesophase nucleates at the substrate surface and grows further in the direction of the polymer-air interface until all of the polymer is taken up in a single crystal¹². In many practical cases, however, the substrates are not as smooth as the silicon wafers used in model studies (roughness within 1 nm). Therefore it is relevant to investigate what effect surface roughness has on the ordering.

For liquid crystals it is known that an appropriate substrate topography can induce a uniform LC alignment^{1,2}. It is quite possible that a certain ordering which is present near the surface is damped further away from the surface. So far, it is unknown whether a patterned substrate does affect smectic layering throughout LC polymer films, or whether only the first few layers near the substrate are distorted. Most probably, the behaviour will depend on the degree of roughness (both with respect to height differences and lateral topography). Since the

crystals nucleate from the substrate, it is conceivable that the layering found for LCPs on smooth substrates is lost when rough substrates are used.

Moreover, it has been found that upon annealing thin liquid-crystalline polymer films on smooth silicon wafers in the isotropic phase the polymer films retract, leaving a single stable LCP-bilayer behind¹¹. We therefore investigate also to what extent surface roughness influences this process.

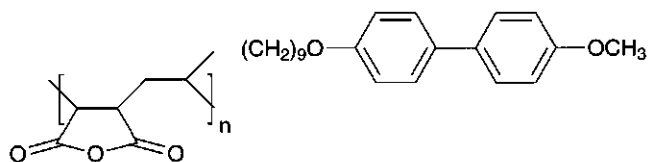
6.2 Experimental

6.2.1 Preparation of rough surfaces

In order to obtain a rough surface, silicon wafers are modified by adsorbing nano-sized silica particles onto them. The size of these particles in dispersion was determined using an ALV dynamic light scattering apparatus equipped with a 35 mW He-Ne Laser (wavelength 632.8 nm). The cleaning procedure of the substrates (Wacker Chemitronics) involves five steps: (i) ultrasonic cleaning for 5 min in demineralised water, (ii) ultrasonic cleaning for 5 min in chloroform, (iii) ultrasonic cleaning for 5 min in demineralised water, (iv) drying in a nitrogen flow, and (v) plasma treatment (Harrick Plasmacleaner/sterilizer PDC-32G) for 2 minutes. This cleaning procedure results in hydrophilic substrates with a water/air contact angle of less than 10°.

The surface modification proceeds as follows: (i) first a quaternary ammonium substituted hydroxyethyl cellulose (QNHEC) with average molar mass of 360 kg·mol⁻¹ (AKZO-Nobel Arnhem) is adsorbed from solution (100 mg·l⁻¹, 0.1 M NaCl, pH = 10) on the silicon wafer for 30 min., (ii) rinsing with demineralised water, (iii) adsorption of negatively charged uniform spheres of silica of different sizes (LUDOX grades HS-40, SM-30 and TM-50, Aldrich Chemical Company, Inc.; the numbers indicate the silica wt% in the original purchased colloidal dispersions) from a dilute suspension (100 mg·l⁻¹, 0.05 M NaCl, pH = 7), and (iv) rinsing successively with demineralised water and acetone. Finally the samples are sintered at 1000 °C for 5 – 10 min. In this way the polymer is burnt away and we end up with a pure silica surface with the same chemical structure as the smooth silicon substrate which has a native oxide layer. After the cleaning procedure the new surface is again found to be hydrophilic ($\theta_{\text{H}_2\text{O}} < 10^\circ$).

The adsorption of QNHEC on silica has recently been studied by Hoogendam et al.¹³. From those results we have chosen our experimental parameters such that we can expect a sufficient adsorption of the polymer on the substrate. Similarly, the conditions for the silica adsorption were taken from Böhmer^{14,15}. By rinsing with water and acetone, respectively, we tried to prevent the deposition of salt at the surface and silica particle aggregation as much as possible.



LCP-C9: $T_g = 99^\circ\text{C}$, $T_{SB \rightarrow SAd} = 112^\circ\text{C}$, $T_{SAd \rightarrow I} = 164^\circ\text{C}$

Figure 6.1: Repeating unit of the used liquid-crystalline polymer and its phase behaviour.

6.2.2 Surface and film characterisation

Ellipsometry (Sentech ellipsometer model SE400, with a rotating analyser) was used to determine the thickness of the QNHEC film. The topography of this film was imaged using a Nanoscope III atomic force microscope, AFM, (Digital Instruments, Santa Barbara, CA). Both contact mode (CM-AFM) (silicon nitride cantilevers with a spring constant of about 0.58 N/m) as well as tapping mode (TM-AFM) (silicon cantilevers with a resonance frequency about 350 – 380 kHz) were used. AFM was also used to study the topography and surface roughness of the (sintered) silica particle layer.

LCP films were prepared by spin-coating from 1,2-dichloroethane. The repeating unit of the LCP used, as well as its phase behaviour, is given in Figure 6.1. The synthesis and characterisation of the phase behaviour has been described by Nieuwhof et al.¹⁶

Also here, the topography was measured by AFM. However, for rough surfaces it is impossible to measure the LCP film thickness accurately by ellipsometry. Therefore, test films of the LCP were spin-coated also onto smooth silicon wafers to determine the film thickness. The phase behaviour and stability of the LCP films were investigated by optical microscopy (Olympus BX60 equipped with a hot-stage and crossed polarisers).

6.3 Results and discussion

Atomic force microscopy (AFM) is used to determine the substrate surface roughness and to investigate the changes in surface topography of the polymer film upon annealing. Also for rough surfaces, we expect that upon annealing at temperatures where the mesophase is stable the polymer will begin to order (starting from the substrate surface) and after a sufficient time the front of the ordered phase will reach the polymer–air interface. Such behaviour was found before for smooth substrates¹². The surface topography of the polymer surface is a reliable indicator for the ordering in the film, i.e., for whether or not layering is present.

6.3.1 Substrate roughening

In order to obtain a rough surface, silicon wafers are modified by adsorbing nano-sized silica particles of different sizes onto them. The deposition of these particles is achieved by first adsorbing a positively charged polyelectrolyte, a quaternary ammonium substituted hydroxyethyl cellulose (QNHEC). This polymer then acts as a bridge between the silicon substrate and the colloidal particles (LUDOX HS-40, SM-30 and TM-50). A similar method was used by Böhmer for adsorbing silica spheres on polymer pre-treated silica wafers^{14,15}.

After 30 min of adsorption the QNHEC layer was dried and characterised. The thickness is always about 2 nm and the surface topography is very smooth, with a roughness less than 1 nm. The AFM-image (contact mode) of the deposited silica particles is very streaky (Figure 6.2a). This is due to the fact that the particles are moved by the tip. After sintering at 1000 °C for several minutes such displacements do not appear anymore (Figure 6.2b,c), even when a high force is applied on a small area. This indicates that the particles are really well fixed. Heating at temperatures of 600 and 800 °C was not sufficient to immobilise the particles and the image remained the same as for the unheated samples.

The AFM-image for HS silica as depicted in Figure 6.2c is about the same as for SM silica. Therefore, the latter one is not shown. Furthermore, it is clear from the black-white contrast in Figure 6.2b and c and the values in Table 6.1 that the differences in height in the TM samples are bigger than the ones in the HS and SM samples. This is as expected.

Due to the friction of the tip (in the contact mode) at the particles and the geometry of the tip (contact and tapping mode), the lateral dimensions of the features (silica particles) will be significantly broadened. In the example given in Figure 6.2c this is quite clear. The structures seem to be rectangular, about 300 × 100 nm, in the scan direction. This convolution results from the fact that the particles are smaller than the dimensions of the AFM tip radius. This also affects the information obtained for the height differences, depending on the surface occupation of the particles and the dimensions of the tip, e.g., whether or not the tip can reach the bottom in between two particles. To correctly determine the height H of the silica patches after sintering, single particles were studied (Table 6.1). This was achieved by lowering the particle density in the silica suspensions (see also Figure 6.5a and Table 6.3). In Table 6.1 also the original radii of the silica particles in solution, as measured by Dynamic Light Scattering (DLS) are presented.

The value H as measured by AFM is expected to correspond to the diameter ($2r$) of the sintered particle. When we compare these values with the ones as measured by DLS, it is clear that in the case of SM and TM particles H and $2r$ do not correspond H is smaller than $2r$. This could be caused by the following effects. First, it might be that the particles melt somewhat during sintering which will result in smaller H -values. Second, the DLS results might be biased by polydispersity effects, because big particles dominate the light-scattering results. Hence, the values as measured by DLS are expected to be larger than those determined by AFM. In case of

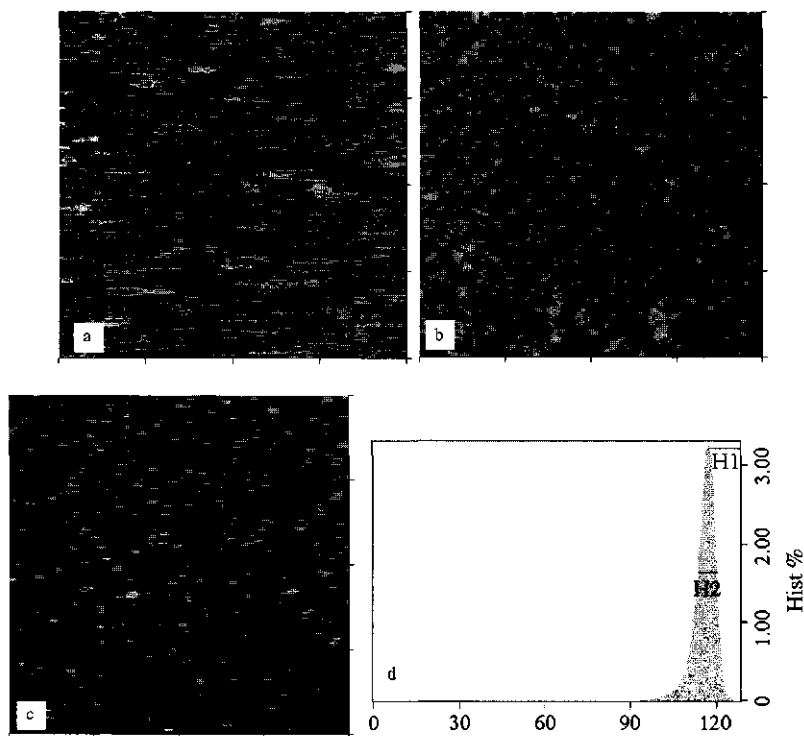


Figure 6.2: Topography of silicon surfaces modified with LUDOX silica particles (TM and HS), adsorbed from 100 mg.l^{-1} suspensions, as measured by AFM: **a)** directly after particle adsorption (TM), **b)** after sintering for 10 min at 1000°C (TM), **c)** as **b)** but now for HS, and, **d)** bearing analysis of **c)** (all images $10 \times 10 \mu\text{m}^2$, and black-white contrast 30 nm).

HS particles this effect is less pronounced as compared to SM and TM. The reason is not clear. Anyway, the height as measured by AFM reflects the outcome of the sintering process.

The height differences in the topography as found in the case of adsorption from concentrated (100 mg.l^{-1}) silica suspensions give us an indication of the surface roughness. Of course one should keep in mind the influence of the tip geometry. Two height values are obtained from the bearing analysis as depicted in Figure 6.2d. Height value *H1* indicates the height which is most frequently found in the sample. Due to the tip geometry the particles in the image are enlarged laterally. Hence, the value *H1* should correspond to the diameter of the particle. *H2* is the peak width (at half height) which gives an indication for the distribution around *H1*. The results for each silica specimen are quite reproducible within one silica batch or measurement. In case of HS also a second batch of substrates was prepared and measured. Between the different batches there are slight differences (several nanometers), which could be most probably due to a difference in surface occupation of the particles. As a result the tip

Table 6.1: Dimensions of the various silica particles as measured by dynamic light scattering and atomic force microscopy. Symbols are explained in the text.

SiO ₂ particle	DLS	AFM	Bearing Analysis	
	r (nm)	H (nm)	$H1$ (nm)	$H2$ (nm)
HS40	8 ± 1	15 ± 2	8 ± 1	6 ± 1
			$11 \pm 2^*$	$9 \pm 1^*$
SM30	14 ± 1	10 ± 2	7 ± 2	6 ± 2
TM50	20 ± 1	22 ± 2	18 ± 3	15 ± 4

* As measured for a second batch.

Table 6.2: $H1$ -values for as-prepared (as-p.) films and after annealing (ann.) at 140 °C. The silica thickness H is 15 nm (HS) and 22 nm (TM).

d (nm)	$H1$ -HS (nm)		$H1$ -TM (nm)	
	as-p.	ann.	as-p.	ann.
10	~5	~6	~10	~14
25	~3	~3	~7	~6
45	~1	~5	~5	~7
90	~1	~12	~3	~9

cannot always reach the bottom of the substrate due to its geometry. At any rate, from the bearing results as given in Table 6.1 the main conclusion is that the particles are adsorbed as a (sub-) monolayer, and that clusters are absent. In the presence of clusters, one would expect $H1$ and $H2$ to be bigger than actually found. The fact that $H1$ is somewhat smaller than H may be due to the impossibility for the tip to reach the surface in between two attached particles in close proximity.

6.3.2 Liquid-crystalline polymer films

When the LCP solution is spin-coated on the roughened substrates the topography varies with the film thickness, i.e. the polymer concentration in the spin-coating process. The various film thicknesses, d , as found for smooth test wafers, are around 10, 25, 45, and 90 nm, respectively. For each film thickness the $H1$ -value is given in Table 6.2 for the as-prepared films on HS- and TM-modified surfaces. With increasing film thickness the surface roughness

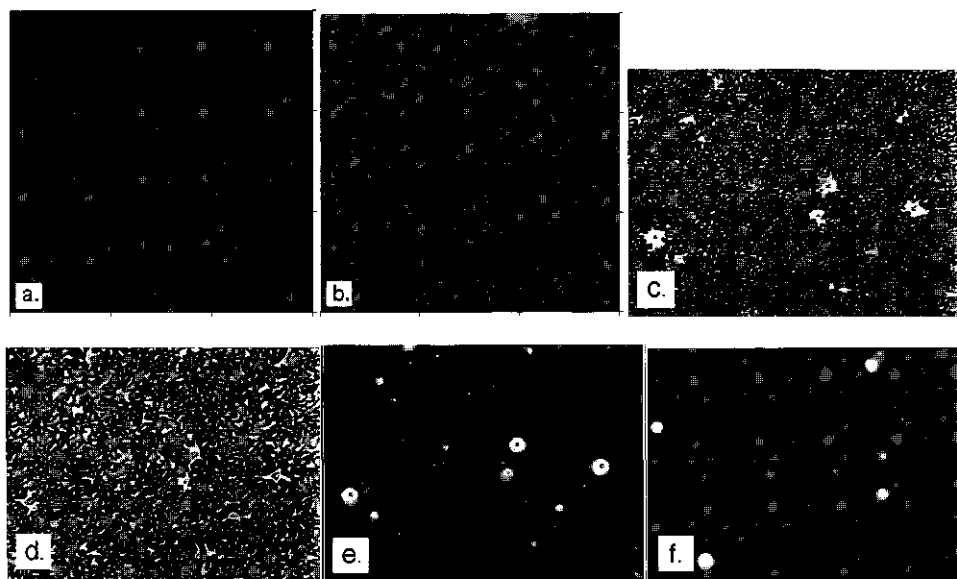


Figure 6.3: The various annealing steps of an about 70 nm thick LCP-C9 film on a SM-roughened silica surface ($H = 10$ nm). Figures a and b are AFM-images ($30 \times 30 \mu\text{m}^2$, b/w-contrast 30 nm) for the as-prepared film (a) and after annealing for 5 min at 140°C (b). The other pictures are optical micrographs ($159 \times 125 \mu\text{m}^2$) after further annealing the sample of diagram b. Pictures c and d show results for annealing at 160°C for 30 s (c) and 10 min (d), respectively, and diagram e for further annealing up to 190°C for 10 min. Situation f corresponds to a film which (starting from a) was directly annealed at 190°C for 5 min.

first becomes less (10 and 25 nm) and then the surface becomes completely smooth (45 and 90 nm). Probably, first the regions in between the silica particles are filled or partly filled: as long as the film is thin, it will follow the surface topography. With increasing film thickness a smooth film is formed on top of the silica.

When these films are annealed in the mesophase at 140°C , the topography changes in some cases. The HI -values measured for the annealed films are also given in Table 6.2. For very thin films ($d < H$) annealing in the mesophase hardly has any effect on the topography (Table 6.2). However, for the films with $d > H$ the surface becomes corrugated when annealed in the mesophase. This is especially clear in case of 45 and 90 nm thick films on HS-silica (Table 6.2).

With increasing temperature from 140 to 160°C there is an increase in corrugation roughness. This process was followed by AFM and optical microscopy. In Figure 6.3a the topography, as measured by AFM, is given for an about 70-nm-thick film on top of SM-silica. It is clear that the surface is smooth. The topography for this film annealed at 140°C for 5 min

is depicted in Figure 6.3b. From previous experiments we know that this annealing step is sufficient to create stable layered structures in such films on smooth substrates^{11,12}. On the rough substrates it is clear that the polymer surface is roughened compared to the as-prepared film (Figure 6.3a); no layering is visible.

At higher temperatures, around 160 °C, random ordered domains become clearly visible by optical microscopy, also under crossed polarisers. We suggest that LC-domains nucleate at the rough substrate patches and grow upwards, thus producing a rough topography. In the course of time the structures increase in size (Figure 6.3c,d). This must be due to some Ostwald ripening process. Apparently the domains can easily grow at this temperature. This is probably due to a low viscosity of the material at that temperature¹¹. After 10 min of annealing at 160 °C, the dimensions of the domains reach values of order 5 μm (length) \times 3 μm (width) \times 120 nm (height), respectively. In between the polycrystalline structures a thin polymer layer of about 10 – 18 nm remains. In addition, the silica surface structures are more or less visible in this polymer film by AFM (not shown in the pictures of Figure 6.3).

A further increase in temperature to above the isotropisation temperature ($T_i = 165$ °C), results in coalescence of the different domains. This material is now in a fluid state and wets the substrate again (Figure 6.3e). In this isotropic phase, the surface tension becomes dominant which is in contrast to the situation in the mesophase where the material is more crystal-like, resulting in a textured surface. In some cases this annealing even resulted in the complete wetting of the substrate. When an as-prepared film is instantaneously heated-up to, e.g., 190 °C, the film also remains stable (Figure 6.3f), which is in agreement with the former result where the isotropic film wets the surface.

We studied also the wetting and/or ordering behaviour on slowly cooling down from the isotropic phase in the mesophase (10 °/min) to see whether a stable liquid film remains or whether crystalline domains appear. Under crossed polarisers bright spots appear, indicating the formation of randomly ordered crystal domains. These domains grow out into needle-shaped structures or so-called batonnets. In case of a 45 nm LCP film on HS-modified silica the dimensions are about 19 μm (length) \times 3 μm (width) \times 150 nm (height), respectively (Figure 6.4). These needles are longer than in case of heating up from the glass phase into the mesophase, namely 19 μm vs. 5 μm . In the latter case more crystallisation points will be present in the film as compared to the cooling down from the liquid. In bulk samples of LCs and/or LCPs such needle-structures are typical for the smectic A phase¹⁷. In bulk, where there is enough material, it is even possible for the batonnets to coalesce forming the so-called focal-conic fan-like textures. Due to the lack of material in thin films no such fan-like structures are formed.

In between the needle-like structures a thin polymer film remains. A square is visible in Figure 6.4, which was deliberately made with the AFM tip under a high load. It has a depth of

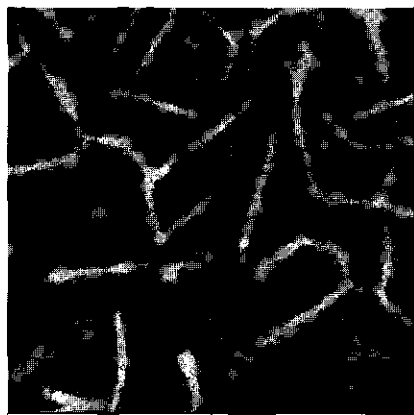


Figure 6.4: AFM-image ($50 \times 50 \mu\text{m}^2$) of needle-like structures in a initially 45 nm thick LCP-film on a HS-modified silica surface after cooling down from the isotropic phase. In the dark square near the centre of the picture a high force is applied to small area (b/w-contrast 250 nm).

Table 6.3: Silica surface coverage after adsorbing various silica suspensions.

SiO ₂ -particle	Coverage (%)		
	100 mg.l ⁻¹ SiO ₂	10 mg.l ⁻¹ SiO ₂	5 mg.l ⁻¹ SiO ₂
HS	~ 100	~ 40 – 50	~ 10 – 20
TM	~ 100	~ 12 – 17	~ 5 – 7

about 8 nm. Again, the silica surface structures are visible in the film (not shown). Concerning the wetting and/or ordering there is no dependence on the original silica particle size.

The experiments described so far are for full coverage by particles, obtained by the deposition from a 100 mg.l⁻¹ silica dispersion. Films which have been prepared on surfaces with a lower density of silica particles were also investigated. In this case only one film thickness (49 nm) and two silica particle specimens (HS and TM) were studied. The silica concentrations in the suspension were 5 and 10 mg.l⁻¹, respectively. In these situations the silica particles are separated from each other. An example of such a modified surface is given in Figure 6.5a. The surface coverage for the different surface modifications is given in Table 6.3.

After spin-coating, films of 49 nm thickness completely cover the rough silica patches. Upon annealing of these films, the ordering and stability behaviour do not seem to be different as compared to the complete surface coverage. Again, the polymer surface gets roughened when annealed at 140 °C for 30 min plus another 16 min at 150 °C. However, after annealing another 3 min at 160 °C layered structures become visible next to the larger polycrystalline

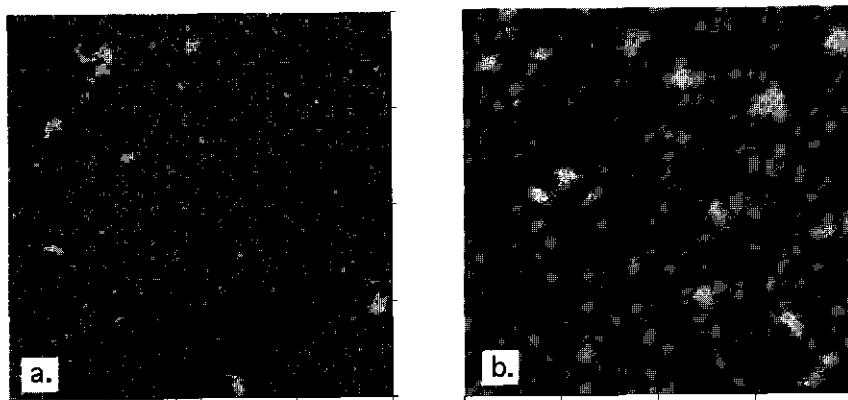


Figure 6.5: Surface topography of: **a)** a bare roughened silica surface (after adsorption of a $10 \text{ mg}\cdot\text{l}^{-1}$ HS-silica suspension), and **b)** of a 49 nm film on a) after annealing in the mesophase (3 min at 160°C) ($10 \times 10 \mu\text{m}^2$, b/w-contrast: 30 nm).

domains (Figure 6.5b). Similar results were obtained for the TM-modified surfaces. The layers have a spacing of about 3 nm which coincides with the thickness of interdigitated bilayers. In a previous study we showed that such layers correspond to a single crystal¹⁰.

After prolonged annealing the monocrystalline layered structures disappear and only large polycrystalline domains remain. Hence, even a minor roughening (5% surface coverage) of the surface suppresses the monocrystalline structure as found on a smooth silica wafer, and leads to a polycrystalline morphology as also found in bulk samples.

6.4 Conclusion

In conclusion, we introduced a new and easy way of controlled nanoscale surface roughening by adsorbing negatively charged colloidal silica particles (radii varying from 8 – 22 nm) onto a positively charged polyelectrolyte pre-adsorbed onto a silicon wafer. This results in a rough surface with the same chemical properties as for a native silica layer on silicon. In this way, model surfaces are obtained that can be advantageously used to investigate the effect of roughness on film formation. We compared thin LCP films on smooth and nano-rough substrates concerning their ordering behaviour and stability. In our case the roughness dimension ($H = 8 - 25 \text{ nm}$) is close to the size of an ordered bilayer, e.g., a bilayer has a 3 nm spacing. We can conclude that even if the wafer surface is only slightly modified by silica particles (5 % coverage) still the layering behaviour of the single crystal, as present on smooth wafers, cannot compete with the formation of random polycrystalline domains. On the other hand, such surface modification results also in an improved film stability against break-up.

Acknowledgement

The authors acknowledge SENTER IOP-verf for financial support of this project and R.P. Nieuwhof (Laboratory of Organic Chemistry, Wageningen University) for providing us with the polymer.

References

- 1) Cognard, J. *Molecular Crystals & Liquid Crystals Suppl. Ser.* **1982**, 1(1), 1.
- 2) Goodman, L. A.; McGinn, J. T.; Anderson, C. H.; Digeronimo, F. *IEEE Transactions on Electron Devices* **1977**, 24(7), 795.
- 3) Li, Z.; Tolan, M.; Höhr, T.; Kharas, D.; Qu, S.; Sokolov, J.; Rafailovich, M. H.; Lorenz, H.; Kotthaus, J. P.; Wang, J.; Sinha, S. K.; Gibaud, A. *Macromolecules* **1998**, 31, 1915.
- 4) Tolan, M.; Vacca, G.; Wang, J.; Sinha, S. K.; Li, Z.; Rafailovich, M. H.; Sokolov, J.; Gibaud, A.; Lorenz, H.; Kotthaus, J. P. *Physica B* **1996**, 221, 53.
- 5) Miller, J. D.; Veeranasuneni, S.; Drelich, J.; Yalamanchili, M. R.; Yamauchi, G. *Polymer Engineering and Science* **1996**, 36(14), 1849.
- 6) Busscher, H. J.; van Pelt, A. W. J.; de Boer, P.; de Jong, H. P.; Arends, J. *Colloids and Surfaces* **1984**, 9, 319.
- 7) Elben, H.; Strobl, G. *Macromolecules* **1993**, 26, 1013.
- 8) Mensinger, H.; Stamm, M.; Boeffel, C. J. *Chem. Phys.* **1992**, 96(4), 3183.
- 9) Henn, G.; Stamm, M.; Poths, H.; Rücker, M.; Rabe, J. P. *Physica B* **1996**, 221, 174.
- 10) van der Wielen, M. W. J.; Cohen Stuart, M. A.; FLeer, G. J.; de Boer, D. K. G.; Leenaers, A. J. G.; Nieuwhof, R. P.; Marcelis, A. T. M.; Sudhölter, E. J. R. *Langmuir* **1997**, 13, 4762.
- 11) van der Wielen, M. W. J.; Cohen Stuart, M. A.; FLeer, G. J. *Langmuir* **1998**, 14(24), 7065.
- 12) van der Wielen, M. W. J.; Cohen Stuart, M. A.; FLeer, G. J.; Schlattmann, A. R.; de Boer, D. K. G. *Phys. Rev. E.*, **1999**, accepted.
- 13) Hoogendam, C. W.; Derks, I.; de Keizer, A.; Cohen Stuart, M. A.; Bijsterbosch, B. H. *Colloids and Surfaces A* **1998**, 144, 245.
- 14) Böhmer, M. R. *Journal of Colloid and Interface Science* **1998**, 197, 251.
- 15) Böhmer, M. R.; van der Zeeuw, E. A.; Koper, G. J. M. *Journal of Colloid and Interface Science* **1998**, 197, 242.
- 16) Nieuwhof, R. P.; Marcelis, A. T. M.; Sudhölter, E. J. R.; Picken, S. J.; de Jeu, W. H. *Macromolecules*, **1999**, 32, 1398.
- 17) Chandrasekhar, S. *Liquid Crystals*; Cambridge University Press: Cambridge, 1992.

Chapter 7

Side-chain liquid-crystalline polymers in bulk and at surfaces[‡]

Abstract

In this chapter we will briefly compare bulk properties on several side-chain liquid-crystalline polymers, synthesised and characterised by R.P. Nieuwhof, with the behaviour in thin films. Also some tentative conclusions concerning the feasibility of the investigated polymers as a primer in the coating technology are drawn.

[‡] Partly based on: M.W.J. van der Wielen, R.P. Nieuwhof, M.A. Cohen Stuart, G.J. Fleer, A.T.M. Marcelis, E.J.R. Sudhölter, *Overview to be published*.

7.1 Introduction

We have seen in the previous chapters that side-chain liquid-crystalline polymers show very interesting characteristics in thin films. The results contribute to surface chemistry in general, and more specifically to ordered fluids and thin film behaviour.

Concerning possible applications of these materials one can think of several fields like nanotechnology, polymer electronics and so on. It goes beyond the scope of this thesis to elaborate on these applications. However, we do want to reflect on the application mentioned in Chapter 1, in which we proposed that LCPs might be suitable as a primer in the coating technology. Therefore, we will summarise some results obtained in bulk measurements, performed by R.P. Nieuwhof¹ in the Laboratory of Organic Chemistry at Wageningen University, and compare them with the properties found in thin films as reported in the present thesis.

7.2 Bulk behaviour versus thin films

The polymer which is mainly described in this thesis, named LCP-C9, is part of a set of side-chain liquid-crystalline polymers, the general molecular structure of which is depicted in Figure 7.1. Several different samples were synthesised by Nieuwhof² by alternating copolymerisation of maleic acid anhydride with 1-alkenes carrying biphenyl mesogens.

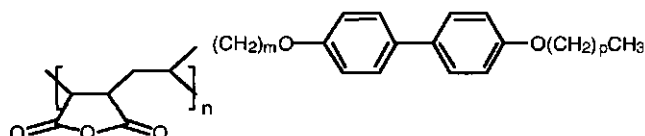


Figure 7.1: Molecular structure of the alternating copolymer of maleic acid anhydride and 1-olefins carrying biphenyl mesogens. The parameter n is the degree of polymerisation, m is the spacer length, and p determines the length of the end group.

7.2.1 Phase behaviour

The phase behaviour of the kind of polymers depicted in Figure 7.1, for varying length of the alkyl spacer (m) in the side chain and/or varying end group length (p), is given in Table 7.1.

The different smectic phases differ in the degree of crystallinity in the order $S_{Ad} + S_{Adt} < S_{Bhex} < S_{Bcryst} < S_E$. The side-chains of the polymers all interdigitate in the mesophase, most of the time with their mesogenic groups, but in some cases with terminal alkyl group overlap $(S_{Adt})^2$.

Table 7.1: Phase transition temperatures, phase types^a and d spacings (d_b in bulk and d_f in thin films) for several polymers with varying spacer length m and end group length p . (Bulk data from R.P. Nieuwhof et al.²)

Polymer (m,p)	Transition temperatures ^a (°C)	d_b spacings (nm)	d_f spacings (nm)
2,0	G 112 I	-	
3,0	G _{Bhex} 146 S _{Ad} 170 I	2.20	1.6 ± 0.2^b
4,0	G _{Bhex} 120 S _{Bhex} 128 S _{Ad} 136 I	2.39	2.5 ± 0.2
6,0	G _{Bhex} 129 S _{Bhex} 140 S _{Ad} 161 I	2.61	2.7 ± 0.1
8,0	G _{Bhex} 103 S _{Bhex} 117 S _{Ad} 156 I	3.01	
9,0	G _{Bhex} 99 S _{Bhex} 112 S _{Ad} 165 I	3.18	3.2 ± 0.2
9,2	G _{Bhex} 142 S _E 156 S _{Ad} 177 I	3.21	3.7 ± 0.2
8,3	G _E 147 S _E 159 S _{Ad} 181 I	3.27	3.4 ± 0.2
6,5	G _{Bhex} 118 S _{Ad/Ad} 163 I	4.30, 3.27	$3.6 \pm 0.5, 1.5 \pm 0.5$
4,7	G 117 S _{Adt} 187 I	4.50	1.5 ± 0.2^c
3,8	G 129 S _{Adt} 208 I	4.53	4.9 ± 0.2

^a G = glass phase; I = isotropic phase; S_{Ad,Adt} = smectic A phases with interdigitation of the mesogenic groups and end groups, respectively; S_{Bhex} = hexatic smectic B; S_{Bcryst} = crystal smectic B; S_E = smectic E.

^b Achieved from an ordered sub monolayer film (spin-coated from 0.05 wt%).

^c Ultrathin non-wettable film (Figure 7.3).

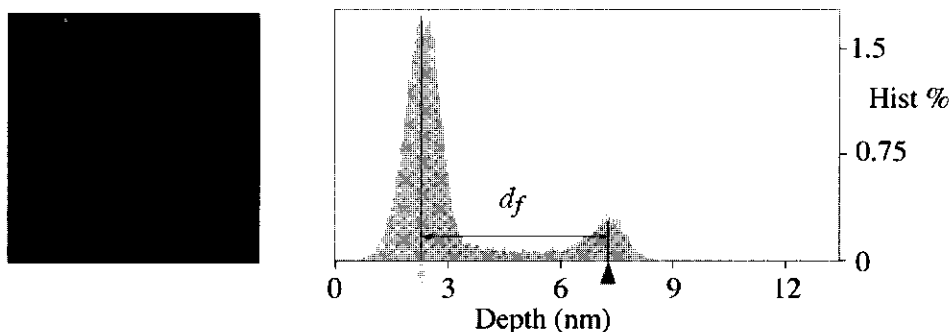


Figure 7.2: Surface topography of a 30 nm thick film of LCP(3,8) on a silicon wafer, annealed at 135 °C for 10 min as measured by AFM (left), and the corresponding bearing analysis from which d_f can be determined (right). The first peak corresponds to the height distribution of the gray areas, the second to that of the black spots. (black-white contrast = 25 nm).

The bulk spacings were measured by X-ray diffraction, whereas for thin films the spacing was determined from the top-layer structures as measured by AFM (Figure 7.2). This has been done in *ordered films* after annealing the films above the glass transition temperature. The procedure is already described in Chapter 2³. It is clear that the spacing values as measured in the top-layer of thin films correspond rather well to the spacings measured in the bulk material. Only in a few cases there is a small difference.

In the case of LCP(4,7) a rather low value for d_p , as compared to the bulk value, is found: 1.5 vs. 4.5 nm. This low value was obtained from a non-wettable ultrathin film (Figure 7.3). After the spin-coating process only this thin layer remained on the substrate. The circular holes in Figure 7.3 indicate that the layer already starts to dewet during the spin-coating process. Apparently, the first LCP layer adjacent to the silicon substrate has a structure different from that in bulk of the LC. The characteristics of this structure, cannot be determined from our data. Possibly, terminal methoxy groups on the mesogens attach to the silanol groups with hydrogen bonds, thus causing the mesogens to orient themselves parallel to the surface rather than in the normal direction. This orientation may be the reason for the autophobic behaviour.

We tried to remove this thin layer by scratching with the AFM tip. Usually after applying a high load to a thin polymer film the material will be removed from that area. This will then result in a black spot in the image, so that the contrast tells us something about the depth. However, in the case of LCP(4,7) it appeared impossible to completely remove the material. Instead of a black square only the two borderlines of the scratched area are visible. These two thin scratches, which are perpendicular to the scan direction, are visible in the center of Figure 7.3. Furthermore, the depth of the scratches is not 1.5 nm, as found for the other holes in the film, but only about 0.9 nm. Hence, the underlying substrate was not yet reached

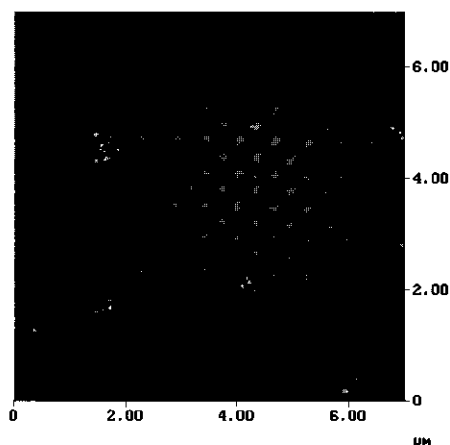


Figure 7.3: Surface topography of an as-prepared sub-monolayer film of LCP(4,7) on a silicon wafer. (black-white contrast = 10 nm).

by this scratching procedure. Both findings indicate that the mechanical properties of this material are different from, e.g., LCP-C9 which can be removed from the substrate.

Non-wetting behaviour was also found for a batch of LCP(6,5). However, when in this case the polymer material was dried for several weeks at 100 °C in a vacuum oven, a solution of this material could then be spin-coated with an improved film formation as a result. This extra drying did not help in case of LCP(4,7).

Drying normally produces condensation of the carboxylic groups to anhydride rings⁴. However, it is hard to believe that the non-wetting behaviour is a result of only the nature of these backbone moieties. It also seems very unlikely that surface active impurities, formed as side-products in the synthesis and which have not been washed out, would be present in the sample. Hence, this non-wetting result remains rather unclear.

Polymer LCP(6,5) exhibits two different mesophases in bulk which coexist, resulting in two different spacings (4.30 and 3.27 nm, respectively). These spacings result from side chain interdigitation with end-group overlap and total side chain overlap, respectively. Different spacings were also found in thin films, as shown in Table 7.1 and illustrated in Figure 7.4a and b. From the bearing analysis it becomes clear that the surface structures have a broad depth distribution. This makes it difficult to extract precise d_f -spacings. Since two kinds of interdigitation coexist, both will contribute to the surface structures, and to the structure of the film in general. This makes the broad depth distribution obvious. Schematically this is depicted in Figure 7.4c.

From all those polymers given in Table 7.1, we have chosen to study the thin film behaviour in particular for LCP(9,0) (which is denoted as LCP-C9 in this thesis), for several practical reasons;

- (i) it was one of the first polymers synthesised in this project with LC behaviour,
- (ii) it was available in sufficient quantities,
- (iii) its mesophase is wide enough to investigate films at different temperatures, and
- (iv) its phase behaviour seems to be suitable for application as a thermally removable primer layer in coatings.

7.2.2 Rheological behaviour

The complex viscosity η^* is defined as the ratio of the shear stress σ to the rate of shear strain $\dot{\gamma}$. In Figure 7.5 the modulus of the complex viscosity ($|\eta^*| = [(\eta')^2 + (\eta'')^2]^{1/2}$) of LCP-C9 is given as a function of temperature. It was measured between oscillating plates at different frequencies¹. In the experimental set-up the harmonic stress results in a harmonic strain of amplitude γ_0 which is proportional to the stress amplitude σ_0 and with a phase lag relative to the stress which is independent of amplitude⁵.

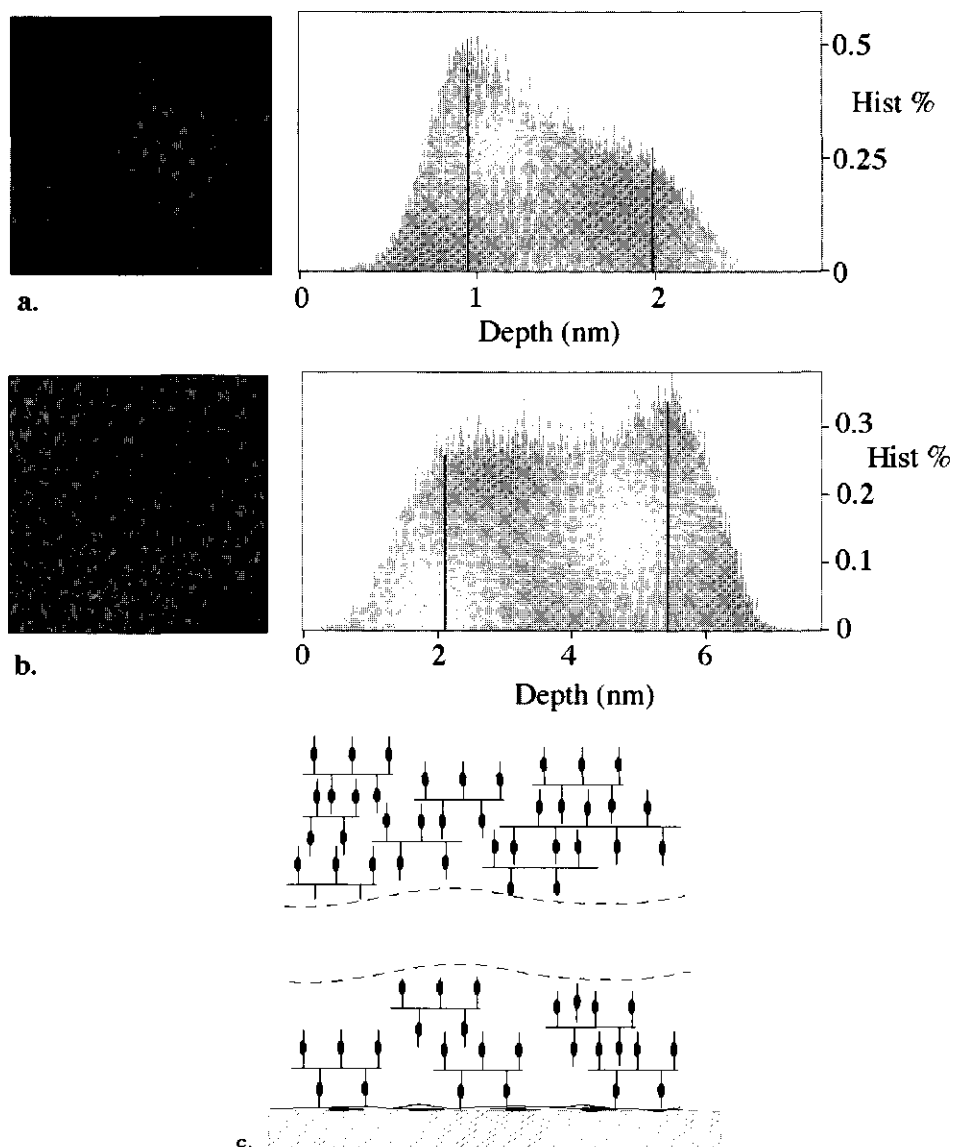


Figure 7.4: Surface topography and corresponding bearing analysis of a 30 nm-thick-film of LCP(6,5) on silicon (a) after annealing for 10 min at 124 °C, (b) after a further 1 min at 165 °C. The bottom diagram (c) gives a schematical representation of the surface structure with 2 coexisting d -spacings in the film. (black-white contrast = 10 nm).

The viscosity slowly drops over about 5 – 6 decades in the mesophase $99\text{ °C} < T < 165\text{ °C}$ and over about 2 decades near the isotropisation temperature $T_i = 165\text{ °C}$ (Figure 7.5). This corresponds to our conclusions from the dewetting experiments over a silicon wafer, described in Chapter 4⁶. In thin films we found a jump in the dewetting velocity around the isotropisation

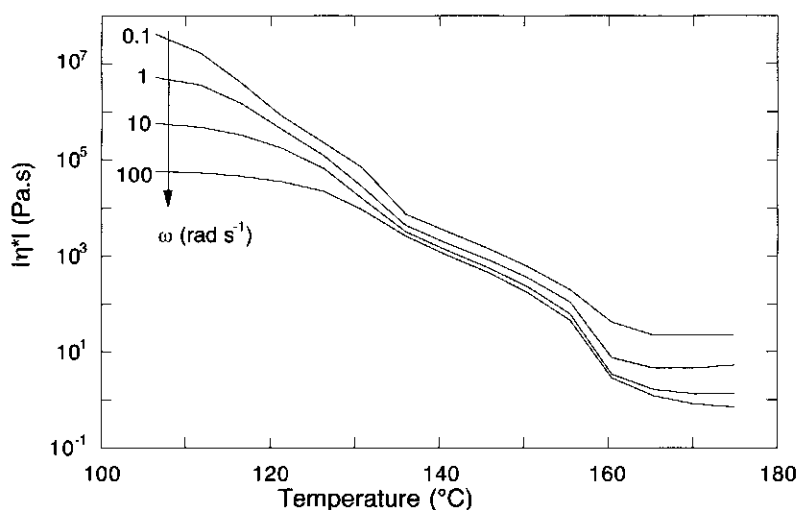


Figure 7.5: The modulus of the complex viscosity of LCP-C9 vs. temperature at various frequencies ω [data from R.P. Nieuwhof¹].

temperature, which we ascribed to the decrease in viscosity. Since the growth rate increased over more than 2 orders of magnitude we speculated that there was also a jump in viscosity of more than two orders of magnitude. This was corroborated by the dynamic oscillatory bulk measurements.

Nieuwhof et al.¹ also measured the storage and loss moduli for different angular frequencies (not shown here). From the frequency independence of the storage modulus at low frequencies, and the value of the resulting rubber plateau, they concluded that even above T_i physical crosslinks are present¹. Since the polymers are rather short, entanglements are not a likely cause of the rubber plateau, so that the mesogens presumably provide the crosslinks.

This behaviour also corresponds to the dewetting experiments described in Chapter 46: we found that in the isotropic phase the film breaks up and the receding polymer material shows a slip behaviour. Such slippage can only occur when the material deforms partly elastically on the relevant timescale and then moves like a solid. For classical polymers such behaviour is found at high molecular weights due to entanglements. In our case of LCP-C9 we do not believe that entanglements are responsible, since the polymer has a rather low molecular weight, but local physical interactions between the mesogens can lead to similar effects.

7.2.3 Variation in backbone architecture

Because of the expected influence of the maleic acid anhydride (MA) moieties in the backbone on the adhesion, also copolymers from maleic acid anhydride and mesogen-containing methacrylates with varying mole fractions of maleic acid anhydride were

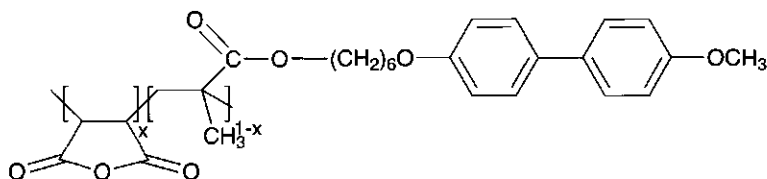


Figure 7.6: General molecular structure of the side-chain liquid-crystalline MA-methacrylate copolymers.

Table 7.2: Phase transition temperatures, phase types and d spacings (d_b in bulk and d_f in thin films) of copolymers depicted in Figure 7.6 (Bulk data from R.P. Nieuwhof et al.¹)

Polymer (x)	Transition temperatures (°C)	d_b spacings (nm)	d_f spacings (nm)
0.30	G _E - S _{EI} 146 I	2.84	
0.26	G _E 137 S _{EI} 146.5 I	2.64*	2.2 ± 0.2
0.20	G _E - S _{EI} 146 S _{AI} 148 I	2.70*	2.1 ± 0.2
0.12	G _E - S _{EI} 138 I	2.68*	2.5 ± 0.2
0	G _E 80 S _{EI} 119 S _{AI} 135 N 137 I	2.64	2.3 ± 0.2

* Based on second order reflection

synthesised¹, in order to see whether the maleic acid anhydride content influences the film properties. The molecular structure is depicted in Figure 7.6 and its phase behaviour is given in Table 7.2 together with the spacing as measured by X-ray diffraction in bulk¹ and as determined by AFM in thin films. In the films the measured spacings are slightly lower than the ones in bulk.

In all cases layers parallel to the surface are obtained by annealing the samples above the glass transition temperature, or just below T_i for those cases that T_g could not be measured (Table 7.2, $x = 0.30$, 0.20 and 0.12). Hence, even without maleic acid anhydride moieties in the backbone ($x = 0$), parallel layering to the substrate surface is achieved.

It might well be possible that the interaction between the ether groups in the side chain and the surface forces some of the side chains to orient themselves parallel to the surface, thereby inducing a certain ordering in the remainder of the molecule. In the case of LCP-C9 we have indications that the side chains in the first layer at the substrate lay flat on the surface as described in Chapter 2.

For a pure methacrylate backbone ($x = 0$), we annealed the sample for a relatively long period above T_g (in meso- and in isotropic phase) to see whether dewetting takes place. From optical microscopy and AFM we concluded that this is not the case: the films remain stable. We

ascribe this to the presence of more physical crosslinks than in LCP-C9, caused by the following properties: (i) the polymer has a much higher molecular weight (275000 vs. 5320 of LCP-C9), (ii) the mesogen density is twice as high (1 side chain per monomer unit vs. 1 side chain per 2 monomer units for LCP-C9), and (iii) for methacrylates it is known that the backbone is not strictly confined between mesogen layers and it shows layer hopping between the smectic layers^{7,8}, which results in a network rather than in a microphase separation of mesogens and backbones, as found for LCP-C9.

7.3 Feasibility of a paint removal concept with side-chain liquid-crystalline polymers as primer

As briefly described in Chapter 1, the background of this fundamental study was the potential use of thermotropic side-chain liquid-crystalline polymers as primer material. In this model study the attention was focussed on the properties of the polymeric material. The next step should be to extend the investigations to a real coating on top of the LCP-primer layer. Hence, at this stage firm conclusions about the feasibility of these polymers in the new paint removal method cannot be made. However, we can use our results to speculate on the possibility for application.

First of all, we succeeded in preparing stable thin films of various LCPs. The film stability against break-up depends strongly on the temperature⁶. Around the isotropisation temperature the films break up very quickly. This is caused by the sudden drop in viscosity, over two orders of magnitude, near this temperature and it makes these polymers suitable for use in thermal paint removal. Since the various polymers all possess different transition temperatures, we can choose the most convenient polymer on the basis of the desired temperature dependence.

In the mesophase the material forms smectic layers parallel to the substrate surface³. This ordering is achieved for a wide range of polymers. The polymers with a biphenyl as the mesogenic group and an ether as end group all exhibit this layering in the mesophase. We believe that the maleic acid anhydride moieties in the backbone and/or the ether groups in the side chains induce this layering. As shown by Gähde et al.⁹ and mentioned in Chapter 1, such ordered layers can act as corrosion protection.

Although the layered films in the mesophase are much more stable than in the isotropic regime, also these LC films can break up, though slowly. The stability is enhanced by increasing the film thickness.

After break-up an ultrathin polymer film remains, even above the isotropisation temperature T_i . This indicates that the adhesion properties of the material are good (as expected from the presence of polar groups¹⁰⁻¹³), which is of course needed in primer layers.

On nanoroughened silica the stability and ordering is rather different¹⁴. In the mesophase polycrystalline domains are present instead of a parallel layering to the substrate surface. Also above the isotropisation temperature, when the polymer is in the liquid state, the film remains stable. This does not agree with the concept described in Chapter 1, but is not necessarily disadvantageous for application purposes. At least the drop in viscosity, which is a property of the material itself, remains most helpful.

Parallel layering is also absent on chemically modified wafers. These modifications result in more hydrophobic surfaces. Polycrystalline domains are present in the polymer film after a short annealing period above the glass transition temperature. However, now the film does not remain stable, but it is very unstable, even in the mesophase. Also the adhesion properties to the surface are worse: no material is left behind after dewetting. Hence, the polymer would be suitable for applications to polar substrates (like metals, or oxides) provided they are thoroughly cleaned. Hydrophobic substrates are less well suited.

In conclusion, we have obtained a clear insight in the properties of thermotropic side-chain liquid-crystalline polymers in thin films. For answering the question if, and under which circumstances, LCPs can be used as a thermally removable primer film, experiments with a coating layer on the model substrates need to be done. Then we can see whether or not the viscosity drop around T_i actually results in an easy way to thermally remove this coating, or whether layering in the primer is needed. These experiments should be compared to the situations in which no layering is present, for example on roughened and/or chemically modified silicon wafers.

References

- 1)Nieuwhof, R. P. Dissertation Wageningen University, 1999.
- 2)Nieuwhof, R. P.; Marcelis, A. T. M.; Sudhölter, E. J. R.; Picken, S. J.; de Jeu, W. H. *Macromolecules* **1999**, *32*, 1398.
- 3)van der Wielen, M. W. J.; Cohen Stuart, M. A.; Fleer, G. J.; de Boer, D. K. G.; Leenaers, A. J. G.; Nieuwhof, R. P.; Marcelis, A. T. M.; Sudhölter, E. J. R. *Langmuir* **1997**, *13*, 4762.
- 4)Nieuwkerk, A. C.; Marcelis, A. T. M.; Sudhölter, E. J. R. *Macromolecules* **1995**, *28*, 419.
- 5)Whorlow, R. W. *Rheological Techniques*; Ellis Horwood: New York, 1992.
- 6)van der Wielen, M. W. J.; Cohen Stuart, M. A.; Fleer, G. J. *Langmuir* **1998**, *14*(24), 7065.
- 7)Noirez, L.; Boeffel, C.; Daoud-Aladine, A. *Phys. Rev. Lett.* **1998**, *80*, 1453.
- 8)Davidson, P. *Prog. Polym. Sci.* **1996**, *21*, 893.
- 9)Gähde, J.; Mix, R.; Goering, H.; Schulz, G.; Funke, W.; Hermann, U. *J. Adhesion Sci. Technol.* **1997**, *11*(6), 861.
- 10)Gähde, J.; Mix, R.; Krüger, R.-P.; Goering, H. *J. Adhesion* **1996**, *58*, 243.
- 11)Frost, A. M.; Kolosentseva, I. A.; Razumovskii, V. V. *Zh. Prikl. Khim.* **1974**, *47*(4), 731.

12)Kurbanova, R. A.; Mirzaoglu, R.; Kurbanov, S.; Karatas, I.; Pamuk, V.; Ozcan, E.; Okudan, A.; Güler, E. *J. Adhesion Sci. Technol.* **1997**, *11*(1), 105.

13)Thery, S.; Jacquet, D.; Mantel, M. *J. Adhesion* **1996**, *56*, 15.

14)van der Wielen, M. W. J.; Cohen Stuart, M. A.; Fleer, G. J. *Advanced Materials* **1999**, *11*, 918.

Summary

Liquid-crystalline polymers, LCPs, possess an ordered liquid state between their crystalline solid state and their isotropic state. In Chapter 1 a short introduction is given on the ordering behaviour of this class of material. It is not only their ordering that makes this material interesting but actually their hybrid character, i.e., they behave both like liquid crystals and like polymers. In the bulk this class of material has been studied extensively and it is still under further study. However, studies of the surface phenomena and thin films of LCPs are very scarce.

What started as a study with a high practical impact, namely the use of side-chain liquid-crystalline polymers as a primer layer for coatings, evaluated into a thorough investigation on surface phenomena of thin films of ordered fluids.

The thin films were prepared by spin-coating solutions of LCP material, based on alternating copolymers of maleic acid anhydride and α -olefins carrying terminal mesogenic methoxybiphenyl groups, onto silicon wafers. This resulted in smooth isotropic thin (nanometer-scale) films. The main topics investigated on these films and described in this thesis are wetting, ordering and dewetting. These phenomena could clearly be made visible by the following three main techniques. By *atomic force microscopy* (AFM) the surface topography and topology can be imaged and structures of only less than a few nanometers in depth can be made visible. This was done for areas in the range of several μm^2 to 0.02 mm^2 . By *optical reflection microscopy* this area could be extended to larger areas up to 0.5 mm^2 , however, without information on the topography. More information on the inner structures in the film was obtained by *X-ray reflectometry*.

In Chapter 2 and 3 we used AFM and X-ray reflectometry, which combination turned out to be very powerful in describing the morphology of and structures in thin films. The initial isotropic spin-coated films became ordered upon annealing above the glass transition temperature, T_g . This ordering was visible in the AFM-images as terrace-like structures with a height corresponding to a bilayer, and in the X-ray spectra as a Bragg peak. The terrace-like structures most probably arise because there is not enough material to complete a full top bilayer. In time the size of the terraces grow and there is a reduction in their number.

From the AFM measurements it became clear that when annealing takes place above T_g , the ordering is achieved much faster than in the case of lower annealing temperatures. Apparently, the short period in the mesophase upon cooling down from the isotropic phase to room temperature was already enough to align the film.

The ordering process described in Chapter 2 concerned films of 30 nm thickness. The layering behaviour and its kinetics are investigated more extensively in films of 200 nm thickness. This study is described in Chapter 3.

Above T_g first randomly oriented micro-crystalline domains are formed which corrugate the polymer–air interface. The size of these corrugations depends on the initial film thickness: it increases with film thickness. At the same time, however, a laterally macroscopic crystal starts to grow from the substrate surface in the direction of the polymer–air interface, at the expense of these domain structures. Finally, a nicely ordered single crystal with parallel ordered bilayers is formed in the film as well as at the polymer–air interface.

This one-dimensional crystallisation, actually recrystallisation, depends strongly on the temperature due to viscosity effects: the ordering was completed much faster at higher temperatures. An Arrhenius-type plot gives an activation energy of 122 kJ/mol, which we ascribe to the expected reorientations of the mesogenic groups during the recrystallisation process.

When the films are heated for a long period they break up. Holes, which are also visible by optical microscopy, appear which then grow in time. This dewetting of the surface is described in Chapter 4.

The growth rate of the holes depends on the temperature and film thickness. At the final stage of dewetting only droplets remain on top of a rather stable bilayer. The bilayer is even present above the isotropisation temperature. This indicates autophobic behaviour which is even more pronounced in the mesophase where a layered film is present, and where dewetting may occur over several ordered layers.

In all cases the dewetting is not linear in time and polymer slippage seems to take place. In the case of polymer slippage, a $t^{2/3}$ dependence is expected for the growth rate, which is indeed found above the isotropisation temperature. In the mesophase the dewetting differs from the “normal” slippage behaviour and a weaker time dependence is observed. We ascribe this deviation to the mesogen–mesogen interactions which have to be broken-up upon dewetting.

Around the isotropisation temperature there is a strong increase in the (initial) dewetting velocity of over more than 2 orders of magnitude. This acceleration is most probably due to the strongly decreasing viscosity because of the breaking up of the mesogen–mesogen interactions.

So far the research concerned the behaviour of thin films on smooth bare silicon wafers. The effect of chemically and physically modified wafers, respectively, on the ordering and stability against break-up is described in Chapters 5 and 6.

In the case of unmodified silicon wafers, we found that the polymer–substrate interaction induces parallel layering in the film, resulting in stable films. By changing the surface groups by surface modification with several silane compounds with different end groups, the interaction between the polymer and the surface can be tuned. In this way we obtained very hydrophobic surfaces for silanes with methyl or allyl end groups, and more intermediate surface properties for silanes with phenyl, chloride, carbomethoxy or cyano end groups. After surface modification film formation was only possible on the intermediate surfaces.

Above T_g these films show a characteristic behaviour which is strongly temperature dependent. At low temperatures in the mesophase holes nucleate which are encircled by unstable rims. Upon further annealing the rim instability decreases and the dewetting velocity increases. This feature also occurs for another completely different side-chain liquid-crystalline polymer with a methacrylate backbone and cyanobiphenyl groups in the side chains. We ascribe the peculiar dewetting behaviour to the presence of polycrystalline domains in the thin films. Especially their size and orientation and their ability to deform under shear are held responsible for the rim instabilities and, consequently, for the droplets remaining behind in the dry patches.

In Chapter 6 we introduce a controllable way to roughen a silicon surface. The idea is to adsorb a positively charged polyelectrolyte on a silicon surface followed by the adsorption of a monolayer of negatively charged nano-sized silica particles. By sintering at 1000 °C, the particles partly fuse with the substrate thus forming a rough, yet pure silica surface. By changing the radius of the adsorbing silica particles the degree of roughness can be tuned.

Different film thicknesses were investigated. When the polymer film thickness is small, the holes between the silica structures are filled and the roughness of the film is smoothed out. Upon annealing no drastic effects are visible. However, when the polymer film thickness exceeds the size of the substrate textures, upon annealing initially smooth films get rough by the formation of ordered domains, i.e., random polycrystalline domains. In time, these ordered domains grow in size and decrease in number. Apparently, the surface structures act as nucleation points for the formation of crystal domains. Big domains grow at the expense of smaller ones (Ostwald ripening).

In the isotropic phase the domains coalesce as an effect of the surface tension. The liquid film then remains stable, which is not the case on smooth substrates. Cooling down from the isotropic phase to the mesophase results in the formation of needle-like structures, so called batonnets, which is a typical texture for smectic A phases as found in bulk experiments.

Decreasing the density of silica particles at the surface results not only in the formation of crystal domains in the film, but also in layered structures. However, this layering disappears upon increasing annealing time and eventually only big crystals remain. Hence, just a few rough silica patches (5% coverage) are enough to suppress the layering behaviour.

In Chapter 7 some bulk properties on several side-chain liquid-crystalline polymers are compared with the behaviour in thin films to reflect on the application of side-chain liquid-crystalline polymers as a primer for coatings as mentioned in Chapter 1. In conclusion, we have obtained a clear insight in the properties of thermotropic side-chain liquid-crystalline polymers in thin films. But, for answering the question if, and under which circumstances, LCPs can be used as a thermally removable primer film, experiments with a coating layer on the model substrates need to be done.

Samenvatting

Vloeibaar-kristallijne polymeren hebben een geordende vloeibare toestand tussen hun kristallijne vaste toestand en hun isotrope vloeibare toestand. Over het ordeningsgedrag van dit type materiaal wordt in Hoofdstuk 1 een korte inleiding gegeven. Niet alleen de ordening maar ook het hybride karakter (het materiaal heeft eigenschappen van zowel vloeibare kristallen als van polymeren) maakt dit materiaal zeer interessant. In bulktoestand is, en wordt, dit soort materiaal al uitgebreid bestudeerd. Echter, het onderzoek naar oppervlakte-eigenschappen en dunne films van vloeibaar-kristallijne polymeren is nog zeer beperkt.

Het onderzoek begon zeer praktijkgericht met als achtergrond het gebruik van vloeibaar-kristallijne polymeren met zijketens in een onderlaag voor verf. Het resultaat is een grondig onderzoek naar de oppervlakte- en filmeigenschappen van dunne geordende vloeibare films.

Met behulp van de zogenoemde spincoating techniek werden deze dunne films bereid op siliciumsubstraten. Hiertoe werd een oplossing van het polymeermateriaal, een alternerend copolymeer van maleïnezuuranhydride en α -olefines met eindstandige mesogene methoxybifenyl-groepen, gebruikt. Dit resulteerde in vlakke ongeordende nanometerdunne films.

De belangrijkste kenmerken van deze films die bestudeerd en beschreven zijn in dit proefschrift zijn bevochtiging (wetting), ordening en filmopbreking (dewetting). Deze processen zijn voornamelijk bestudeerd met de volgende 3 technieken: (i) *Atomic force microscopy* (AFM) werd gebruikt om de oppervlaktetopografie en topologie te bestuderen. Met deze techniek kunnen structuren van minder dan enkele nanometers in hoogte of diepte zichtbaar gemaakt worden. Dit is gedaan voor oppervlakken van enkele μm^2 tot 0.02 mm^2 in afmeting. (ii) Met *optische reflectiemicroscopie* konden gebieden tot 0.5 mm^2 bekeken worden echter zonder informatie over de topografie. (iii) Meer informatie over de structuren in de film werd verkregen met *röntgenreflectometrie*.

In de Hoofdstukken 2 en 3 zijn zowel AFM als röntgenreflectometrie gebruikt. Deze combinatie bleek zeer geschikt te zijn in het beschrijven van de morfologie van de structuren in de dunne films. Boven de glasovergangstemperatuur, T_g , ordenen de oorspronkelijk ongeordende gespincoate films zich. Dit is zichtbaar in de AFM-beelden als terrasachtige structuren met een hoogte die correspondeert met een bilaag, en in de röntgenspectra als Bragg-pieken. Deze terrasachtige structuren ontstaan waarschijnlijk omdat er niet genoeg materiaal aanwezig is om er precies een volledige bilaag mee te vullen. Wordt de ordening in de tijd gevolgd, dan blijken deze terrassen te groeien en hun aantal af te nemen.

Uit de AFM-metingen bleek verder dat na verwarming boven de isotropisatietemperatuur, T_i , de ordening veel sneller plaatsvond dan bij lagere temperaturen. Blijkbaar is een korte periode in de mesofase, bij afkoeling vanuit de isotrope fase naar kamertemperatuur, al genoeg om de film te ordenen.

Dit ordeningsproces is beschreven in Hoofdstuk 2 voor films met een dikte van 30 nm. Hoe en hoe snel de laagvorming tot stand komt, is onderzocht voor films met een dikte van 200 nm. Dit is beschreven in Hoofdstuk 3.

Boven de T_g worden eerst willekeurig georiënteerde micro-kristallijne domeinen gevormd die het polymeer–lucht-grensvlak verruwen. De mate van verruwing is afhankelijk van de initiële filmdikte: het neemt toe met de filmdikte. Op hetzelfde moment begint echter ook een lateraal macroscopisch kristal vanaf het substraatoppervlak te groeien in de richting van het polymeer–lucht-grensvlak ten koste van die domeinstructuren. Uiteindelijk is zowel in de film als aan het polymeer–lucht-grensvlak een mooi geordend 1-kristal met parallel geordende bilagen gevormd. Deze ééndimensionale kristallisatie, eigenlijk een herkristallisatie, hangt sterk af van de temperatuur ten gevolge van de viscositeitseffecten, dat wil zeggen, de ordening was veel sneller voltooid bij hogere temperaturen. Uit een Arrhenius-type grafiek halen we een activeringsenergie van 122 kJ/mol die we toeschrijven aan de verwachte heroriëntering van de mesogene groepen tijdens het herkristallisatieproces.

Als de films langdurig worden verwarmd breken ze op. Er ontstaan gaten die ook zichtbaar zijn met optische microscopie en vervolgens groeien deze in de tijd. Deze filmopbreking, ofwel dewetting, is beschreven in Hoofdstuk 4.

De groeisnelheid van de gaten is afhankelijk van de temperatuur en de filmdikte. Aan het eind van de dewetting zijn er alleen nog druppels aanwezig die op een redelijk stabiele bilaag achterblijven. Deze bilaag is zelfs nog aanwezig boven de isotropisatietemperatuur. Dit geeft een autofoob gedrag aan dat zelfs nog duidelijker zichtbaar is in de mesofase. Daar is een gelaagde film zichtbaar en dewetting treedt op over verscheidene geordende lagen.

In al de gevallen verloopt de dewetting niet lineair in de tijd en treedt waarschijnlijk polymeerslip op. In geval van polymeerslip zou de groeisnelheid van de gaten evenredig moeten zijn aan $t^{2/3}$. Dit wordt inderdaad gevonden boven de T_i . In de mesofase verschilt de dewetting van het “normale” slipgedrag en wordt er een zwakkere tijdsafhankelijkheid gevonden. Dit schrijven we toe aan de mesogeën–mesogeën interacties die verbroken moeten worden tijdens de dewetting.

Rond de isotropisatietemperatuur is er een sterke toename in de (initiële) dewettingsnelheid over meer dan 2 ordes van grootte. Deze versnelling is hoogstwaarschijnlijk ten gevolge van de sterk dalende viscositeit vanwege de verbreking van de mesogeën–mesogeën interacties.

Tot nu toe betrof het beschreven onderzoek het gedrag van dunne films op vlakke kale siliciumoppervlakken. Het effect van chemisch en fysisch modificeren van het oppervlak op de ordening en de filmstabiliteit is beschreven in respectievelijk Hoofdstuk 5 en 6.

In geval van ongemodificeerde siliciumsubstraten werd de parallelle gelaagdheid in de film opgelegd door de polymeer–substraat-interactie, dat resulteerde in stabiele films. Door de oppervlaktegroepen te veranderen met behulp van diverse chloorsilaanverbindingen met

verschillende eindgroepen kan de interactie tussen het polymeer en het oppervlak ingesteld worden. Zo zijn zeer hydrofobe oppervlakken verkregen voor silanen met methyl- of allyl-eindgroepen, en intermediaire oppervlakken voor silanen met fenyl-, chloride-, carbomethoxy- of cyano-eindgroepen. Na oppervlaktemodificatie was er alleen filmvorming mogelijk op deze intermediaire oppervlakken.

Boven de T_g vertoonden deze films een karakteristiek gedrag dat sterk temperatuursafhankelijk was. Bij lage temperaturen in de mesofase ontstonden gaten omringd met instabiele randen. Bij verhoging van de temperatuur verminderde deze randinstabiliteit en nam de dewettingssnelheid toe. Dit gedrag werd ook gevonden bij een ander vloeibaar-kristallijn polymeer met een methacrylaat-hoofdketen en cyanobifenyl-groepen in de zijketens. Dit aparte dewettinggedrag schrijven we toe aan de aanwezigheid van polykristallijne domeinen. Vooral de domeingrootte en orientatie en de mogelijkheid om te vervormen ten gevolge van afschuiving, worden verantwoordelijk geacht voor de randinstabiliteiten, met als resultaat de achterblijvende druppels op de droge plaatsen.

In Hoofdstuk 6 wordt een nieuwe manier om gecontroleerd een silicaoppervlak te verruwen voorgelegd. Het idee hierachter is om een positief geladen polyelectrolyte op een silicaoppervlak te laten adsorberen, gevolgd door de adsorptie van een monolaag van negatief geladen silicananometerdeeltjes. Door vervolgens te verhitten bij 1000 °C versmelten deze deeltjes gedeeltelijk met het substraat waardoor het oppervlak wordt verruwd. Het oppervlak blijft hierdoor van silica. Door te variëren in de straal van de te adsorberen silicadeeltjes kan de mate van ruwheid ingesteld worden.

Op deze verruwde oppervlakken zijn vervolgens films van diverse diktes aangebracht en onderzocht. Voor een dunne polymeerfilm worden de gaten tussen de silicastructuren gevuld en neemt de ruwheid van de film af. Bij verwarming zijn er geen drastische veranderingen zichtbaar. Echter, als de dikte van de polymeerfilm de substraattextuur overstijgt, dan worden de oorspronkelijk vlakke films ruw bij verwarming ten gevolge van de vorming van willekeurig geordende polykristallijne domeinen. Als de verwarming wordt voortgezet groeien deze geordende domeinen in de tijd en als gevolg daarvan neemt hun aantal af. Blijkbaar zorgen de (ruwe) oppervlaktestructuren voor nucleatiepunten voor de vorming van kristallijne domeinen. Grote domeinen groeien ten koste van de kleinere (Ostwaldrijping).

In de isotropefase vloeien de domeinen samen ten gevolge van de oppervlaktespanning. De vloeistoffilm blijft stabiel, wat niet het geval was op de vlakke substraten. Afkoeling vanuit de isotropefase in de mesofase resulteert in de vorming van naaldachtige structuren, zogenaamde batonnets, wat een typische textuur is voor smectische A fases zoals die in bulk worden gevonden.

Verlaging van de dichtheid aan silicadeeltjes resulteert niet alleen in de vorming van kristallijne domeinen in de film, maar ook in gelaagde structuren. Echter deze gelaagdheid verdwijnt als er langer wordt verwarmd en uiteindelijk blijven er alleen grote kristallen achter.

Slechts een paar ruwe silicaplekjes (5% bezetting) zijn al genoeg om de laagvorming te onderdrukken.

In hoofdstuk 7 wordt teruggeblikt op de toepassing van zijketen vloeibaar-kristallijne polymeren als primer voor verf, zoals beschreven in hoofdstuk 1. Daartoe worden bulkeigenschappen van enkele zijketen vloeibaar-kristallijne polymeren vergeleken met het gedrag in dunne films. Concluderend kunnen we zeggen dat een duidelijk beeld is verkregen van de eigenschappen van thermotrope zijketen vloeibaar-kristallijne polymeren in dunne films. Echter, om de vraag te kunnen beantwoorden of, en onder welke omstandigheden, vloeibaar-kristallijne polymeren gebruikt kunnen worden als thermisch verwijderbare primer-films, moeten er nog experimenten gedaan worden met een coating op de modelsubstraten.

Curriculum vitae

Maarten Willem Josephus van der Wielen was born in Hulst, the Netherlands, on February 12th, 1970. In 1988 he graduated from secondary school (Atheneum B) at the 'R.K. Jansenius Scholengemeenschap' in Hulst. In September of the same year, he started the 4-year course in Laboratory Science with a specialisation in Chemistry at Larenstein International Agricultural College in Wageningen. In June 1992, he obtained his BSc degree after which he continued his studies in Molecular Sciences at the Wageningen Agricultural University. His majors were Molecular Physics and Colloid and Interface Chemistry. Furthermore, he spent 5 months of practical research at the Institute of Inorganic, Analytical and Physical Chemistry at Bern University, Switzerland. He graduated in June 1995. In July 1995 he started the research described in this thesis as a PhD at the Laboratory of Physical Chemistry and Colloid Science, Wageningen Agricultural University.

Dankwoord

Een mooie periode van vier jaar sluit ik nu met deze laatste pagina's af. Een periode waar ik met veel plezier op zal blijven terugkijken. Dit is mede te danken aan de diverse bijdragen van mijn collega's, familie en vrienden die ik bij deze daarom wil bedanken. Enkele van hen wil ik in het bijzonder noemen.

Allereerst mijn ouders en mijn vrouw Jacqueline. Pa en ma, bedankt voor de mogelijkheden die jullie me gaven om te studeren en de ondersteuning daarin. Jacqueline, jij bent er altijd voor mij en ik heb op velerlei manieren op je kunnen rekenen. Je zorgt samen met ons zoontje Thierry voor vele mooie momenten.

Graag wil ik mijn promotoren Gerard Fler en Martien Cohen Stuart bedanken voor de begeleiding en samenwerking. Gerard en Martien, jullie gaven me het vertrouwen te werken in dit voor ons drieën nieuw terrein. Ik ben trots op onze samenwerking en behaalde resultaten. Gerard, op je vraag "Kom je op mijn geweten werken?", als ik weer eens bij je langskwam om te kijken of je al naar mijn manuscripten had gekeken, kan ik antwoorden: "Ja", en weet je, het hielp nog ook!

De directe projectcollega's René Nieuwhof, Ernst Sudhölter en Ton Marcelis, allen werkzaam binnen het Laboratorium voor Organische Chemie, wil ik bedanken voor onze samenwerking. Hieruit vloeiden niet alleen vloeibaar-kristallijne polymeren voort, maar ook zeer nuttige besprekingen! René, zonder jouw polymeren had dit proefschrift er heel anders uitgezien. Ik kwam graag effe bij je shoppen, maar om al je produkten uit je winkeltje in mijn vier jaar te onderzoeken was een beetje veel van het goede.

De halfjaarlijkse rapportages aan de IOP-verf begeleidingscommissie, onder leiding van Frans Willemse, waren zeer nuttig omdat vooral tijdens deze bijeenkomsten de vertaalslag naar de praktijk naar voren kwam. Van deze commissie wil ik in het bijzonder Hans Kloosterboer (Philips nat. lab., Eindhoven) en Wim de Jeu (AMOLF, Amsterdam) bedanken bij het bediscussiëren en interpreteren van mijn resultaten.

Niet al mijn metingen konden in ons eigen lab. worden gedaan. Gelukkig kon ik daarvoor bij anderen aankloppen. Zo kon ik, voordat we zelf een ellipsometer hadden aangeschaft, altijd terecht bij James Lichtenbelt (AKZO-Nobel, Arnhem) voor filmdiktemetingen. James, niet alleen bedankt voor het gemak waarmee ik telkens weer je opstelling kon gebruiken, maar ook voor je interesse in mijn metingen.

De samenwerking met Dick de Boer, Ann Leenaers en Bart Schlatmann (allen op dat moment werkzaam bij Philips nat. lab. en CFT, Eindhoven) heb ik ook als zeer prettig ervaren. De röntgenresultaten hebben een belangrijke bijdrage geleverd aan mijn proefschrift. Bedankt voor de fijne samenwerking.

Hoewel het niet in dit proefschrift terug te vinden is, heb ik nogal wat tijd gestoken in het toepassen van infraroodspectroscopie aan dunne LCP-films. Van buiten onze groep heeft

Willem Nissink (Universiteit Utrecht) hiervoor enkele metingen verricht. Willem, bedankt dat je, ondanks je eigen schrijverij, hiervoor nog wat tijd vrij wilde maken.

Gedurende mijn promotie heb ik Stefan Jansen en Edwin Baars begeleid tijdens hun doctoraalvak. Dat was voor mij een zeer leuke ervaring en afwisseling. Beide bedankt.

Natuurlijk is het aanwezig zijn van de faciliteiten en ondersteuning onmisbaar binnen elke groep, maar zeker ook de sfeer speelt een belangrijke rol. Ik wil hiervoor ons gehele laboratorium, inclusief ex-collega's, bedanken. Enkele wil ik nog even met name noemen: Marcel *ESC'97* Giesbers, Martijn *karting* Tinus Oversteegen, Joost *mooi he mensen* Maas, Bert *zullen we een spelletje doen* Torn, Remco *is een goed plan* Fokkink, Monique *Borsato chips* Bremer, Desiree *bij mij gaan alle baby's huilen (Thierry niet trouwens!)* Barten, en Henri *geen zoon van Bert* Bijsterbosch.

Het eerste dat je opvalt aan een proefschrift is de omslag. In mijn geval zijn hierop enkele voorbeelden weergegeven van wat je uit AFM-resultaten kunt toveren. De omslag is ontworpen door Patrick van Gerner. Patrick, fijn dat je dat wilde doen, en voortaan zal ik het geen kافت meer noemen.

Tot slot dank ik familie en vrienden voor de belangstelling die ze toonden voor mijn werk en voor de ontspanning naast het werk.

Bedankt allemaal,

Maarten